# UNIVERSITÉ DE STRASBOURG

ÉCOLE DOCTORALE Science de la Vie et de la Santé (ED 414)

[EA 3072 Mitochondries, Stress Oxydant et Protection Musculaire]

# THÈSE présentée par: Manuel BARBERIO

Soutenue le : 10 décembre 2019

Pour obtenir le grade de : **Docteur de l'Université de Strasbourg**

Discipline/ Spécialité : Sciences Médicales

**Real-time intraoperative quantitative assessment of gastrointestinal tract perfusion using hyperspectral imaging (HSI).**

THÈSE dirigée par :

| | |
|---|---|
| M. Diana Michele | Medical-Scientific Director, Research Institute against Cancer of the Digestive System, Strasbourg, France.<br><br>HDR, Université de Strasbourg, France |

EXAMINATEURS :

| | |
|---|---|
| M. Spinoglio Giuseppe | PU-PH, Director Robotic Surgery and Educational IEO (European Institute of Oncology) IRCCS, Milan, Italy |
| M. Forgione Antonello | PU-PH, Consultant General Oncologic Mini-invasive Surgery at General Surgery Department of the Niguarda Cà Granda Hospital, Milan, Italy |

AUTRES MEMBRES DU JURY :

| | |
|---|---|
| M. Eric Noll | HDR, Université de Strasbourg, France |

INVITE :

| | |
|---|---|
| M. Bernard GENY | PU-PH, Nouvel Hôpital Civil, Université de Strasbourg, France |

# Summary

# ABSTRACT

Anastomotic leakage (AL) is a severe complication in digestive surgery, presenting high incidence rates, particularly after esophageal (20-35%) and colorectal resections (4-19%), as well as high morbidity and mortality rates.

An adequate local perfusion is a fundamental variable to control in order to promote anastomotic healing. It also contributes to reduce the risk of AL. However, clinical criteria are often unreliable to evaluate bowel perfusion, leading to misinterpretation. Consequently, an intraoperative tool allowing to objectively detect the anastomotic blood flow intraoperatively is highly desirable. In this regard, fluorescence angiography (FA) has been incrementally explored over the last few years, to assess perfusion during digestive surgical procedures. FA is an optical imaging technique, which requires a near-infrared (NIR) camera coupled with the intravenous injection of an exogenous fluorescent dye. Applied to digestive resections, FA allows to visualize bowel perfusion by means of fluorescence enhancement, based on the rationale that the injected fluorophore is distributed solely to areas with preserved blood supply. Several clinical trials have shown promising results. However, a well-designed randomized controlled trial is currently missing. Consequently, the evidence level of the available studies remains low. Additionally, there is a need for a standardized and quantitative evaluation of the fluorescent signal during FA. Quantitative FA has been previously introduced and validated. However, FA remains limited by the need of injecting a fluorophore.

Hyperspectral imaging (HSI) is a promising optical imaging technique allowing for a contrast-free, real-time, and quantitative tissue analysis, which couples a spectroscope with a photo camera. Through tissue-light interactions (absorption, reflectance) at the analyzed surface, it is possible to analyze the intrinsic biochemical properties. HSI acquires bidimensional spatial images across the electromagnetic spectrum, subsequently providing a tridimensional dataset called hypercube (x, y as spatial coordinates, and $\lambda$ as the spectral coordinate). In the past, this technology was used for medical purposes, including tissue perfusion, but given the large dimension of the produced data, data

extraction and perfusion quantification was not possible. With recent technological advances, systems capable of quantifying several physiological tissue parameters, including oxygen saturation ($StO_2$), near-infrared perfusion index (NIR), hemoglobin index (THI), and tissue water index (TWI) as an immediate output have been developed. One of the drawbacks of HSI is that it provides static color-coded images, which contain perfusion parameters. Those images with enhanced information are displayed side-by-side and not overlaid on the standard white light, RGB real images. It is a limiting factor for intraoperative use, since spatially dynamic accurate images are essential to precisely identify and co-localize the structures along with the augmented physiology information in the surgical field.

Through a customization of the HSI system and a proprietary software solution, we developed an hyperspectral-based enhanced reality (HYPER) environment, to allow for a contrast-free precise intraoperative perfusion assessment. This thesis describes the steps of the development and validation of the HYPER concept.

# RESUME EN FRANÇAIS

## Positionnement de la recherche

Les fuites anastomotiques constituent une complication grave de la chirurgie digestive, présentant des taux d'incidence élevés, en particulier après des résections œsophagiennes (20-35 % [1]) et colorectales (4-19 % [2]), ainsi qu'une morbidité et une mortalité élevées [1].

Une perfusion locale adéquate est un facteur déterminant qui favorise la cicatrisation anastomotique et contribue ainsi à réduire le risque de fuites anastomotiques. Cependant, les critères cliniques sont souvent peu fiables pour évaluer la perfusion intestinale [3]. Par conséquent, un outil peropératoire permettant de détecter objectivement le débit sanguin majeur dans les anastomoses est nécessaire. À cet égard, l'angiographie par fluorescence (AF) a progressivement fait l'objet d'études au cours des dernières années pour évaluer la perfusion lors des interventions chirurgicales digestives. L'AF est une technique d'imagerie optique qui nécessite une caméra proche infrarouge (NIR) couplée à l'injection intraveineuse d'un colorant fluorescent exogène. Appliquée aux résections digestives, l'AF permet de visualiser la perfusion intestinale grâce à une fluorescence améliorée, en partant du principe que le fluorophore injecté se diffuse uniquement dans les zones où l'apport sanguin est conservé [4-6]. Plusieurs essais cliniques ont montré des résultats prometteurs lorsque l'AF était utilisée dans la chirurgie du tube digestif haut et bas [7-10]. Cependant, les études sont très hétérogènes en matière de protocoles et la qualité des preuves est globalement faible [11-13]. Par ailleurs, il est nécessaire d'effectuer une évaluation normalisée et quantitative du signal fluorescent lors d'une AF [14]. Notre groupe a déjà introduit et validé plusieurs expériences quantitatives de l'AF [15-17]. Cependant, l'AF reste subordonnée à la nécessité d'injecter un fluorophore, posant ainsi une limite.

La spectro-imagerie (abrégée par HSI dans sa version anglaise) est une technique d'imagerie optique prometteuse qui offre une analyse quantitative, en temps réel et sans contraste des tissus et qui couple un spectroscope à une caméra optique. Les interactions tissu-lumière (absorption, réflectance) au niveau de la surface analysée dépendent des propriétés biochimiques intrinsèques.

La spectro-imagerie acquiert des images spatiales bidimensionnelles sur l'ensemble du spectre électromagnétique, fournissant ainsi un ensemble de données tridimensionnelles appelé hypercube (x, y comme coordonnées spatiales et λ comme coordonnée spectrale). La spectro-imagerie a récemment été utilisée à des fins médicales [18], notamment pour la perfusion tissulaire. Akbari et al. [19] ont d'abord identifié la longueur d'onde optimale (765-830 nm) afin d'évaluer l'ischémie intestinale, en utilisant un prototype de spectro-imagerie avec un large éventail de longueurs d'onde (400 à 1700 nm), sur un modèle porcin. Toutefois, le système n'a pas fourni d'analyse quantitative de l'oxygénation.

Récemment, un système de spectro-imagerie compact a été mis au point, ainsi disponible sur le marché et capable de fournir des informations quantitatives sur la saturation en oxygène (StO2), l'indice de perfusion dans le proche infrarouge (NIR), l'indice d'hémoglobine (THI) et l'indice d'eau dans les tissus (TWI) en sortie immédiate [20]. Le système a été initialement conçu pour détecter les changements microcirculatoires pendant le suivi de la cicatrisation de la plaie. L'un des inconvénients de la spectro-imagerie est qu'elle fournit des images statiques codées par couleur, qui contiennent des paramètres de perfusion. Ces images avec des données augmentées sont affichées côte à côte et ne sont pas superposées aux images réelles RVB en lumière blanche standard. C'est un facteur limitant pour une utilisation peropératoire, car des images précises et dynamiques dans l'espace sont essentielles pour identifier avec précision et colocaliser les structures et les informations physiologiques augmentées dans le champ opératoire.

**Objectif de la recherche**

Dans un premier temps, notre objectif a consisté à valider la spectro-imagerie en quantifiant précisément la teneur en oxygène des tissus (StO2) dans un modèle d'ischémie-reperfusion des muscles squelettiques. Successivement, grâce à une personnalisation du système de spectro-imagerie, obtenue par l'ajout d'une webcam HD et d'un capteur de distance infrarouge et grâce à la mise en place d'un logiciel propriétaire, il a été possible de superposer les images pseudo-couleur générées par la spectro-imagerie, comportant la cartographie de StO2 sur la vidéo en temps réel. Ceci a débouché sur un effet de réalité augmentée (HYperspectral-based Enhanced Reality, HYPER), qui a permis une localisation peropératoire précise des caractéristiques spectrales mises en évidence par le système de spectro-imagerie. Afin de valider ce nouvel outil, nous avons utilisé une anse ischémique de l'intestin grêle porcin comme modèle de travail. La capacité d'HYPER à quantifier avec précision la StO2 a été testée par rapport à des marqueurs d'ischémie fiables : 1) le lactate capillaire local (LCL) ; 2) la production des espèces réactives de l'oxygène (ROS) et 3) l'analyse histopathologique. La troisième étape de la recherche visait à comparer la détection et la quantification de l'ischémie de l'intestin grêle dans le modèle porcin entre l'effet HYPER et l'angiographie par fluorescence quantitative bien établie en utilisant le logiciel FLER (FLuorescence-based Enhanced Reality) créé par notre groupe [16, 21]. En quatrième étape, nous avons évalué l'utilité de la spectro-imagerie dans deux contextes chirurgicaux cliniques différents : lors d'une résection œsophagienne et lors d'une résection du côlon [22, 23].

**Étapes expérimentales**

**1) Hyperspectral imaging quantification of mouse limb microcirculation in ischemia-reperfusion model with phosphodiesterase 5 inhibitor preconditioning**

Le fondement rationnel de cette étude était de découvrir si le préconditionnement pharmacologique est protecteur dans les lésions de reperfusion de l'ischémie des membres postérieurs, en utilisant le sildénafil comme inhibiteur de la phosphodiestérase de type 5. La spectro-imagerie a été utilisée pour quantifier la StO2 tout au long de l'expérience. *Matériels et méthodes :* Une ischémie unilatérale des membres postérieurs (120 minutes) suivie d'une reperfusion (30 minutes) a été créée. Cinq souris ont reçu du sildénafil (1 mg/kg par voie parentérale 30 minutes avant l'ischémie) et 5 souris ont servi de témoins. La StO2 à T0, 5, 30, 60, 120 minutes après l'ischémie (T5, 30, 60, 120) et la StO2 à 5, 15 et 30 minutes après la reperfusion (T 125, 135, 150) ont été mesurées par spectro-imagerie. *Résultats :* Le groupe témoin a montré une StO2 significativement inférieure à T120 (24,8±17 %) par rapport à T0 (53,3±7,04 %) (p=0,0113) et T150 (76,8±3,77 % ; p=0,0008). T150 a montré une StO2 statistiquement significative supérieure à T0 (p=0,0134). Dans le groupe du sildénafil T120, la StO2 (28,6±20 %) était inférieure à T0 (63,3±8,46 % ; p=0,0312) et T150 (73,3±19,1 % ; p=0,0075). Aucune différence statistique n'a été observée entre T0 et T150. Les valeurs de la StO2 ne différaient pas statistiquement entre le sildénafil et le groupe témoin. *Conclusion :* La spectro-imagerie est un outil qui permet de quantifier les phases d'ischémie et de reperfusion. Le préconditionnement au sildénafil n'a pas amélioré les valeurs de la StO2.

2) **HYPerspectral Enhanced Reality (HYPER): a physiology-based surgical guidance tool**

Cette étude expérimentale évalue la précision de la spectro-imagerie, afin de quantifier la perfusion intestinale et d'obtenir une superposition des données de spectro-imagerie aux images en temps réel. *Matériels et méthodes :* Chez 6 porcs, 4 anses intestinales ischémiques ont été créées (A, B, C, D) et soumises à imagerie à des moments précis (de 5 à 360 min). Un système de spectro-imagerie

disponible sur le marché a fourni des cartographies pseudo-couleur de l'état de la perfusion (StO2, perfusion en proche infrarouge) et de l'indice tissulaire de l'eau (TWI). Un logiciel ad hoc a été mis au point pour superposer les données de spectro-imagerie à la vidéo diffusée en direct et créer le logiciel HYPerspectral Enhanced Reality (HYPER). Sept régions d'intérêt (ROI) ont été identifiées dans chaque anse intestinale selon les amplitudes de la StO2, c'est-à-dire vasculaire (VASC proximal et distal), vasculaire marginal (MV proximal et distal), ischémique marginal (MI proximal et distal) et ischémique (ISCH). Les lactates capillaires locaux (LCL), le radical des espèces oxygénées (ROS) et l'histopathologie ont été mesurés au niveau des ROIs. Un algorithme de prédiction du LCL basé sur l'apprentissage machine, basé sur le HSI-StO2%, a été utilisé sur les 6 porcs et testé sur 5 animaux supplémentaires. *Résultats :* Les paramètres de spectro-imagerie (StO2 et proche infrarouge) étaient congruents avec les niveaux de LCL, la production de ROS et les scores de lésions histopathologiques au niveau des ROIs mis en évidence par le système HYPER. L'erreur moyenne globale de prédiction du LCL était de 1,18±1,35 mmol/L. Pour des valeurs de la StO2 > 30 %, l'erreur moyenne était de 0,3±0,33. *Conclusions :* L'imagerie par le système HYPER a permis de quantifier avec précision les changements de perfusion sur la durée dans ce modèle d'ischémie intestinale [24].

**3) Quantitative fluorescence angiography vs. hyperspectral imaging to assess bowel ischemia: a comparative study in enhanced reality**

L'objectif de cette étude était de comparer la performance de la spectro-imagerie et du système FLER afin d'évaluer la perfusion intestinale, dans un modèle expérimental d'ischémie sans survie. *Méthodes :* Chez 6 porcs, un segment ischémique de l'intestin grêle a été créé et soumis à imagerie. Les modalités d'imagerie ont été appliquées séquentiellement à la même zone. La spectro-imagerie a d'abord été réalisée pour acquérir les amplitudes de la StO2 en utilisant le système TIVITA™ (Diaspective Vision ; Allemagne). Par la suite, l'AF a été réalisée à l'aide d'une caméra laparoscopique dans le proche infrarouge (D-Light P, Karl Storz, Allemagne), après injection

intraveineuse de 0,2 mg/kg de vert d'indocyanine. Le signal de fluorescence jusqu'au pic de concentration a été analysé à l'aide d'un logiciel propriétaire (FLER, IHU/IRCAD Strasbourg, France) pour obtenir une cartographie virtuelle de perfusion. La cartographie virtuelle a été superposée à des images en temps réel pour obtenir une FLER. Dix régions d'intérêt adjacentes ont été sélectionnées à partir d'ensembles de données de spectro-imagerie et ont été superposées aux cartographies générées par le système FLER à l'aide d'une fonction logicielle plug-in personnalisée, permettant ainsi une comparaison quantitative des deux modalités d'imagerie. Des lactates capillaires locaux (LCL) ont été échantillonnés au niveau des ROIs. Un modèle prédictif LCL a été extrapolé à partir de la pente de spectro-imagerie-StO2 et de la pente FLER. *Résultats :* La concentration systémique moyenne de lactate était de 2,09±0,35 mmol/L, la concentration moyenne de LCL était de 2.09±0.35 mmol/L, la valeur moyenne de la StO2 était de 48.62±18 % et la pente moyenne du pic de concentration était de 598.6±658.1. Le coefficient de corrélation r2 entre spectro-imagerie-StO2 et la pente FLER était de 0,42 et la corrélation de Spearman était de 0,66 (p=8,32-05). La corrélation de Spearman entre les valeurs LCL et la pente FLER, et entre les valeurs LCL et spectro-imagerie-StO2 était de -0,56 (p=0,001). Le modèle de prédiction du lactate de la spectro-imagerie a démontré une performance significativement plus élevée comparativement à la prédiction du lactate basée sur le FLER (p=0,027). *Conclusion :* La spectro-imagerie sans contraste a permis d'obtenir des résultats plus précis en termes de prédiction du LCL.

**4) Discrimination between arterial and venous bowel ischemia via computer-assisted analysis of the fluorescent signal**

L'objectif de cette étude était d'identifier les schémas de l'ischémie intestinale artérielle ou veineuse par analyse logicielle du signal de fluorescence.

*Matériels et méthodes :* Chez 18 porcs, deux clips ont été appliqués sur l'artère mésentérique inférieure (groupe A : n = 6) ou la veine (groupe V : n = 6) ou sur les deux (groupe A-V : n = 6). Trois régions d'intérêt ont été identifiées sur le côlon sigmoïde : P = proximal au premier clip ; C =

central, entre les deux clips ; et D = distal au second clip. Le vert d'indocyanine a été injecté par voie intraveineuse. Le signal de fluorescence a été capté au moyen d'un laparoscope dans le proche infrarouge. Le pic de concentration (secondes) et l'intensité maximale de fluorescence ont été enregistrés à l'aide d'un logiciel. Une unité d'intensité de fluorescence normalisée (UIFN : 0 à 1) a été attribuée, en utilisant une carte de référence. Les variations du NFIU sur la durée ont été calculées toutes les 10 minutes pendant 50 minutes. Les lactates capillaires ont été mesurés sur le côlon sigmoïde au niveau des 3 ROIs. Différents algorithmes de machine learning (ML) ont été appliqués pour la reconnaissance des schémas d'ischémie.

*Résultats :* Le délai de pointe à la région d'intérêt ischémique C était significativement plus long dans le groupe A versus groupe V (20,1±13 versus 8,43±3,7 ; p = 0,04) et dans le groupe A-V versus groupe V (20,71±11,6 versus 8,43±3,7 ; p = 0,03). L'UIFN maximale à la région d'intérêt C était plus élevée dans le groupe V (1,01±0,21) comparativement à A (0,61±0,11 ; p = 0,002) et A-V (0,41 ± 0,2 ; p = 0,0005). Les lactates capillaires à la région d'intérêt C étaient plus faibles en V (1,3±0,6) qu'en A (1,9±0,5 ; p = 0,0071) et A-V (2,6±1,5 ; p = 0,034). Le plus proche voisin K et les algorithmes SVM linéaires ont fourni à la fois une précision de 75 % dans la discrimination entre A et V et de 85 % dans la discrimination entre A et A-V. La précision est tombée à 70 % lorsque la ML a dû identifier simultanément la région d'intérêt et le type d'ischémie. *Conclusions :* L'analyse dynamique assistée par ordinateur du signal de fluorescence permet de distinguer les différents modèles d'ischémie intestinale [25].

**5) Evaluation of hyperspectral imaging (HSI) for the measurement of ischemic conditioning effects of the gastric conduit during esophagectomy**

L'objectif de cette étude était d'évaluer la spectro-imagerie pour mesurer les effets du conditionnement ischémique au cours d'une œsophagectomie. *Matériels et méthodes :* Des images hyperspectrales peropératoires du tube gastrique par mini-thoracotomie ont été enregistrées chez n = 22 patients, dont 14 ont subi une gastrolyse laparoscopique et un conditionnement ischémique de

l'estomac avec œsophagectomie transthoracique en deux temps et un conduit gastrique avec anastomose intrathoracique après 3-7 jours. L'extrémité du tube gastrique (a posteriori anastomose œsophagogastrique) a été mesurée par spectro-imagerie. Le logiciel d'analyse fournit une image RVB et 4 images fausses couleurs représentant les paramètres physiologiques de la zone tissulaire enregistrée en peropératoire. Ces paramètres comprennent l'oxygénation des tissus (StO2), l'indice de perfusion (indice de perfusion en proche infrarouge), l'hémoglobine des organes (OHI) et l'indice d'eau dans les tissus (TWI). *Résultats :* La spectro-imagerie peropératoire du conduit gastrique a été possible chez tous les patients et n'a pas prolongé l'intervention opératoire classique en raison de son applicabilité rapide. En particulier, l'oxygénation tissulaire du conduit gastrique était significativement plus élevée chez les patients ayant subi un conditionnement ischémique (moyenne du préconditionnement de la StO2 = 78 % ; moyenne de non-préconditionnement de la StO2 = 66 % ; p = 0,03). *Conclusions :* La spectro-imagerie convient à l'évaluation sans contact, non-invasive et peropératoire des paramètres physiologiques des tissus dans les conduits gastriques. Par conséquent, la spectro-imagerie est une méthode utile pour évaluer les effets du conditionnement ischémique et peut contribuer à réduire les complications anastomotiques. Des études supplémentaires sont nécessaires pour établir les valeurs normales et les seuils des paramètres présentés pour le site anastomotique du conduit gastrique [23].

**6) New intraoperative imaging technologies: Innovating the surgeon's eye toward surgical precision**

L'imagerie est l'un des piliers de l'évolution continue de l'oncologie chirurgicale vers un paradigme de précision. Dans le présent aperçu, certaines technologies d'imagerie peropératoire établies ou émergentes sont décrites à la lumière de la vision et de l'expérience de notre groupe en chirurgie guidée par l'image, en particulier en oncologie chirurgicale digestive [26].

# INTRODUCTION GENERALE

## (Partie en anglais)

## 1. Image-guided surgery

Over the last years, given the rapid advances in computer science, the concept of "precision medicine" [27] has been introduced. It is based on the increasing interaction between a human and a machine, obtained thanks to the incremental availability of computers with high computational power, which has enabled the processing of patient-related big data.

Similarly, in surgical science, the availability of highly accurate intraoperative imaging techniques coupled with the remarkable advances of minimally invasive or robotic procedures has generated the novel concept of precision surgery.

The introduction of minimally invasive surgery (MIS) approximately 30 years ago was considered a groundbreaking revolution, resulting in a dramatic reduction of surgical trauma as compared to a conventional open approach. Simultaneously, other disciplines such as interventional radiology and interventional flexible endoscopy have made enormous progress. Nowadays, they represent a valid alternative to the surgical therapeutic approach for an increasing number of clinical scenarios. Interventional radiologists can benefit from cutting-edge imaging systems, in order to perform advanced image-guided percutaneous procedures, which are progressively taking over some previous surgical indications. An analogous evolutive process occurs in flexible endoscopy, with advanced tools which allow gastroenterologists to perform effective endoluminal surgery for early stage cancers.

Such changes hold the potential to produce patient-tailored management algorithms making it possible to treat diseases with less invasive and targeted strategies.

Similarly, intraoperative imaging techniques, associated with advanced computer algorithms capable of augmenting the surgical field beyond the surgeon's naked eye capabilities have generated the concept of image-guided surgery [28]. The images provide extra information which enhances the surgeon's vision, potentially leading to intraprocedural strategy changes.

Today, medical imaging offers a large variety of different technologies (CT, MRI, positron emission tomography or PET-scan, ultrasound and optical visualization techniques), which have reached a remarkable degree of sophistication over the past 10 years and have made it possible to obtain more detailed images of the human body [29].

With this view, the Research Institute against Digestive Cancer (IRCAD) launched a large translational research project aiming at the development and implementation of hybrid, image-guided, computer-assisted therapies. This effort culminated with the foundation of the Institute of Image-Guided Surgery, IHU Strasbourg. The IHU comprises cutting-edge experimental and clinical platforms fully equipped with multiple imaging systems **(Figure 1)**. In collaboration with the University of Strasbourg, the institute houses various research groups working on advanced imaging medical robotics, and artificial intelligence, in tight collaboration with surgeons, interventional radiologists, and endoscopists.

**Fig. 1:** Hybrid operative room with multidetector CT-scan and robotic C-arm Artis Zeego

## 2. Gastrointestinal anastomosis

### 2.1. Definition

The term "anastomosis" is derived from the Greek language and literally signifies “by means of an opening”. It refers to the artificially established continuity between two spaces or tubular structure, such as blood vessels.

A surgical digestive anastomosis is the connection between two segments of the gastrointestinal tract, which is performed either to restore continuity after removal of an intermediate segment housing, for example, a tumor, or to short circuit the passage of food, in order to induce a reduction in nutrient absorption and weight loss and an improvement in the metabolic profile (obesity surgery: gastric bypass).

Many techniques have been developed to produce digestive anastomoses, e.g. manual suture, mechanical stapler suture with metal staples, mechanical or magnetic compression anastomosis [30], anastomosis with biological glues and many others [31]. Manual suturing and staple suturing are the two most common techniques in the daily practice **(Figure 2)**.

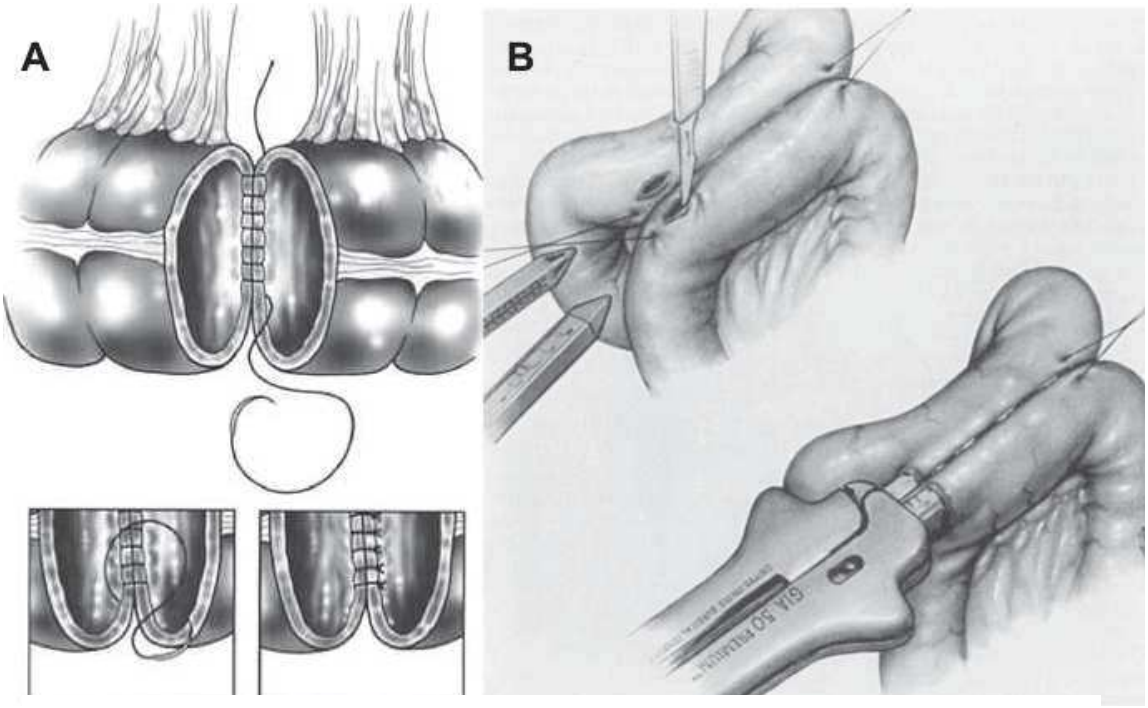


**Fig. 2:** Schematic representation of a hand-sewn colonic anastomosis (A) and of a small bowel anastomosis using the GIA mechanical stapler (B).

## 2.2 The healing mechanism of digestive anastomoses

The "normal" healing process of a digestive anastomosis has not been fully clarified and several questions remain open in the pathophysiological understanding [32]. Simplifying the healing of an anastomosis was compared to that of skin tissue and following the same repair phases, controlled by a cascade of cytokines and growth factors, namely hemostasis (I), inflammation (II), proliferation (III), and remodeling (IV). In an extremely schematic way, phase I is above all a hemostatic response, with the formation of a fibrin and fibronectin matrix, the role of which is to ensure the tightness of the joined ends of the intestine (anastomotic stumps). Next, phase II is characterized by the infiltration of the anastomotic site by inflammatory cells at the submucosal level with destruction of pre-existing collagen from proteinases (such as matrix metalloproteinases, MMP). From the third day, the provisional matrix is gradually converted into granulation tissue, containing neo-vessels, fibroblasts, and macrophages. Collagen synthesis reaches its peak around the 7th day. In order for this process to be carried out correctly, which in reality is very complex and requires a lot of energy resources, it is necessary that the anastomotic site be sufficiently well perfused.

## 2.3. Anastomotic complications

Alterations in the anastomotic healing process might lead to complications, such as stenosis (reduction in the digestive tract lumen) and/or leakages.

Any defect of the anastomosis integrity which allows communication between the endoluminal and the extraluminal compartment is called anastomotic leakage (AL). AL is an extremely severe complication in digestive surgery, with high morbidity and mortality rates [1]. It still presents a high incidence, particularly after esophageal (20-35% [33]) and colorectal resections (4-19% [2]).

A large number of risk factors involved with anastomotic leakages have been reported. They include poor nutritional status, immunosuppression, preoperative chemotherapy, consumption of tobacco, obesity, and a poor surgical technique [31, 34, 35].

Although a mechanical anastomosis shows very little inflammatory response when compared to the hand-sewn one [36], there is no evidence demonstrating the superiority of one technique over the other [37].

Certainly, an adequate local perfusion is a key factor to promote anastomotic healing [38]. It also contributes to reduce the risk of AL. Consequently, it is mandatory to assess the perfusion of the anastomotic limbs intraoperatively. However, clinical criteria alone are often unreliable to accurately evaluate bowel perfusion [3], and a device capable of intraoperatively assessing perfusion accurately, with minimal repercussion on the surgery workflow is highly desirable.

## 3. Techniques for the intraoperative evaluation of intestinal perfusion

The availability of a tool capable of objectively estimating the blood supply of the anastomotic limbs intraoperatively is of paramount importance in digestive surgery. A large number of techniques have been developed for this purpose [1]. However, most of them are only used for research purposes since they are either time-consuming, operator-dependent, or provide pinpoint results, impairing a real-time, objective intraoperative assessment.

In this respect, fluorescence angiography (FA) has been incrementally explored over the last few years, to assess perfusion during digestive surgical procedures. FA is a user-friendly intraoperative method to assess gastrointestinal perfusion and is relatively easy to integrate in the surgical workflow [11]. The equipment has a relatively low cost, and the results are accurate and obtained in real time. FA is an optical imaging technique, which requires a near-infrared (NIR) camera coupled with the intravenous injection of an exogenous fluorescent dye, typically indocyanine green (ICG). Applied to digestive resections, FA allows to visualize bowel perfusion by means of fluorescence enhancement, based on the rationale that the injected fluorophore is distributed solely to areas with preserved blood supply [4-6]. Several clinical trials have shown promising results with FA in both upper and lower GI surgery [7-10]. However, the studies are highly heterogeneous in terms of protocols and the evidence quality is globally low [11-13]. Additionally, in most cases, FA is performed without quantifying the fluorescent signal [14]. As a result, perfusion is assessed exclusively in a subjective manner. Two main factors affect the performances of FA and should be taken into consideration. The first one is the progressive ICG diffusion over time through the serosal capillary network into the margins of the ischemic zones, leading to an overestimation of the vascularized area. The second one is the quadratic inverse relationship between the target-endoscope distance and fluorescence intensity [15, 16]. When distance is not controlled and/or fluorescence intensity is not normalized with a calibration system, the presence of a fluorescent signal in the tissue is not representative of the actual perfusion. To overcome those interpretation

biases, a software-based quantitative FA has been introduced, based on the analysis of fluorescent signal dynamics [15-17]. Fluorescence-based Enhanced Reality (FLER) is a software solution which computes the time-to-peak (TTP) fluorescent signal pixel-by-pixel during FA. TTP is converted into a quantitative perfusion cartography, generated by analyzing the velocity of the fluorescence signal until reaching its maximal intensity peak. The perfusion cartography is a color-coded image, which can be used as a last image hold function and overlaid onto the real-time laparoscopic video. The accuracy of the quantification software has been confirmed experimentally by our research group in the past [15]. However, the routine use of FA in the daily clinical practice is limited by the need to inject ICG, which is still off-label for this specific indication and can occasionally be associated with severe adverse events [39, 40].

For this reason, another optical imaging technology, hyperspectral imaging (HSI) has been explored by our group to assess perfusion in the gastrointestinal tract. HSI, which has been used since decades in the industrial sector or for remote sensing [18] is a promising optical imaging technique coupling a spectroscope with a photo-camera and allowing for a contrast-free, real-time, and quantitative tissue analysis. Tissue-light interactions (absorption, reflectance) at the analyzed surface depend on intrinsic biochemical properties. HSI acquires bidimensional spatial images across the electromagnetic spectrum, consequently providing a tridimensional dataset called hypercube (x, y as spatial coordinates, and $\lambda$ as the spectral coordinate). HSI has been recently used for medical purposes [18], including tissue perfusion. Akbari et al. [19], in a proof-of-concept experimental study, first identified the optimal wavelength (765-830nm) in order to detect bowel ischemia, using an HSI prototype with a broad wavelength range (400 to 1700nm), in the porcine model.

Recently, HSI was successfully used in medical and surgical applications, including tumor identification [18], intraoperative parathyroid recognition [41], and real-time quantitative perfusion assessment during open digestive surgical procedures [23, 42].

Compared to fluorescence imaging, HSI gives a larger amount of information and quantifies several tissue components, including water, oxygen, and hemoglobin content. Additionally, a remarkable

advantage when compared to FA is that HSI does not require the use of any contrast agents. In other words, HSI is an optical, contrast-free, and non-destructive *in vivo* "biopsy" of the surgical field, allowing one to virtually discriminate anatomical structures and characterize tissue physiology. However, the large HIS-generated datasets (hypercubes) require complex data processing algorithms in order to extrapolate useful discriminative features from the spectral curves.

In the following chapter, a state-of-the-art on hyperspectral imaging in the medical field is briefly presented, with a special attention to clinical applications in digestive surgery, in which the IRCAD-IHU of Strasbourg specializes and in particular visceral perfusion, which is the main subject of this thesis.

# 4. Hyperspectral imaging

## 4.1. Introduction and basic principles

Hyperspectral imaging (HSI), also called imaging spectrometer, originated from the remote sensing of the earth surface [43] and has been explored for various applications by NASA. Given the capacity to acquire two-dimensional images across a wide range of the electromagnetic spectrum **(Figure 3)**, HSI can show the invisible, ranging beyond the borders of the visible light and extending the information to the ultraviolet (UV) and near-infrared (NIR) frequencies. It has been applied to numerous areas, including vegetation and water resource control [44, 45], archeology and art conservation [46, 47], food industry and safety control [48, 49], forensic medicine [50, 51], crime scene detection [52, 53], and biomedicine [18, 20, 54].

HSI is a hybrid modality combining conventional imaging and spectroscopy. Most traditional optical imaging methods can only capture gray or color images. The regions of interest in these kinds of images are exclusively analyzed by their spatial properties (size, shape, and texture). It has been widely recognized that monochrome and RGB color imaging methods have limitations in detecting early tissue abnormalities [55]. The quality of diagnostic information obtained is poor, since in most cases the metabolic or biochemical alterations occurred during the progress of the disease do not alter the chromatic characteristics of pathological tissues consistently. The probe-based spectroscopic diagnostic technology can also obtain an entire spectrum of a single tissue site within a wavelength region of interest. The drawback of this method is represented by the fact that it provides point measurements of each area of interest without spatial information. The main advantage of HSI is that combining imaging and spectroscopy, it can acquire reflectance, absorption, or fluorescence spectrum pixel-by-pixel in the image, which can be used to detect the chemical composition changes of objects which cannot be identified with traditional imaging or spectroscopy methods alone [56].

HSI allows to obtain a contact-free and non-destructive quantitative and qualitative analysis of the living tissue. Light delivered to biological tissue undergoes multiple scattering derived from the inhomogeneity of biological structures and absorption of natural chromophores (hemoglobin, melanin, and water) as it propagates within the tissue. According to the electromagnetic theory, different biochemical constituents have different spectral signatures [57]. These signatures are usually generated by the interactions between tissue and light radiation, such as electron transition, atomic and molecular vibration or rotation. The biological and pathological changes in tissues and organs also have a close relationship with the spectra. Spectral characteristics in different wavelength regions yield specific spectral features, making pathological changes distinguishable. As a result, the reflected, fluorescent, and transmitted light from tissue captured with HSI carries quantitative diagnostic information about tissue pathology. Additionally, HSI holds the potential to discriminate different anatomical structures from one another, since every tissue generates specific spectral patterns from its interaction with the light.

This technology opens new perspectives in the medical field, allowing researchers to identify and quantify the relationships among tissue components at molecular level, observe living organisms non-invasively, enhance histopathological analyses, thereby globally augmenting the biological understanding of diseases.

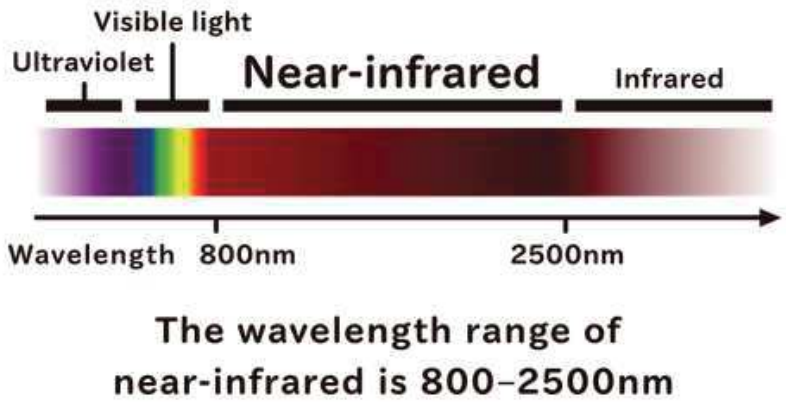


**Fig. 3:** Schematic representation of the electromagnetic spectrum. HSI systems can typically acquire images across a wide range of the electromagnetic spectrum, beyond the visible light.

## 4.2. The hypercube

By collecting spectral information at each pixel of a two-dimensional (2-D) detector array, HSI generates a three-dimensional (3-D) dataset in which x and y are spatial coordinates and λ is the spectral coordinate, known as hypercube **(Figure 4)**. Thanks to the spatial information, the source of each spectrum on samples can be located, which gives a high diagnostic value to this technology.

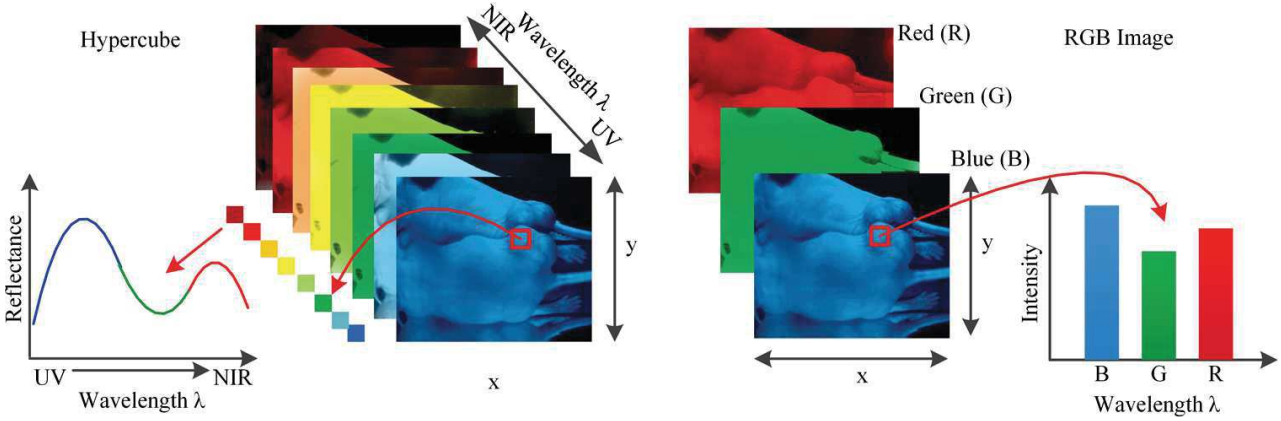


**Fig. 4:** Comparison between hypercube and RGB image. Hypercube is a 3D dataset of a two-dimensional image on each wavelength. The lower left is the reflectance curve (spectral signature) of a pixel in the image. The RGB color image only has three image bands on red (R), green (G), and blue (B) wavelengths respectively. The lower right is the intensity curve of a pixel in the RGB image (from Lu and Fei: Medical hyperspectral imaging: a review).

The spectral signature of each pixel in the images allows HSI to identify various pathological conditions. HSI generally covers a contiguous portion of the light spectrum with more spectral bands (up to a few hundreds) and higher spectral resolution than multispectral imaging (MSI). Consequently, HSI has the potential to capture the minimal differences in the spectrum under different non-physiological conditions while multispectral imaging may miss significant spectral information. The main differences between optical imaging, spectroscopy, multispectral and hyperspectral imaging are shown in **Table 1**.

| Feature | 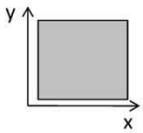 | 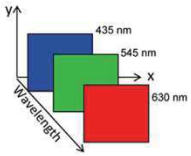 | 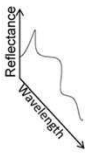 | 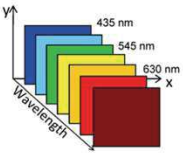 | 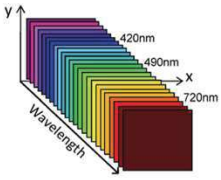 |
|---|---|---|---|---|---|
| | Monochrome | RGB | Spectroscopy | Multispectral | Hyperspectral |
| Spatial information | Yes | Yes | No | Yes | Yes |
| Band numbers | 1 | 3 | From several dozens to hundreds | 3 to 10 | From several dozens to hundreds |
| Spectral information | No | No | Yes | Limited | Yes |
| Multiconstituent information | No | Limited | Yes | Limited | Yes |
| Sensitivity to minor components | No | No | No | Limited | Yes |

**Table 1:** Main differences between monochrome, RGB, spectroscopy, multispectral imaging and hyperspectral imaging *(Li Q et al. Review of spectral imaging technology in biomedical engineering: achievements and challenges).*

## 4.3. Imaging systems

HSI acquisition systems represent a challenge to engineers, who have to handle sophisticated optical and electronic systems to generate a hypercube. There are several types of HSI cameras, and although a number of HSI cameras are commercially available, most devices used in the experimental procedures reported in the literature are prototypes. However, depending on how data are acquired, there are two main large categories of HSI devices, namely spatial scanning cameras and spectral scanning cameras.

***Spatial scanning* cameras:** Based on the push-broom technique, they are capable of simultaneously acquiring a single spatial dimension (a narrow portion of an image) and the entire spectral information for a given scene. To capture a hypercube in this way, it is necessary to perform a spatial scanning, where either the camera or the captured object(s) move their position while the camera is acquiring frames. The scanning can also be performed by using a mirror in front of the optic and moving the mirror to image the whole object. Although the use of mirrors allows to develop more compact devices (more appealing for the clinical use), it is necessary to consider the geometric distortions that mirrors can generate. The core of these cameras is an optical element which splits the incoming radiation into specific wavelengths values [58]. The advantage of this type of camera is that it captures images with high spectral resolution, also offering an excellent compromise between spatial and spectral resolution. Thanks to their acceptable spatial resolution, these types of cameras have been described for various applications in the medical field. Nevertheless, given the complex image acquisition methodology through a scanner, it is technically demanding to attach those cameras to medical instrumentation, such as a laparoscope or a microscope. Additionally, real-time imaging is currently not available with this type of devices.

**Spectral scanning cameras:** They use an optical element which filters the incoming radiation, registering the entire spatial information of a single wavelength at each moment. Hypercube

acquisition requires a change in the wavelength of the filter in order to perform spectral scanning. There are several types of spectral scanning cameras:

- Filter wheel cameras: which require the manual shift of the optical filter,
- Liquid Crystal Tunable Filter (LCTF) or Acousto-Optic Tunable Filter (AOTF) are devices where spectral transmission can be electronically controlled.

These cameras provide lower spectral resolution than the push-broom cameras and are not suitable for applications where the captured object is moving, because spatial information may vary in the different wavelengths. Nevertheless, these HSI systems can be easily attached to medical instruments and can offer high spatial resolutions. Additionally, also for this camera system, a real-time imaging is currently not available.

**Snapshot cameras:** This technology is intended to deal with the main limitation imposed by the previously described HSI technologies, namely real-time acquisition. It is not possible to collect hypercube in real time using the abovementioned technologies, since a scan (either spatial or spectral) is necessary. These technologies are restricted to static situations, or scenarios where the object that is moving has a slightly lower speed as compared to the scan speed. For these reasons, where it is necessary to obtain spectral information of non-static scenes (e.g. living cell imaging) a snapshot camera represents the best choice. Additionally, snapshot cameras can theoretically be directly attached to clinical instrumentation, such as endoscopes or laparoscopes. However, both the spectral and the spatial resolution of snapshot cameras are lower as compared to both abovementioned technologies. Given their low spatial and spectral resolution, snapshot cameras are rarely used in experimental or clinical surgical scenarios, in which a high spatial localization is essential.

## 4.4. Spectral range and resolution

- **Spectral range** refers to the wavelength regions covered by HSI systems. Most systems can cover ultraviolet (UV), visible (VIS), near-infrared (NIR), and mid-infrared (mid-IR) spectral ranges **(Table 2)**. The most widely used spectral range in the literature falls in VIS and NIR regions. While visible light penetrates only 1 to 2mm below the skin, hence providing superficial information, light in the NIR region penetrates deeper into the tissue than VIS or mid-IR radiation.·NIR light is ideal for surgical guidance due to its deep penetration into the tissue, which can help the surgeon visualize critical anatomical structures of interest which are not visible with the naked eye. By expanding the eyesight beyond the visual spectrum, additional information can be obtained to further characterize structures of interest.

- **Spectral resolution** of an HSI system refers to the capability of separating two adjacent spectral features emitted by a point in the image [59]. Spectral resolution measures the narrowest spectral feature which can be resolved with an HSI system. High spectral resolution allows accurate reconstruction of the spectral profile of a given object. Another important parameter of an HSI system is spectral bandwidth, which is defined as the full width at half maximum. HSI systems with a higher spectral resolution and a narrower bandwidth potentially provide a more accurate spectral signature of the sample.

| Abbreviation | Full name | Spectral range (nm) |
|---|---|---|
| UV | Ultraviolet | 200-400 |
| VIS | Visible | 400-780 |
| NIR/near-IR | Near-infrared | 780-2500 |
| MIR/mid-IR | Mid-infrared | 2500-25,000 |

**Table 2:** Spectral range of the different wavelengths. The most common HSI cameras range from UV to NIR wavelengths.

## 4.5. Data analysis

Image analysis is of paramount importance in order to diagnostically extract useful information from a large hyperspectral dataset at the tissue and cellular levels. It is therefore critical for disease screening and diagnosis. The hypercube with high spatial and spectral resolution may potentially contain more diagnostic information. However, high spatial and spectral dimensions generate large datasets, which complicate the automatic analysis of hyperspectral data. In particular, the complexity is given by the high data redundancy and the variability of hyperspectral signatures. With a large number of spatial and spectral information available, advanced image classification methods for hyperspectral datasets are required to extract, unmix, and classify relevant information. Although hyperspectral image analysis methods have been intensively investigated in the remote sensing field, their development and application in medical disciplines remain at a preliminary stage. The relationships between spectral features and underlying biomedical mechanisms are not well understood. The basic steps for hyperspectral image analysis generally involve preprocessing, feature extraction and feature selection, and classification or unmixing. Hyperspectral data extraction is rather complex since it uses advanced “big data” algorithms such as support vector machine (SVM) or convolutional neural networks (CNN). The detailed description of those steps is fairly technical and goes beyond the purposes of a thesis in medical science.

## 4.6. Medical applications

### 4.6.1. *In vivo* cancer detection

Ferris et al. [60] performed a clinical study in a population of women in order to screen cervical malignancies using a HSI system covering the UV and VIS regions, and measured tissue fluorescence and reflectance of the cervical epithelium. This system had a multichannel spectrograph capable of hyperspectral resolution of ~5nm and spatial resolution of the ectocervix of ~1mm. They showed that the system could discriminate high-grade cervical lesions from less severe lesions and normal cervical tissue. In addition, the device could detect cervical cancer precursors with a greater accuracy than a simultaneously collected Pap smear.

Later, a multispectral digital colposcope (MDC) was built by Benavides et al. [61]. It was concluded that a MDC could provide significant diagnostic information to discriminate between cervical intraepithelial neoplasia lesions and normal cervical tissues, and that excitation wavelengths across the spectral range of 330 to 360nm and 440 to 470nm appeared important in cervical cancer diagnosis.

Hattery et al. [62] built a six-band multispectral NIR imaging prototype to identify thermal signatures of blood volume in patients with Kaposi's sarcoma, a skin cancer affecting prevalently immunosuppressed individuals. Results showed that relative spatial tissue blood volume and blood oxygen saturation values could be used as indicators of tumor angiogenesis and tumor metabolism.

Roblyer et al. [63] reported the use of a multispectral-enhanced microscope for the detection of oral neoplasia in a pilot clinical trial. They observed decreased blue/green autofluorescence and increased red autofluorescence in the lesions and increased visibility of vasculature overall.

Another research group analyzed malignant colorectal tumors, adenomatous polyps, and different types of normal mucosa [64]. They built a flexible endoscopic HSI system and performed *in vivo* analysis of the colonic mucosa in several patients. The system was capable of capturing HSI images in the wavelength range from 405 to 665nm, acquiring 27 spectral bands using a tunable filter

wheel. A total of 21 HSI cubes from 12 different patients were acquired. The HSI endoscopic device was capable of identifying colorectal tumors in real time with an average accuracy of 92.9±5.4%. In addition, through HSI the authors were able to enhance the visualization of the microvascular network on the mucosal surface.

Another group focused on the *in vivo* identification of gastric malignant ulcers using HSI [65] using a customized multispectral video endoscopy system capable of capturing a multispectral video composed of bands located in the visual spectral range. These research works suggest that HSI and MSI can be used as guidance tools both for diagnosing and outlining gastric tumor margins accurately.

In an experimental rat breast cancer model, Panasyuk et al. [64] successfully detected residual small tumors (0.5 to 1.0mm) with HSI, that were intentionally left in the operative bed **(Figure 5)**. The rat breast tumors were exposed and imaged via HSI, then intentionally incompletely removed, and then imaged again with HSI. They could identify and differentiate tumors, blood vessels, and muscle according to their spectral characteristics. The authors reported a sensitivity of 89% and a specificity of 94% for the detection of residual tumors, which is comparable to that of histopathological examination.

With the aid of HSI, more extensive neoplasia resection and more effective biopsy locations may be achieved. This technology is totally in line with the principles of precision surgery, since the complete resection of a neoplasia and the conservation of normal tissue may improve surgical results and lead to tailored, tissue-sparing procedures, hence preserving organ function and improving quality of life.

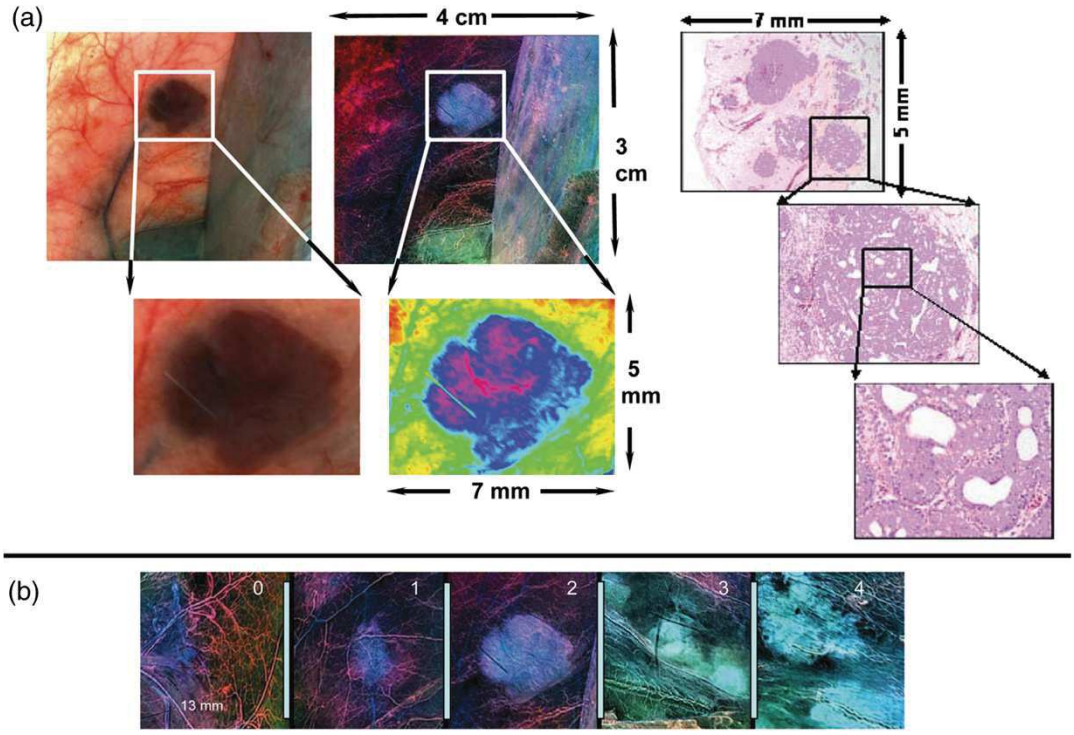


**Fig. 5:** (a) Photomicroscopic and corresponding hyperspectral image from breast tumor in situ (4 × 3cm) (upper left and upper middle panels). Resected tumor and surrounding tissue (5 × 7mm) stained with hematoxylin and eosin and evaluated via histopathology after resection. Microscopic histological images with further resolution are displayed (right panels). (b) Representative examples of normal tissue (grade 0), benign tumor (grade 1), intraductal carcinomas (grade 2), papillary and cribriform carcinoma (grade 3), and carcinoma with invasion (grade 4) are displayed (from *Panasyuk et al. Medical hyperspectral imaging to facilitate residual tumor identification during surgery*).

### 4.6.2. Limbs perfusion and peripheral arterial disease

Zuzak et al. [66, 67] measured the changes in the spatial distribution of regional tissue oxygenation during vascular occlusion and reperfusion in healthy individuals. In this manner, the authors were able to non-invasively differentiate between normal and ischemic tissue. In a clinical study [68], the same group used a visible reflectance HSI system to examine a model of vascular dysfunction involving both ischemia and reactive hyperemia during tissue perfusion. The system could detect oxyhemoglobin and deoxyhemoglobin signals from spectral images in the 525- to 645-nm region. Peripheral arterial disease (PAD) involves the progressive atherosclerotic narrowing of the arterial vessels mainly in the lower extremity, which may lead to rest pain, ulceration, and amputation. Effective diagnostic and prognostic technologies are necessary for an earlier detection and treatment. However, traditional methods, such as ankle-brachial index, Doppler, segmental limb pressure, etc., do not provide a high specificity and sensitivity for the prediction of the healing of tissue loss in PAD patients. HSI has the capability to measure oxyhemoglobin and deoxyhemoglobin concentrations to create an oxygenation map in a non-invasive fashion. Chin et al. [69] scanned patients with and without PAD with a HSI system and acquired the concentration of oxyhemoglobin and deoxyhomoglobin **(see Figure 6)**. The results showed that HSI might be useful in detecting differences in oxygenation levels in the lower extremities of patients with and without PAD. Their data also suggested that HSI may become a useful tool for the diagnosis and follow-up of patients with PAD.

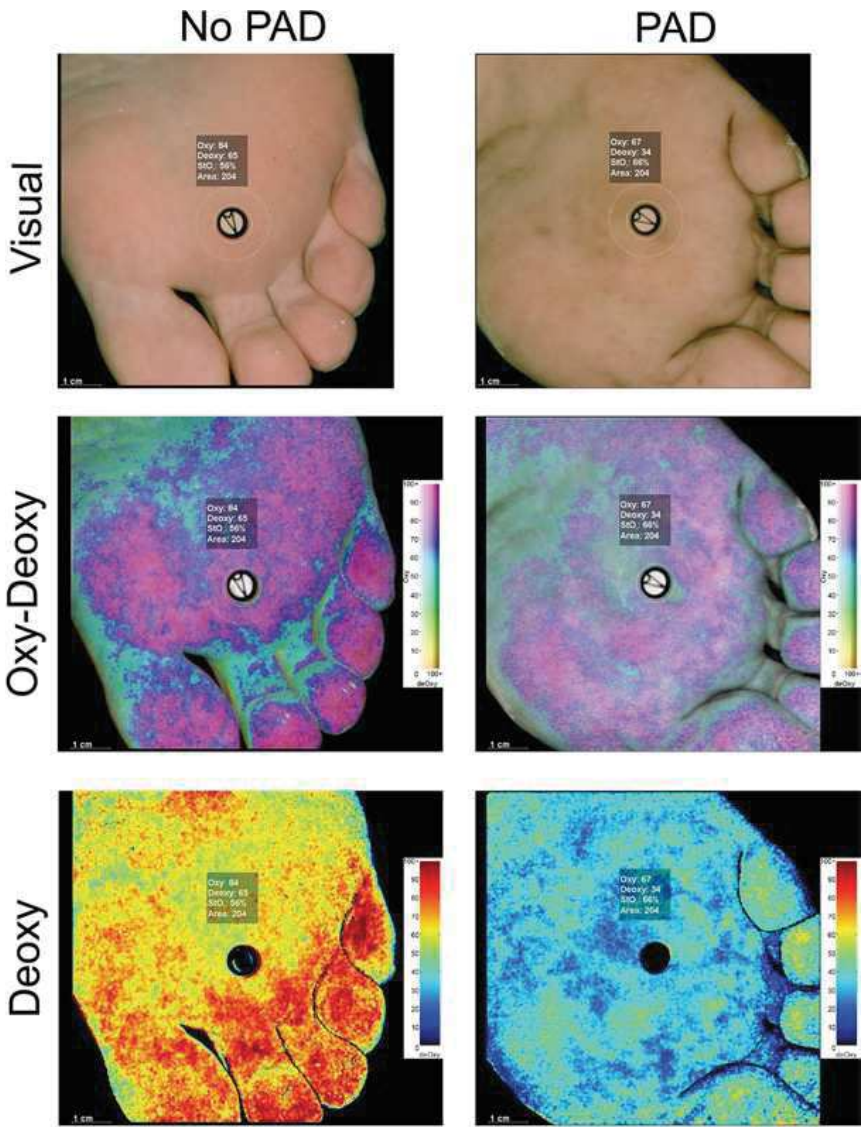


**Figure 6:** Visual, integrated oxyhemoglobin-deoxyhemoglobin, and deoxyhemoglobin hyperspectral images are shown of the plantar metatarsal angiosome for **(left)** a foot with no peripheral arterial disease (*PAD*) and **(right)** a foot with PAD. The foot with PAD has substantially decreased oxyhemoglobin and deoxyhemoglobin values throughout the angiosome (from *Chin et al. Evaluation of hyperspectral technology to assess the presence and severity of peripheral artery disease)*.

### 4.6.3. Gastrointestinal surgery

Zuzak et al. built a laparoscopic HSI system based on a tunable filter [70]. They used this system in order to explore the structures within the hepatoduodenal ligament in a contactless way. They found that the wavelength of 930nm, at which lipids are normally absorbed could be used as an optical biomarker to visualize the lipid-containing bile ducts. Although their system had a poor spatial resolution, a long acquisition time, and was incapable of a video rate, the authors successfully identified the biliary duct using this miniaturized HSI prototype.

Biliary duct injuries during cholecystectomy are relatively rare. However, they represent an extremely feared complication with terrible consequences for patients. As a result, the availability of a system allowing for a real-time and contrast-free identification of key structures intraoperatively might have a great impact in the clinical practice.

In a further study, the same authors [71] modified the previous system by widening its spectral range into the NIR wavelength. With this device, they were able to identify all the structures of the hepatoduodenal ligament prior to dissection. Again, they confirmed that the common bile duct reflected spectra at the lipid shoulder at 930nm and a strong water peak at 970nm. The venous structures showed absorption peaks at 760nm (deoxyhemoglobin), 800nm (oxyhemoglobin), and 970nm (water) whereas arterial vessels had absorption peaks at 800 and 970nm, which would be expected for oxyhemoglobin and water. Therefore, they demonstrated the capability of HSI in discriminating biliary duct, arterial and venous vessels intraoperatively without dissecting the surrounding connective tissue **(Figure 7)**. Due to the difficult operability of the device, given mainly by the low spatial resolution and the long acquisition time, this remarkable miniaturization effort that the authors developed failed to translate into the clinical setting.

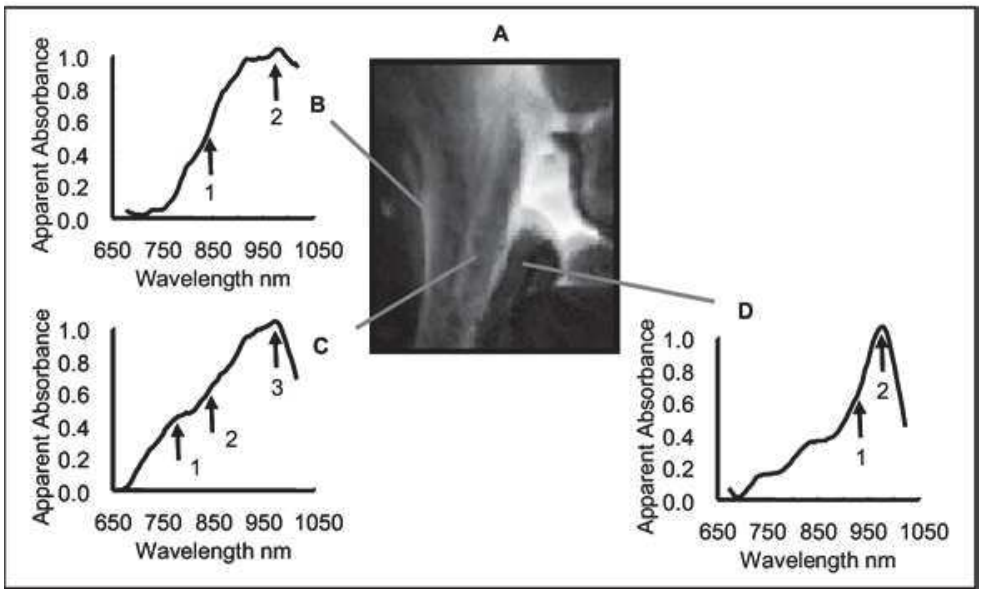


**Fig. 7.** NIR laparoscopic hyperspectral image of the hepatoduodenal ligament. (A) During a laparoscopic procedure in live anesthetized pigs, the artery, vein, and the anteriorly placed common bile duct were identified through connective tissue by measuring NIR spectra. (B) An artery indicated with spectra has a very pronounced broad oxyhemoglobin peak around 800nm (arrow 1) and a small water peak at 970nm (arrow 2). (C) A venous structure produces spectra with a deoxyhemoglobin shoulder at 760nm (arrow 1), a broad oxyhemoglobin peak around 800nm (arrow 2), and a small water peak at 970nm (arrow 3). (D) The common bile duct is identified using spectra containing a lipid shoulder at 930nm (arrow 1) and a prominent water peak at 970nm (from: *K.J. Zuzak et al. Intraoperative bile duct visualization using near-infrared hyperspectral video imaging).*

### *4.6.3.1. Intestinal ischemia*

Intestinal (or mesenteric) ischemia occurs when the blood supply to the bowel is not sufficient to meet the energetic requirements of the organ. This condition in the acute situation is related to a high mortality rate. Additionally, the visual perception of the surgeon alone is often not enough to accurately delineate the extent of the ischemic bowel. Patients must often undergo reiterated bowel resections, which increase morbidity and mortality. Akbari et al. [72] created a prototype push-broom HSI system composed of two cameras and capable of analyzing the spectrum from 400 to 1700nm. In a single pig model, they created an ischemic bowel segment and could identify the extent of the ischemic area using HSI. Additionally, they observed a characteristic peak in the wavelength of the ischemic segment at 765 to 830nm. In their remarkable work, the authors demonstrated that it is possible to identify ischemic bowel loops using HSI. Nevertheless, the

system that they used was outsized, and subsequently unsuitable for daily surgical use and did not allow for a quantitative analysis of ischemia.

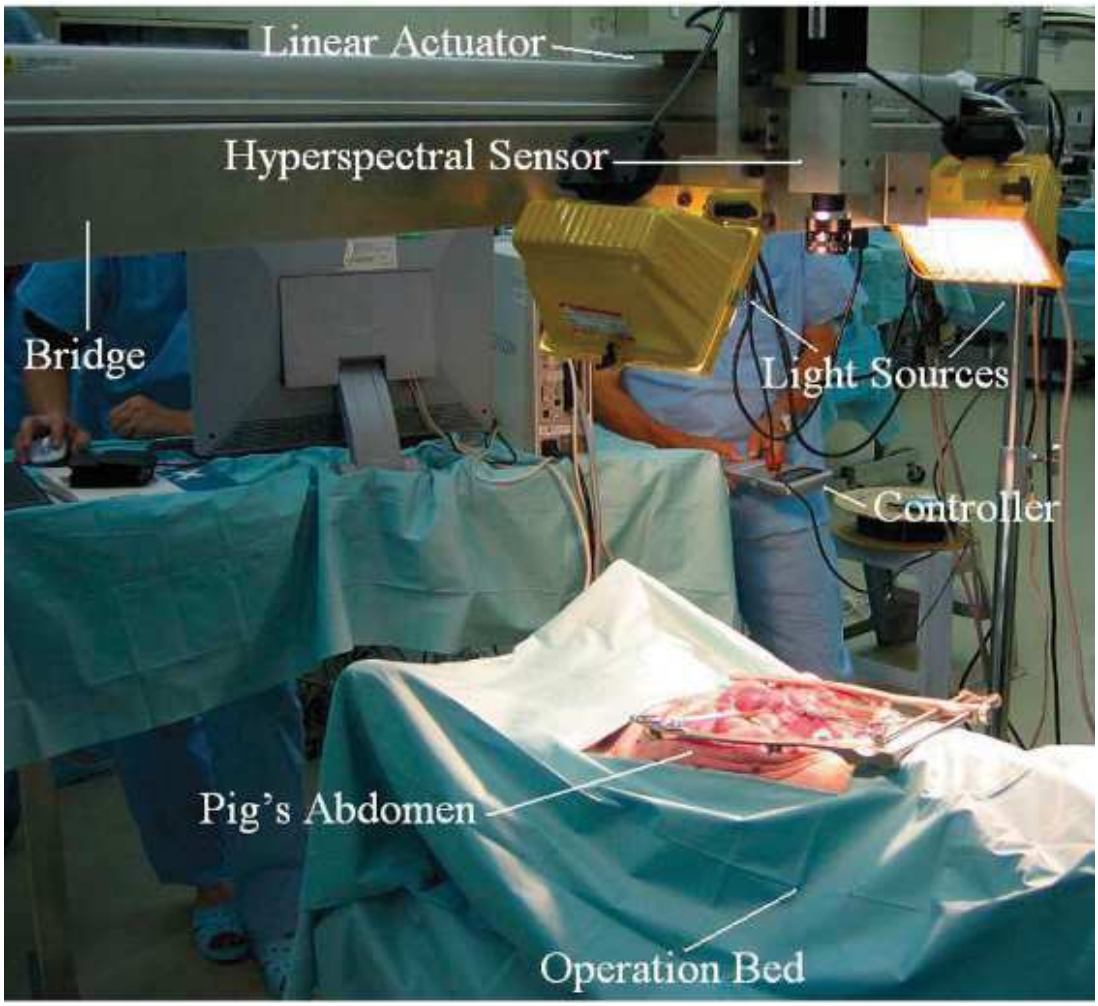


**Fig. 8.** Experimental setting for the detection of bowel ischemia. The authors used a bulky HSI system composed of 2 cameras in order to analyze the spectrum in a wide range (400-1700nm). *(From: Akbari et al. Detection and analysis of intestinal ischemia using visible and invisible hyperspectral imaging).*

# 5. Fluorescence-guided surgery: state-of-the-art

## 5.1. Basic principles

The term fluorescence-guided surgery refers to a real-time medical imaging technique designed to guide the surgeon through the surgical procedure [73], using the optical phenomenon. In a simplified way, fluorescence is characterized by a light emission from a molecule (i.e. the fluorophore) after being excited by the absorption of a photon of energy. In other words, the fluorophore (fluorescent contrast agent) absorbs light energy (excitation) and passes into an electronically excited state. The fluorophore then passes to the initial state by the emission of a photon. This light emission after excitation can be of the same wavelength as the excitation, smaller or larger. The magnitude of the displacement of the emission signal in the spectrum is correlated with the fluorescence detection capacity. Although the phenomenon concerns the entire electromagnetic spectrum, for FIGS we refer to fluorescence in the visible spectrum (optical spectrum) in near-infrared wavelengths. The basic FIGS scheme includes the use of (Figure 3):

1) A fluorescent contrast agent, administered to the patient

2) A laser light source

3) A camera with a filter

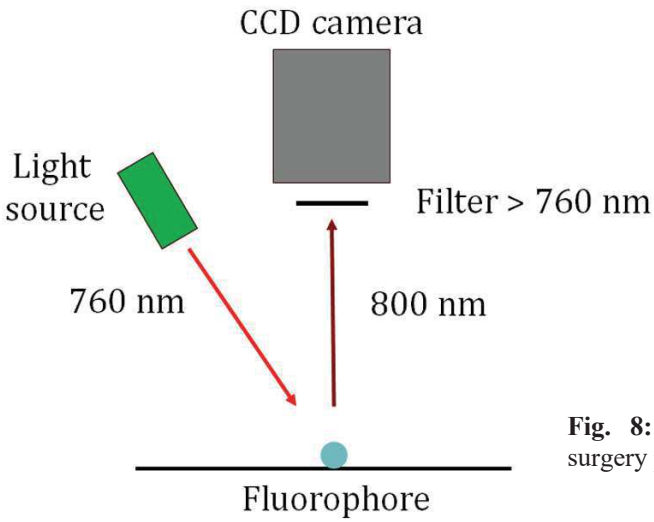


**Fig. 8:** Basic representation of the fluorescence-guided surgery principle

Fluorescence of the fluorophore allows to identify anatomical structures invisible to the naked eye, or even metabolic processes, such as organ perfusion.

The fluorescent signal can be viewed directly in the surgical field, in the case of open surgery, or it can be captured using a specific camera and displayed on a screen, during minimally invasive procedures.

At present, fluorescence-guided surgery is the most used navigation system intraoperatively, since it presents a certain number of advantages [74]:

1) visual information is provided in real time,

2) imaging devices have a reduced size,

3) the surgical workflow is respected,

4) costs are reduced.

## 5.2. Fluorophores

There is a wide variety of fluorophores, already available or in development, which can be characterized by excitation and emission spectra and can be broadly classified into non-targeted and targeted ones. In the current practice, non-targeted fluorophores are the most common ones. Only a

limited number of clinical studies have been conducted using targeted agents. Below is a list of the most important fluorophores.

In general, the choice of fluorophore should take into account the following factors:

1) dosage,

2) time between administration and visualization,

3) pharmacodynamics, and

4) route of administration (systemic vs. local).

### 5.2.1. Non-targeted agents

**Indocyanine green (IndoCyanine Green = ICG):** is the most commonly used non-targeted fluorophore. ICG has been used since the 1950s and is approved for:

1) liver function measurement,

2) heart function measurement, and

3) eye angiography.

In France, the use of ICG for imaging is still considered outside the scope of the 27 AMM ("autorisations de mise sur le marché") regulatory functions in 2016. Consequently, it is to be considered "OFF-LABEL". The emission wavelength of the ICG is 820nm [75]. It is a very safe molecule, with a risk of side effects corresponding to about 1/60,000 injections, and reactions are rarely severe [76]. The pharmacodynamic properties of ICG are well-known (http://www.drugs.com/pro/indocyanine-green.html): ICG is extracted from the bloodstream by the liver through an energy-dependent mechanism mainly, but not exclusively, by the OATP (organic anion-transporting polypeptide) B1 and B3 carriers and is very rapidly excreted in the bile via the Multidrug Resistance-associated Proteins MDR3, MRP3 and MRP2 carriers, without excretion in the urine.

**Methylene blue (MB):** MB has fluorescence properties much lower than ICG, expressing a lower quantum efficiency (ratio between the number of photoelectrons released in the internal photoelectric effect and the number of incident photons). The emission length of the MB is 680nm. MB is partially excreted in the urine, and for this reason, it may be useful in visualizing ureters [77].

**Fluorescein sodium (SF):** FDA-approved for ophthalmological applications (angiography and angioscopy of the retina and iris), it is used in research as a fluorescent contrast agent in multiple applications [78]. SF is the essential fluorophore for obtaining images with confocal laser endomicroscopy (CLE). Its emission length is 520nm.

**5-Aminolevulinic Acid (5-ALA):** This is a bioactive fluorophore, i. e. an *in vivo* enzymatic reaction makes the substrate fluorescent. 5-ALA is mainly used for fluorescence-guided surgery in neurosurgery, particularly in guided ablation of malignant gliomas. In addition, 5-ALA has been successfully used in the detection of bladder cancer (90%) [79], and most recently in the detection of colon and rectal cancers [80]. The mechanism of selective accumulation in tumors is not known. Its emission length is 635nm.

## 5.2.2. Targeted agents

Target agents are constructed in such a way that they can be conjugated to specific sites (ligands) allowing the clear visualization of a target tissue/structure, where such ligand is hyper-expressed. The targeted agents currently developed aim to visualize cancer cells to make it possible:

1) to detect the tumor at a very early stage, and

2) to verify that the tumor has been completely resected.

Nanoparticles can offer a valuable opportunity in the development of targeted agents, thanks to the modularity of their composition. However, there is a significant regulatory barrier to this type of

approach, considering the extremely long times to obtain authorization for the clinical translation of these agents [81].

**Currently available devices for fluorescence-guided surgery**

Fluorescence optical imaging takes advantage of the deep penetration of light photons into the tissues in the near infrared spectrum. This provides a fast and relatively inexpensive imaging of endogenous and/or exogenous contrast agents which emit fluorescence between 700 and 900nm. The penetration limit with current technologies is limited to about 1cm [82]. The typical fluorescence imaging system has been described in detail in various publications [83, 84]. In summary, it consists of a light source (broadband filtered source, light-emitting diode (LED), or laser diode), which excites a fluorophore. The light emitted by this fluorophore is then captured with a charge-coupled camera (CCD), with a filter to narrow the excitation light. The various design parameters of the device (field of view, light source, wavelength, etc.) will all have an impact on performance and, in particular, on the signal-to-noise ratio [73]. For instance, an adjustable field of view is the fundamental prerequisite for effective surgical navigation and can be achieved by using zoom or fixed magnification lenses. In general, the field of view should be at least 10cm and preferably 20cm in diameter for most surgical procedures. It should be noted that the power of the light source must be progressively higher as the size of the field of view widens. In addition, magnification to achieve a minimum field of view reduces the final resolution, if the CCD camera has a finite number of 31 pixels. The different technologies which can excite fluorophores in the near-infrared include the following:

1) broadband filtered sources,

2) LEDs, and

3) laser diodes [73].

An increasing number of companies or academic research groups are now developing systems for fluorescence-guided surgery. The different systems differ in several characteristics, including:

1) the type of excitation source (laser, LED),

2) the signal detection system,

3) the wavelength of exercise,

4) the optimal working distance,

5) the possibility of superimposing white light images onto infrared fluorescence imaging, in order to obtain a kind of augmented reality.

## 5.3. Common clinical applications of fluorescence-guided surgery

To date, the most common clinical applications in digestive surgery are as follows:

1) intraoperative cholangiography during cholecystectomy,

2) intraoperative navigation to identify the sentinel node,

3) real-time evaluation of organ perfusion.

The targeted detection of tumor tissue is still at a practically experimental stage, with very few clinical cases performed with this technique worldwide to date. However, real-time identification of cancer cells through fluorescent contrast agents targeting tumor expressed antigens is surely the most revolutionary application of FIGS.

### 5.3.1. Intraoperative cholangiography using fluorescence imaging

Intraoperative cholangiography reduces the risk of biliary tract injuries during cholecystectomy. Indeed, the rate of iatrogenic lesions of the biliary tract is about 0.15-0.6% [85].

As cholecystectomy is one of the most commonly performed surgical procedures, with about 700,000 procedures per year in the United States and about 50,000 in France, it is easy to calculate that despite their low incidence, biliary duct injuries represent a major public health problem. The

most frequent etiology of these injuries is a misinterpretation of the anatomy due to anatomical variants or a significant inflammatory state [86], because in the presence of cholecystitis their rate increases 20 times. Intraoperative X-ray cholangiography [87, 88] is a frequently used and highly effective technique to localize bile ducts and/or assess the presence of lesions. However, this technique presents several limitations:

1) it is a relatively long procedure, during which the cystic duct is catheterized to inject radiopaque contrast into the bile duct,
2) it is necessary to mobilize additional human resources,
3) the patient and team are exposed to ionizing radiation,
4) the radiological image obtained is 2D and cannot be superimposed on the surgical field.

To date, fluorescence cholangiography through the injection of indocyanine green has been evaluated in a significant number of clinical trials and has proven to be an effective and safe means of visualizing biliary anatomy [89-91], with promising results as shown by a systematic review of the recently published literature [92].

One of the most important disadvantages of fluorescence cholangiography after systemic injection of indocyanine green is related to a strong liver uptake, and this gives a very intense background signal due to intrahepatic ICG accumulation. This accumulation can sometimes interfere with the optimal visualization of the cystic duct.

In order to reduce the background noise of strong fluorescence from the liver, it is possible to inject the ICG 24 hours before the operation, as demonstrated by Verbeek [93]. Indeed, this interval allows for the evacuation of ICG from the liver, while a sufficient quantity of ICG will still be present in the biliary tree, which will then be the only illuminated structure. However, such an interval poses economic and logistical problems, as it requires patient hospitalization in advance to administer the contrast medium. An appropriate compromise would probably be to inject the

contrast medium between 6 and 10 hours before the procedure in case of scheduled surgery. However, this attitude could not apply to emergencies (cholecystitis), which are precisely the cases where fluorescence guidance is the most appropriate. In these situations, we proposed to administer ICG locally, directly into the gallbladder. This cholecystocholangiography technique has shown significant promising results in the experimental model, with very clear images of the bile ducts [94].

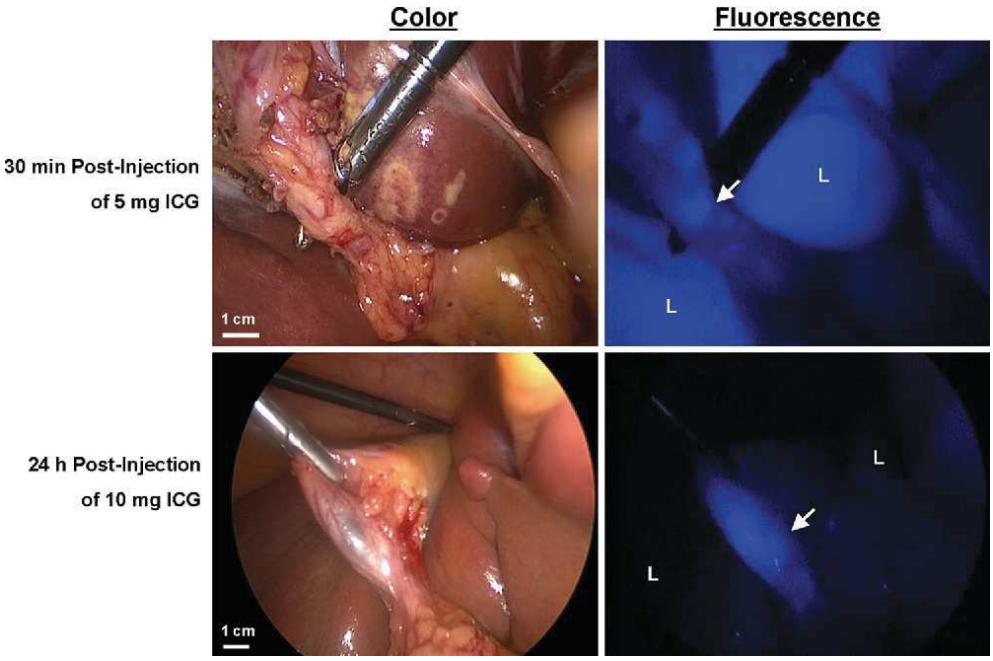


**Fig. 9:** Color and fluorescence images after ICG injection at different timepoints. The liver signal interference in the images taken 30 min after ICG injection is much higher than in the ones taken after 24 hours *(Verbeek FP et al. Optimization of near-infrared fluorescence cholangiography for open and laparoscopic surgery)*.

### 5.3.2. Sentinel node detection

The sentinel node (SLN) is the first lymph node to receive lymphatic drainage from a tumor. A sentinel node without metastases also suggests that there is no metastasis in the downstream nodes. The identification and analysis of SLN is of crucial importance in surgical decision-making, especially in minimally invasive procedures with organ preservation [95]. The detection of SLN

using fluorescence imaging, after peritumoral injection of ICG, is a relatively recent technique, already applied in a variety of tumors, especially breast and melanoma [73]. This is a well-established procedure in the Asian world for early stage stomach cancer [96]. A margin of improvement in navigation technique can be considered, given that ICG is too small a molecule, tending to diffuse very rapidly to multiple lymph nodes. As a result, ICG can clearly delineate the lymphatic "basin" [97], but this is less the case for the sentinel node. Indeed, Miyashiro et al. of the Japan Clinical Oncology Group (JCOG) [98] found too many false negatives with ICG.

### 5.3.3. Organ perfusion evaluated with infrared fluorescence angiography

Systemic (intravenous) injection of a fluorophore allows to assess the presence of blood circulation (perfusion) through the generalized distribution in the body.

Perfusion analysis, using fluorescence angiography, has been used in several surgical areas, ranging from plastic/reconstructive surgery, with evaluation of the infusion of musculocutaneous flaps [99], to transplant, especially renal and hepatic transplantation [100] to evaluate the adequate vascularization of grafts. Several groups have published their experience with post-transplant angiography [101].

Special consideration should be given to the evaluation of gastrointestinal tract perfusion, as intestinal vascularization at the time of anastomosis creation is a fundamental parameter for healing, as already discussed in Section 2.2.

Indeed, poor vascularization at anastomotic level leads to energy failure and this will deteriorate the tissue's healing capabilities. The first step of an oncological surgical resection of an intestinal segment is to cut off the vascularization of that segment. This vascular approach causes ischemia of the intestinal segment, which depends on the distribution of the branches of the artery which have been controlled. The extent of the ischemic segment is subsequently not entirely predictable. When

removing a bowel segment, the surgeon estimates the extent of the resection taking into consideration not only the pathological aspects (for example, in the case of a tumor, the resection must take into account the location of the tumor and additional safety margins of up to several centimeters), but also the perfusion of remaining stumps which will be anastomosed. As mentioned above, clinical evaluation is very subjective because it is based on variable parameters such as the color of the serosa after the vascular "cut" and on whether or not vascular pulsations and peristalsis are present.

## 6. Markers of perfusion and tissue energy status

In order to validate the digestive perfusion evaluation system using hyperspectral and fluorescence imaging, we studied biomarkers of perfusion and tissue metabolism (reactive oxygen species production and capillary lactatemia) at the intestinal level, allowing a correlation between biological and morphological data. Below are some general physiological reminders.

### 6.1. Reactive oxygen species (ROS)

ROS, also known as free radicals, are produced from all eukaryotic cells and they are needed in a number of physiological processes, such as proliferation, migration, differentiation, and metabolism [102]. Free radicals lodge an unpaired electron (s) in the outer orbit. Given this configuration, they are extremely reactive and take part in a number of physiological chemical reactions with vital cell components in the body. ROS are mainly responsible for oxidative stress (OS) and are accountable for causing damage to proteins, lipids and DNA [103]. OS causes irreversible damage in cells and it is related with the development of several pathologies such as cancer, Alzheimer’s and Parkinson’s diseases, atherosclerosis, diabetes mellitus, etc. [104]. Additionally, OS contributes in various forms of aging-related pathophysiology. ROS are continuously produced during respiration. However, their production results increased in the course of prolonged ischemia or ischemia and consecutive

reperfusion. Since their half-life is extremely short and the body possesses several defense mechanisms against ROS (redox homeostasis), their detection on fresh tissue might be very complicated. Currently, electron paramagnetic resonance (EPR) is the method of choice to quantify ROS since it is able to detect short-lived radicals with a high specificity and sensitivity [105].

### 6.1.1. Electron paramagnetic resonance (EPR)

EPR **(Figure 10)**, first discovered in 1945, is a technique to analyze materials with unpaired electrons. The basic concept is similar to that of nuclear magnetic resonance (NMR). The difference is given by the fact that in EPR the electron spins are excited and not the atomic nuclei spins themselves. EPR detects transitions of unpaired electrons into a magnetic field. The concentration of free radicals can be obtained as the double integrals of the EPR spectrum of a spin adduct, which then allows to investigate ROS qualitatively and quantitatively [106].

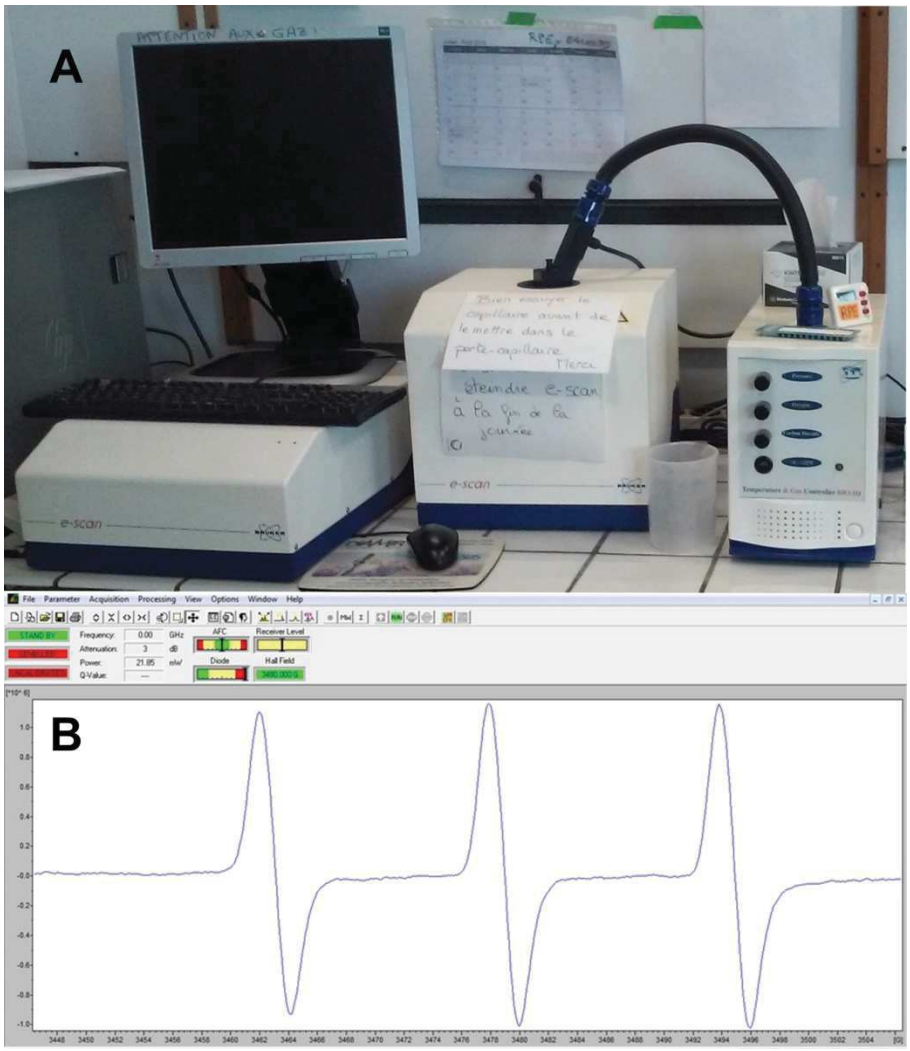


**Fig. 10.** EPR. In A, the device is shown and in B, an example of the measurement software used for the analysis during our experiments is provided.

## 6.2. Lactate

Lactate (2-hydroxypropanoate) is a salt of hydroxycarboxylic acid. Lactate forms a conversion couple via oxidation-reduction with pyruvate catalyzed at cytosolic level by the enzyme lactate dehydrogenase (LDH): **Lactate + NAD+ ⇄Pyruvate + NADH + H+**.

The reduction of pyruvate to lactate results in oxidation of NADH to NAD and vice versa, the oxidation of pyruvate from lactate results in the reduction of NAD to NADH.

Lactate is produced mainly from glucose catabolism. A second source of lactate is the metabolism of L-alanine, catalyzed by alanine aminotransferase (ALAT) [107], present at cytoplasmic and mitochondrial levels. Pyruvate is an intermediate common to these production routes. In addition, lactate may be derived from the catabolism of other amino acids such as serine, threonine, and cysteine [108]. In terms of bioenergetics, one glucose molecule per glycolysis will produce two lactate molecules, two ATP molecules, and two protons. This metabolic pathway is of low energy efficiency and is responsible for acidification of the cytosol via proton production.

Lactate production is increased under conditions of tissue hypoxia [109]. When the oxidative energy metabolism is no longer functional due to lack of oxygen, pyruvate from glycolysis accumulates and is transformed into lactate via LDH [110]. However, there is no true linear relationship between hyperlactatemia and tissue hypoxia, as changes in oxygen delivery which may occur at the microcirculation level, such as in septic shock, or hyperlactatemia may be accompanied by an increase in tissue oxygen pressure, and this needs to be taken [111] into account.

In the clinical practice, the measurement of systemic lactatemia is used in multiple situations, such as monitoring and stratification of patients at high risk of mortality from sepsis and/or digestive ischemia (mesenteric ischemia). Indeed, persistent elevated lactatemia is a predictive mortality index [112], while rapid lactate clearance is a sign of favorable prognosis [113]. However, for digestive ischemia, the measurement of systemic lactates, while remaining a predictor of mortality, does not correlate well with either the timing of ischemia [114], nor with the extent of intestinal necrosis [115].

In contrast, "local" lactatemia undergoes much more rapid and consistent variations with perfusion, as demonstrated in models of acute limb ischemia [116].

It was demonstrated that local capillary intestinal lactatemia is a reliable biomarker of enterocyte energy status, and that it correlates in a reliable fashion with perfusion [117-120]. Today, it is possible to measure capillary lactatemia using portable devices with test strips, such as glycemia measuring devices in diabetic patients. Several devices for the measurement of capillary lactates are available on the market. Initially, these devices were developed for the assessment of newborns in the delivery room and to determine the maximum aerobic physical capacity in sports medicine. These devices incorporate electrochemical sensors capable of measuring lactate levels in a few seconds, in a minimal amount of blood (in the order of microliters). The operation of the sensors is based on an enzymatic reaction producing a change in the electrical voltage measured with the device. The test strip contains an enzyme (e. g. lactate oxidase) using lactate as a substrate and the products of this reaction are responsible for the amperometric variation measured in the solution, the intensity of which is proportional to the initial amount of lactate [121].

# EXPERIMENTAL WORKS

## BACKGROUND AND AIMS

The incidence of gastrointestinal anastomotic leakage (AL) remains high, ranging from 20 to 35% [33] after esophageal and from 4 to 19% [2] after colorectal procedures. AL is a major concern in digestive surgery, since it is linked to high morbidity and mortality rates [1].

As already described, proper anastomotic healing is a multifactorial process, including non-modifiable patient-related factors, such as age, gender, and relevant comorbidities. An insufficient blood supply to the anastomotic limbs is a recognized and partially modifiable factor playing a central role in anastomotic breakdown [1, 122]. The intraoperative evaluation of gastrointestinal perfusion using clinical judgment is unreliable, irrespective of the surgeon's experience.

Basic techniques, such as mechanical anastomotic leak tests, have mild if no benefits at all in terms of complication prevention [123]. Additionally, it has been proven that improvement of the anastomotic blood flow through collaterals is unlikely to take place before postoperative day 5 [124]. As a result, anastomotic perfusion is exclusively dependent on the blood flow at the time of surgery and this should be assessed intraoperatively.

Another issue that should be addressed is that the viability of the flap/graft is dependent not only on the arterial inflow but also on the venous outflow in reconstructive and transplant surgery. As an example, venous congestion is linked to flap failure, and the ability to identify a venous outflow deficiency could lead to perform salvage procedures [125]. Similarly, in gastrointestinal surgery, discriminating between ischemia caused by arterial blood inflow or venous congestion could be useful in a number of clinical situations. For instance, venous congestion often affects gastric conduits after pull-up for esophageal reconstruction and might be related to complications [126]. Additionally, during acute mesenteric ischemia, an intraoperative FA which can discriminate between arterial and venous etiology might prove useful in choosing the appropriate surgical strategy [127-129].

Although a number of techniques are available to assess tissue perfusion in real time, given their scarce reproducibility and/or high costs and/or prolongation of the surgical workflow, they did not find acceptance within the surgical community [1]. FA is currently the method of choice to visualize perfusion intraoperatively given its low cost and the possibility to obtain a real-time assessment. In a retrospective case-matched study with 201 patients, Kudszus et al. evaluated the impact of indocyanine green FA. They concluded that FA may significantly reduce the rate of severe complications as well as the rate of anastomotic leakage [7]. Despite the initial optimism in a recent systematic review with a meta-analysis, it has been shown that FA does not reduce the rate of AL [11]. The reason for this might be provided by the heterogeneity of the existing studies in terms of ICG dose, injection time, and system used and by the lack of published randomized controlled trials.

Additionally, in most existing studies, FA is merely judged subjectively in a qualitative way. Recently, two authors reported quantitative FA, using software solutions which can measure the speed of the fluorescence signal to reach its maximum intensity [130, 131] with promising results. Both authors analyzed the contrast agent velocity pattern, without translating it into images, and this could limit the intraoperative usability. Our group introduced and validated the quantitative FA using the FLER enhanced reality software several years ago [15, 119, 120]. The FLER software, explained in the previous section of this thesis, has recently been evaluated in a series of patients (not published yet) within a prospective study showing promising results.

However, FA is limited by the need to inject ICG, which is still off-label in this specific indication, which therefore represents a regulatory burden.

Hyperspectral imaging (HSI) is an optical imaging technique, coupling a spectroscope with a photo camera, which allows for a contrast-free, real-time, qualitative and quantitative tissue analysis [19]. Lately, a new compact HSI system, TIVITA® (Diaspective Vision, Germany) capable of performing spectral acquisition in a short time (approximately in 6 seconds) is commercially available. The system provides the datasets as hypercubes and additionally generates as an

immediate output pseudo-color images quantifying several physiological parameters such as $StO_2$ and $H_2O$ [20].

The accuracy of this technology in detecting tissue ischemia *in vivo* has never been validated in a controlled experimental setting.

Additionally, the downside of HSI lies in the lack of a video rate and in that the hyperspectral information is provided as a static side-by-side image and not superimposed onto the surgical field. This impairs the intraoperative usability and surgical navigation.

In the present experimental project, we tested the performance of FLER in distinguishing between arterial, venous or mixed bowel ischemia models using a machine learning (ML) approach. Besides, we assessed the reliability of HSI to determine *in vivo* tissue ischemia in a mouse hindlimb ischemia/reperfusion model (currently submitted) in a stepwise fashion. In addition, by extrapolating the experiences with FLER, we developed the concept of HYPER (HYPerspectral Enhanced Reality). Through a customization of the HSI system and a proprietary software, the static HSI perfusion images were superimposed onto a real-time video, in order to generate a HSI-powered augmented reality environment, enabling for a precise surgical navigation. The accuracy of HYPER to quantify bowel perfusion has been experimentally validated using robust surrogate markers of bowel ischemia, such as LCL, ROS production, and histopathological evaluation [24]. Additionally, given the high correlation of $StO_2$ with LCL, implementing a ML approach, a LCL prediction algorithm based on $StO_2$ values was obtained and tested. In a second step, HYPER was compared to FLER in a controlled experimental setting using LCL as ground truth (currently submitted).

In addition, HSI was tested in 22 patients undergoing esophageal resection for cancer in a pilot study which aimed to assess its intraoperative usability within the surgical workflow [23].

# MATERIALS AND METHODS

## EQUIPMENT ENABLING FLER

### Near-infrared (NIR) optimized laparoscope

The incoherent light source D-Light P (Karl Storz, Tuttlingen, Germany) was used **(Figure 11)** to capture the fluorescent signal. The filter of the D-light P can be switched into the light transmission path. The filter transmits light in a range of 690 to 780nm and completely blocks light >800nm. In addition, switching the filter out of the light path allows for a standard white light observation.

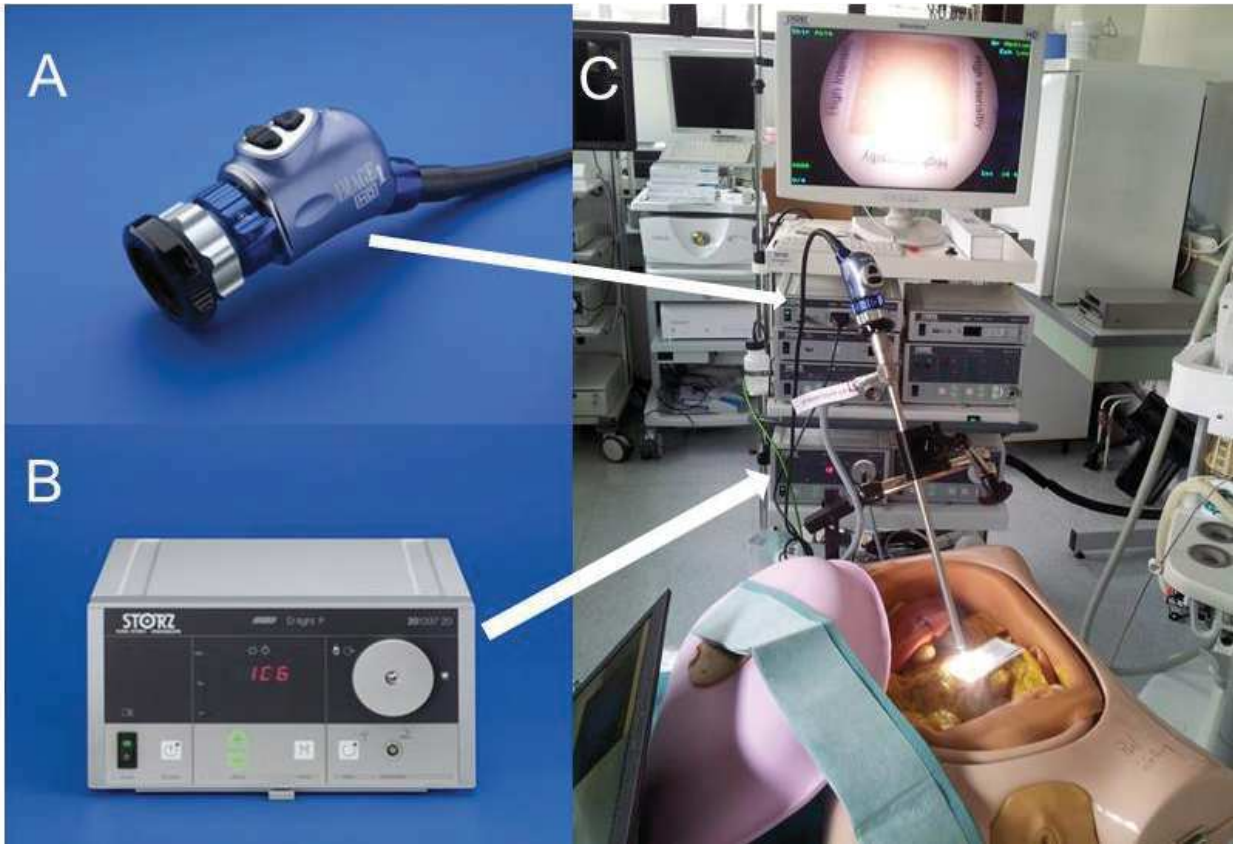


**Fig. 11.** NIR system D-Light P (Karl Storz, Tuttlingen, Germany). A) camera head, B) light source capable of emitting near-infrared light, C) testing of the camera system within a surgical simulator.

**ER-PERFUSION software**

The Research and Development department of the IRCAD has developed a dedicated image analyzer software (ER-PERFUSION, IRCAD, France), using the Python Scientific Package. The ER-PERFUSION can correlate fluorescence intensity over-time changes to tissue perfusion and allows to construct a virtual cartography based on fluorescence time-to-peak (TTP). TTP is inversely correlated to perfusion level. Virtual cartography can be overlapped onto real-time laparoscopic images in order to obtain the FLuorescence-based Enhanced Reality (FLER) effect. The perfusion analysis based on time-to-peak is 1) independent from the distance-to-target, and 2) dynamic: virtual perfusion cartography is created by averaging signals over a 20-40 second video at the speed of 5-25 frames per second and by attributing a color code based on the time required to reach the maximum intensity of each pixel. Each single pixel of perfusion cartography is a dynamic image (2D + diffusion time) representing the average of several images (from 100 to 200) **(Figure 12)**.

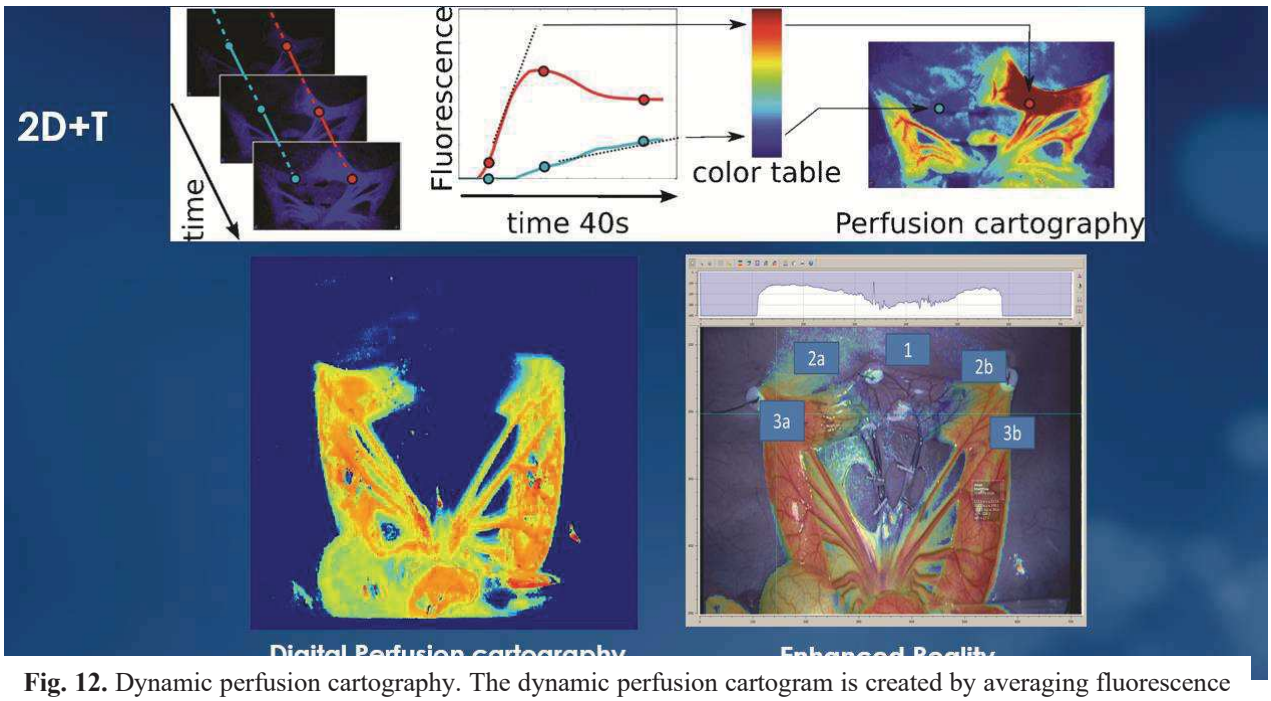


**Fig. 12.** Dynamic perfusion cartography. The dynamic perfusion cartogram is created by averaging fluorescence signals over a 20 to 40s video at a speed of 5 to 25 frames per second and by attributing a color code based on the slope intensity/time of each pixel. Each single pixel of the cartogram results from the average of multiple subsequent images.

More precisely, TTP is obtained as a difference $T_{75}$- $T_{25}$, where $T_{25}$ and $T_{75}$ represent timepoints corresponding to the first and last quartile of fluorescent intensity over time respectively **(Figure 13)**. Other authors used time-to-peak defined as the difference between $T_{100}$ (maximum intensity of fluorescent signal) and $T_0$ (minimum intensity of fluorescent signal) [17]. However, we found that it is often difficult to precisely determine the timepoints of the minimum (given the frequent presence of signal noise) and maximum (given the presence of a long signal plateau phase) fluorescence intensity. As a result, we arbitrarily chose $T_{25}$ and $T_{75}$, which are more robust timepoints.

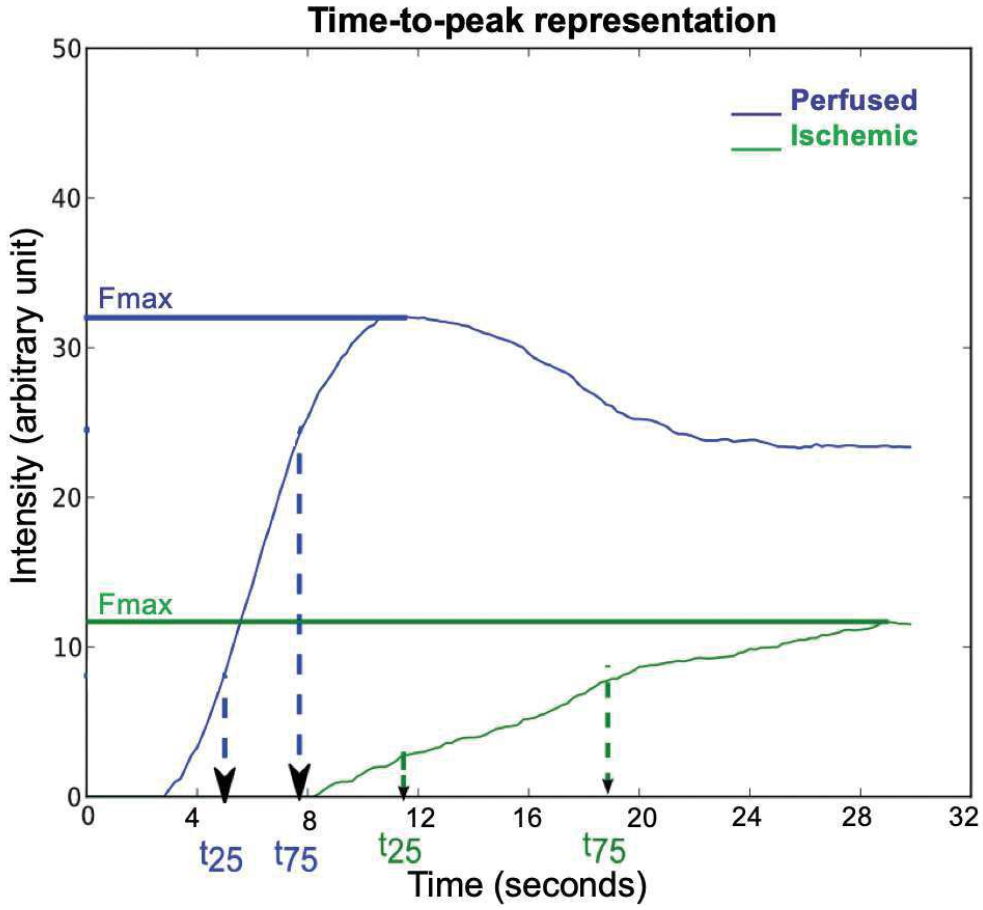


**Fig.13.** Graphical representation of time-to-peak in a well-perfused (blue) and in an ischemic area (green), in which very different maximum fluorescent intensity peaks (Fmax) are reached. TTP is the time required (in seconds) for the intensity curve to go from the first to the last quartile of fluorescent intensity over time. As represented, TTP is shorter for the perfused zone when compared to the ischemic one.

## EQUIPMENT ENABLING HYPER

### Hyperspectral imaging system

The CE-marked push-broom HSI camera (TIVITA™ Tissue; Diaspective-Vision GmbH, Am Salzhaff, Germany) is a medical Class I product. The HSI system performs an imaging remission spectroscopy in the visible (VIS) and near infrared (NIR) portions of the electromagnetic spectrum, emitting light through 6 halogen lamps. The device generates a three-dimensional (3D) Hyper-Cube with the spatial dimensions x and y and the spectral dimension λ. As already described in the introduction section of this thesis, according to the push-broom imaging principle, an objective lens creates an image and a slit selects a row (y-axis) in the image plane (y-λ-plane) [132]. Differently, out of many HSI systems described in the literature, TIVITA™ is compact and light, enabling the acquisition of a hypercube with high spectral (5nm) and spatial (640 × 480 pixel) resolution in approximately 6 seconds. The system scans in the range from 500 to 1000nm, generating 100 spectral values.

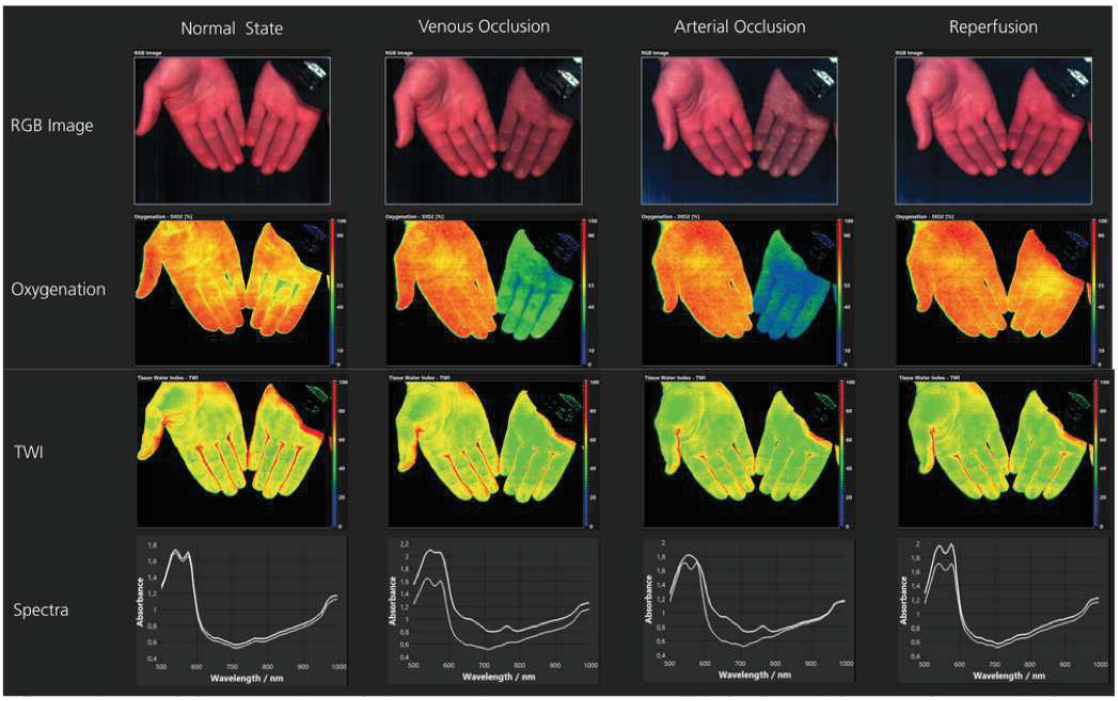


**Fig. 14.** Hand occlusion test performed in healthy individuals to validate the oxygenation and TWI algorithms. On the top row, the RGB images generated with the HSI system are visible. On the 2nd and 3rd row, the $StO_2$ and TWI pseudo-color images are displayed.

Additionally, implementing different algorithms in the software, the camera can calculate several biological tissue parameters as an immediate output and represent them into pseudo-color images. Among those parameters, StO2, near infrared perfusion index (NIR), and tissue water index (TWI) can be found (Figure 14). The detailed mathematical principles of those algorithms stand beyond the purpose of a thesis in life sciences and are described elsewhere [132, 133]. In a nutshell, StO2, which provides the tissue oxygenation of the superficial tissue layer, is calculated through an algorithm based on the second derivate of spectral regions in which an oxygenated hemoglobin peak is present (500-650nm and 700-815nm). NIR is intended to measure the perfusion in the NIR region, hence reaching deeper tissue layers (until 5mm) and the algorithm is based on the mean of 2 subregion within the NIR domain, separated by the isosbestic point at 797nm. The TWI algorithm is extrapolated using water peak regions (880-900nm and 955-980nm).

**System customization and HYPER software**

Since the TIVITA™ system generates static-side-by-side pictures, in order to allow surgical navigation and precisely detect fine perfusion changes on the gastrointestinal tract intraoperatively, we introduced the HYPER solution. The first step consisted in a customization of the TIVITA™ system by integrating an HD video camera (HD Pro C920, Logitech, Switzerland) and a laser-based distance sensor **(Figure 15)**. In a second step, a Python-based computer vision solution was used to align StO2 cartography images obtained with the HSI camera with the real-time video delivered via the HD camera, in order to obtain HYPerspectral-based Enhanced Reality (HYPER) **(Figure 16)**. The alignment of the two cameras was achieved using a calibration chessboard at the beginning of each experiment.

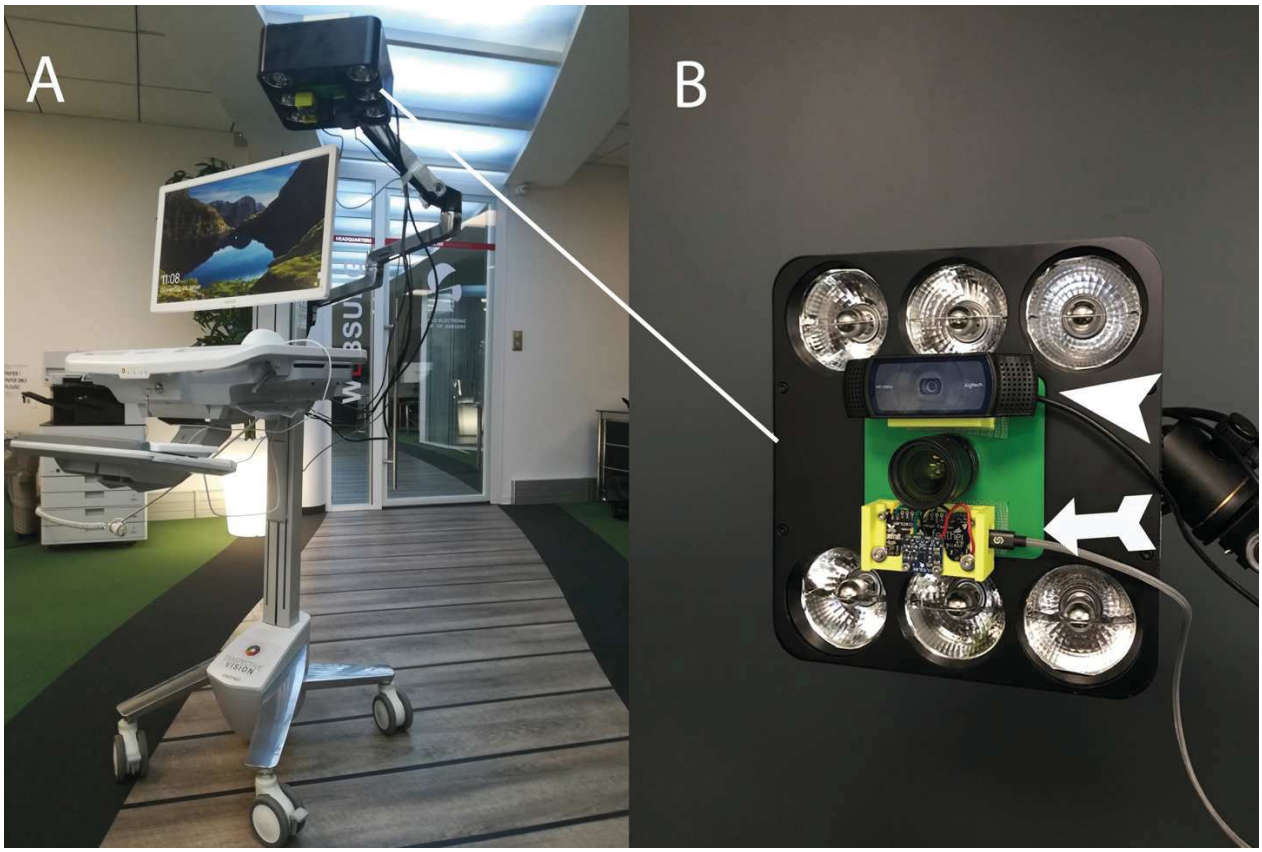


**Fig. 15**. Hyperspectral camera (A). Customization with distance sensor (arrow) and HD webcam (arrowhead), next to the camera lens.

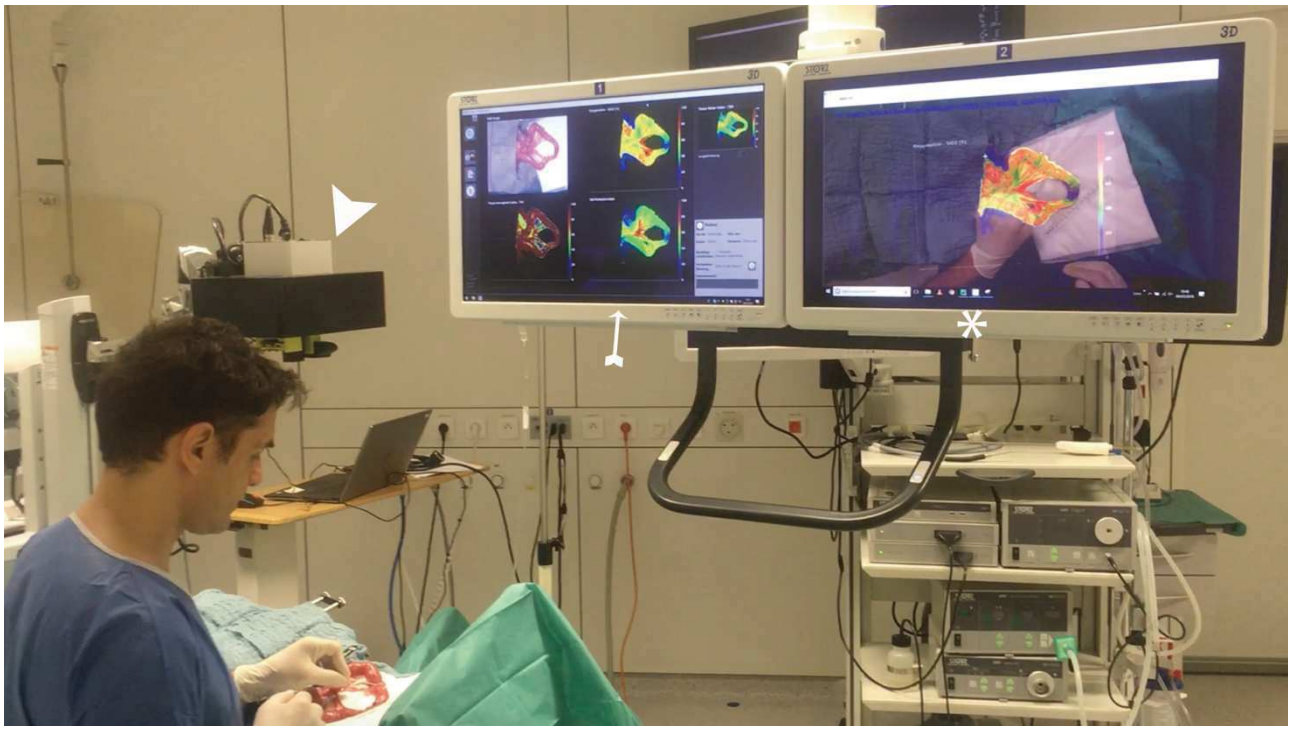

**Fig. 16**. The HSI camera (arrowhead) placed on top of an exposed ischemic bowel loop. The left monitor (arrow) displays static HSI images. The right monitor (*) shows the superimposed HSI images on the real-time running video, creating the HYPerspectral-based Enhanced Reality (HYPER) effect.

To measure the accuracy of HYPER, we have used various analytics to confirm that the perfusion quantification obtained through the light/tissue interaction generated at the level of the bowel is consistent with the biological changes occurring at tissue level:

1) **Capillary lactates**. A strip-based, portable lactate analyzer (EDGE®, ApexBio, Taipei, Taiwan) was used to assess lactate levels on blood sampled from serosal capillary vessels in correspondence with well-defined ROIs. The device is capable of delivering lactatemia levels, within a measuring range from 1.1 to 22.2mmol/L, in 45 seconds, using just a few microliters of blood **(Figure 17)**.


**Fig. 17.** Portable strip-based lactate analyzer "The Edge".

2) **Reactive oxygen species (ROS) formation quantification by means of electron paramagnetic resonance (EPR) (Figure 18)**. The ROS concentration was directly determined with a specific spin probe: 1-hydroxy-3-methoxycarbonyl-2, 2, 5, 5-tetramethylpyrrolidine hydrochloride (CMH). Briefly, tissues were cut into 10 pieces and washed twice with the Krebs Hepes buffer (NaCl 99mM, KCl 4.69mM, CaCl2 2.5mM, MgSO4 1.2mM, NaHCO3 25mM, KH2PO4 1.03mM, D(+)Glucose 5.6mM, Na-hepes 20mM, pH 7.4, deferoxamine 25µM and diethyldithiocarbamate

(DETC) 5µM). They were then incubated at 37°C with the CMH (200µM) spin probe for 30 minutes under 20mmHg of oxygen partial pressure with a Gas-Controller (Noxygen Sciences Transfer, Elzach, Germany). Supernatants were injected into a capillary, and registered by an e-scan spectrometer (Bruker, Germany) at 15°C. The EPR settings were as follows: Centre Field: 3477.4g, microwave power: 21.85mW, modulation amplitude: 2.40 G, sweep time: 5.24 sec (10 scans), sweep width: 60 G, number of lag curve points: 1). The amplitude of the signal was measured and expressed in µM/min/mg dry weight [134].

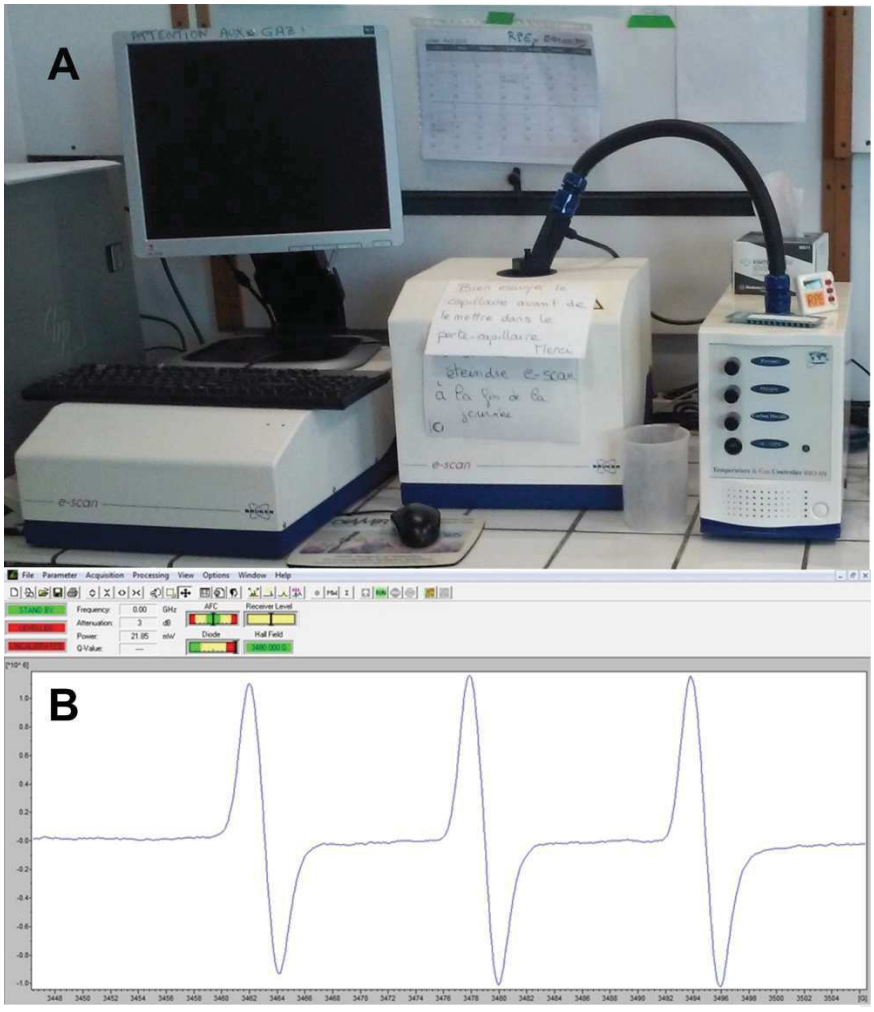


**Fig. 18.** EPR device (A) with analyzing software (B).

3) **Pathological examination.** The specimens were fixed in 4% formalin for at least 24 hours. Sections of 4µm in thickness were cut from paraffin-embedded tissues and stained with hematoxylin

and eosin. During the validation study of HYPER, biopsies were taken from each ROI at all time-points (from 1 hour to 6 hours of ischemia). Assessments were made using Chiu's score for intestinal ischemic damage [135]: grade 0 = normal mucosa; grade 1 = subepithelial space at villous tip; grade 2 = extension of subepithelial space with moderate lifting; grade 3 = massive lifting down the sides of the villi, some denuded tips; grade 4 = denuded villi, dilated capillaries; grade 5 = disintegration of lamina propria; grade 6 = transmural infarction.

4**) Machine learning-based lactates prediction from HSI StO2.** A predictive model was built in order to predict capillary lactate values from corresponding HSI-StO2 images. The 6 pigs involved in the HYPER protocol were used as a training set for an automatic curve-fitting, machine learning algorithm. In 5 additional recovery pigs, used during other experiments, which were used as a validation dataset, 2 ischemic bowel loops were created and imaged in a similar fashion. At random timepoints and ROIs, HSI-StO2 values were obtained and capillary lactates were sampled simultaneously.

## ETHICS AND ANIMAL MODELS

The preclinical experiments were part of the ELIOS project (Endoscopic Luminescent Imaging for Oncology Surgery), which received full approval from the local Ethical Committee on Animal Experimentation (ICOMETH No. 38.2016.01.085), and from the French Ministry of Superior Education and Research (MESR), under the following reference: APAFIS#8721-2017013010316298-v2. All animals used in the experimental laboratory were managed according to French laws for animal use and care, and according to the directives of the European Community Council (2010/63/EU) and ARRIVE guidelines [136]. The animals were fasted for 24 hours with free access to water before surgery. Animals were premedicated 10 minutes before surgery, by means of

an intramuscular injection of ketamine (20mg/kg) and azaperone (2mg/kg) (Stresnil, Janssen-Cilag, Belgium). Intravenous propofol (3mg/kg) combined with rocuronium (0.8mg/kg) were used for induction. Anesthesia was maintained with 2% isoflurane. At the end of the procedures, pigs were sacrificed with an intravenous injection of Pentobarbital Sodium (40mg/kg) (Exagon®, AXIENCE, France), under 5% isoflurane anesthesia.

For the preclinical studies included in this thesis, 10 male Swiss mice (12-16 weeks old) and a total of 30 pigs (Sus scrofa domesticus, ssp. Large White) were used. Five additional pigs were included after being used for training purposes at the IRCAD surgical training center and served as a test sample for the lactate prediction algorithm. The protocol for the use of living animals in surgical training was approved by the MESR, under the following reference number: APAFIS#2981-2015120212324587-v2. The additional use of those animals is encouraged by the ethical principle of reduction.

Concerning the clinical study part of this thesis, 22 patients undergoing hybrid (laparoscopic gastrolysis and open thoracic part) esophagectomy for cancer were included.

*In vivo* experimental steps, in murine and porcine models of ischemia and/or hypoperfusion, were the following:

1) Hyperspectral imaging quantification of mouse limb microcirculation in ischemia-reperfusion model with phosphodiesterase 5 inhibitor preconditioning: the hindlimb ischemia model was created by applying a tourniquet to the limb for 2 hours, followed by 30 minutes of reperfusion, N=10 (unpublished).

2) HYPerspectral Enhanced Reality (HYPER): a physiology-based surgical guidance tool: A 10cm long ischemic segment was created in 4 small bowel loops (coded A, B, C, D) by dividing the arcade branches, N=11 [24].

3) Quantitative fluorescence angiography vs. hyperspectral imaging to assess bowel ischemia: a comparative study in enhanced reality: One 10cm long ischemic segment was created in every animal, N= 8 (submitted).

4) Discrimination between arterial and venous bowel ischemia via computer-assisted analysis of the fluorescent signal: by clipping the inferior mesenteric artery, the inferior mesenteric vein or both, a sigmoid arterial, venous or mixed ischemia model was created (n=18) [137].

5) Evaluation of hyperspectral imaging (HSI) for the measurement of ischemic conditioning effects of the gastric conduit during esophagectomy: n=22 patients undergoing hybrid esophagectomy were divided into 2 equal groups: group 1 received an operation in two steps with laparoscopic gastrolysis as ischemic preconditioning (step 1), esophagectomy and reconstruction (step 2). Group 2 received a standard esophagectomy in a single step [23].

**STUDY 1: Hyperspectral imaging quantification of mouse limb microcirculation in ischemia-reperfusion model with phosphodiesterase 5 inhibitor preconditioning**

Peripheral arterial disease (PAD) has a high incidence and complication rate. Vessel recanalization represents the only therapy, but it induces reperfusion injury. Preconditioning with Sildenafil, a phosphodiesterase 5 inhibitor, has been advocated for protection against this injury. The aim of the present study was to show a real-time, non-invasive quantitative assessment using hyperspectral imaging of the Sildenafil effect. A one-sided hindlimb ischemia (120 minutes) followed by reperfusion (30 minutes) was created using an elastic tourniquet. Five mice received Sildenafil (1mg/kg i.p. 30 minutes before ischemia) and 5 mice received a 9% NaCl injection, serving as control. The $StO_2$ at T0, 5, 30, 60, 120 minutes after ischemia (T5, 30, 60, 120) and 5, 15 and 30 minutes after reperfusion (T 125, 135, 150) were measured by means of hyperspectral imaging (HSI) **(Figure 19)**.

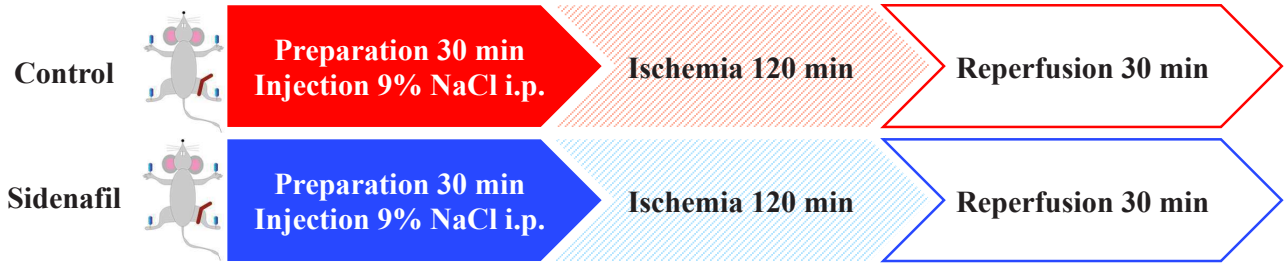


**Fig. 19.** Experimental set-up diagram.

**STUDY 2: HYPerspectral Enhanced Reality (HYPER): a physiology-based surgical guidance tool**

The aim of this experimental study was to evaluate the accuracy of HSI, to quantify bowel perfusion, against robust ischemia surrogates and to obtain a superimposition of the hyperspectral information onto real-time images, through the HYPER effect.

In 6 pigs, 4 ischemic bowel loops were created (A, B, C, D) by dividing the mesentery over 10cm and imaged at set timepoints (from 5 to 360 min). A commercially available HSI system provided pseudo-color maps of the perfusion status (StO2) and the tissue water index (TWI). The *ad hoc* software was developed to superimpose HSI information onto the live video, creating the HYPerspectral-based Enhanced Reality (HYPER). Seven regions of interest (ROIs) were identified in each bowel loop according to StO2 ranges, namely: 2 vascular (VASC proximal and distal), 2 marginal vascular (MV proximal and distal), 2 marginal ischemic (MI proximal and distal) and 1 ischemic (ISCH) **(Figure 20)**. Local capillary lactates (LCL) and histopathology were measured at the ROIs. Radical of oxygen species (ROS) was restricted to only one time point (2h ischemia in all 6 animals). This was done for logistic reasons, since the ROS analysis needed to be performed simultaneously for all ROIs, and considering the large number of samples (ROIs=291), it would not be feasible.

A machine learning-based prediction algorithm of LCL, based on the HSI-StO2%, was practiced in the 6 pigs and tested on 5 additional animals.

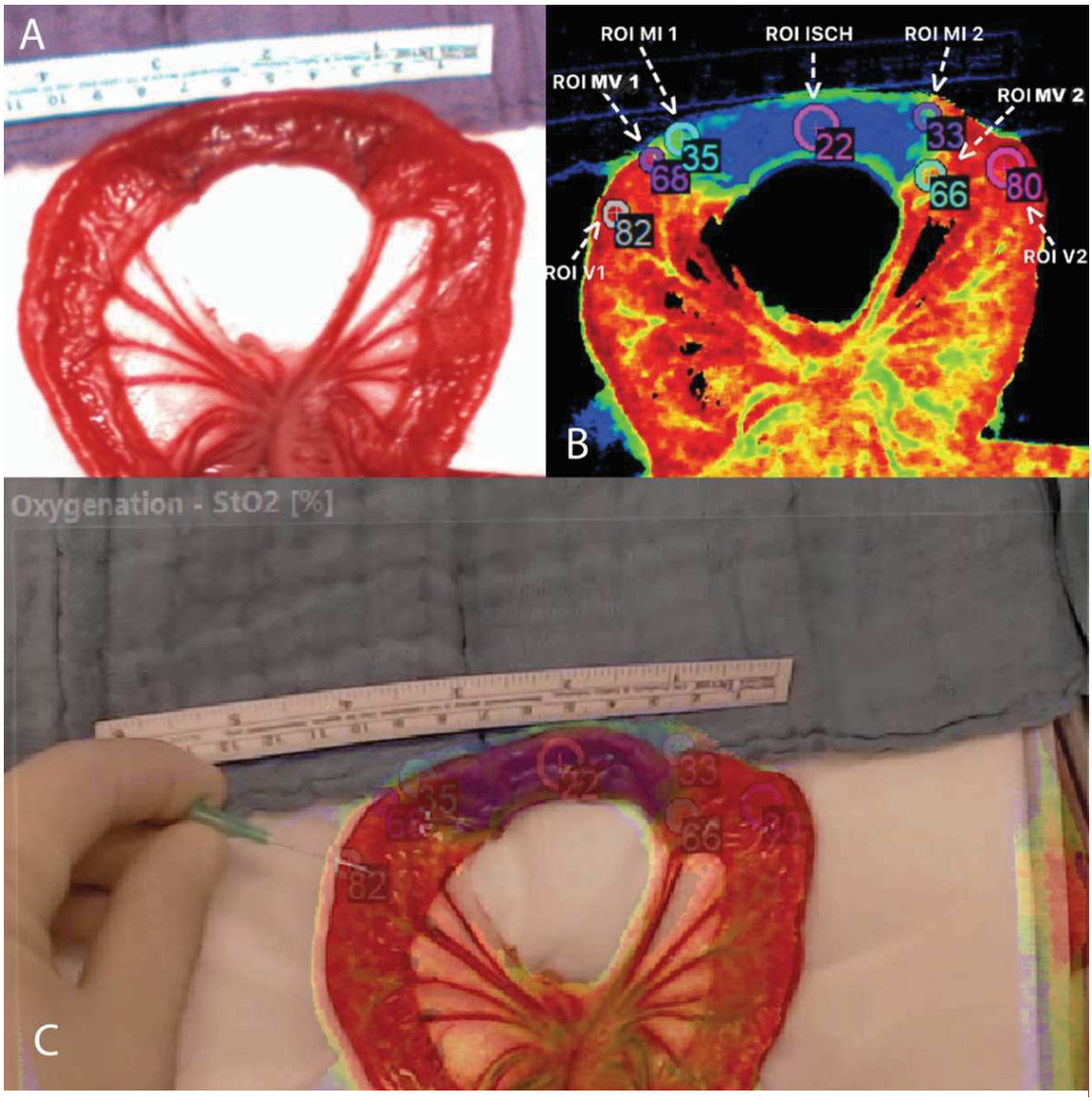


**Fig. 20.**
A) RGB image captured with the camera integrated to the HSI system, 5 minutes after the onset of ischemia.
B) HSI-generated pseudo-color image displaying the StO2 cartography. Once the HSI dataset has been acquired, the ROIs are placed manually according to the defined levels of StO2. ROIs are set at every timepoint (5, 15, 30, 45, 60 minutes for loop A, 120 minutes for loop B, 240 minutes for loop C and 360 minutes for loop D). ROIs are defined as follows: proximal and distal vascularized areas (V1 and V2, StO2 range: 70-100%); proximal and distal marginal vascularized (MV1 and MV2; StO2 range: 50-70%), proximal and distal marginal ischemic (MI1 and MI2; StO2 range: 30-50%); and 1 ischemic area (ISCH; StO2 range: 0-30%).
C) The StO2 pseudo-color image was registered onto the real-time video stream, and the ROIs were displayed as HYPerspectral-based Enhanced Reality (HYPER).

**STUDY 3: Quantitative fluorescence angiography vs. hyperspectral imaging to assess bowel ischemia: a comparative study in enhanced reality**

The aim of this study was to compare the performance of HYPER and FLER in the assessment of bowel perfusion using an experimental model of ischemia.

An ischemic bowel segment was created in 8 pigs as in STUDY 2, and imaged using HSI and fluorescence angiography. HSI was performed to acquire the $StO_2$, and FA was then performed after intravenous injection of 0.2mg/kg of indocyanine green. The time-to-peak fluorescence signal was analyzed using a proprietary software (ER-Perfusion, IHU/IRCAD Strasbourg, France) to obtain a perfusion map. This was overlaid onto real-time images to obtain FLER. Nine adjacent regions of interest (ROIs) were selected and were superimposed onto the real-time video to obtain HYPER. FLER and HYPER were successfully superimposed allowing a comparison of both imaging modalities. Local capillary lactates (LCL) were sampled at the ROIs. Two LCL predictive models were extrapolated based on both imaging modalities **(Figure 21)**.

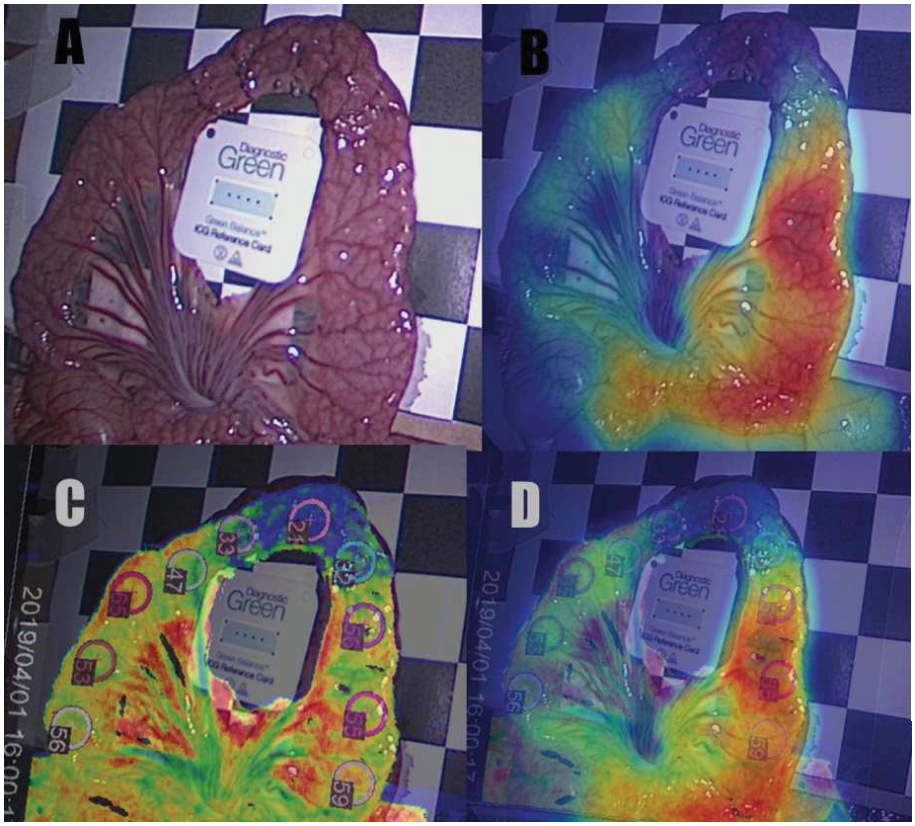


**Fig. 21.** Ischemic small bowel model displayed under white light (A), with ICG reference card visible in the center of the bowel loop. FLER (B) with superimposing of the fluorescence-based quantitative perfusion cartography. HYPER (C) generated through the superimposing of the StO2 pseudo-color image captured with HSI. (D) shows the warping of FLER and HYPER simultaneously, over the real-time video captured with the laparoscopic camera. The selected ROIs are precisely identifiable in the surgical scene.

**STUDY 4: Discrimination between arterial and venous bowel ischemia using computer-assisted analysis of the fluorescent signal**

The aim of the present study was to evaluate a software-based analysis of the fluorescence signal to recognize the patterns of bowel ischemia and discriminate between arterial occlusion, venous congestion and a combination of both.

In 18 pigs, two clips were applied on the inferior mesenteric artery (group A: *n* = 6) or vein (group V: *n* = 6) or on both (group A-V: *n* = 6). Three regions of interest (ROIs) were identified on the sigmoid: P = proximal to the first clip; C = central, between the two clips; and D = distal to the second clip. Indocyanine Green was injected intravenously. The fluorescence signal was captured by means of a near-infrared laparoscope. The time-to-peak (seconds) and the maximum fluorescence intensity were recorded using software. A normalized fluorescence intensity unit (NFIU: 0-to-1) was attributed, using a reference card. The NFIU's over-time variations were computed every 10 min for 50 min. Capillary lactates were measured on the sigmoid at the 3 ROIs. Various machine learning algorithms were applied to recognize ischemia patterns **(Figure 22)**.

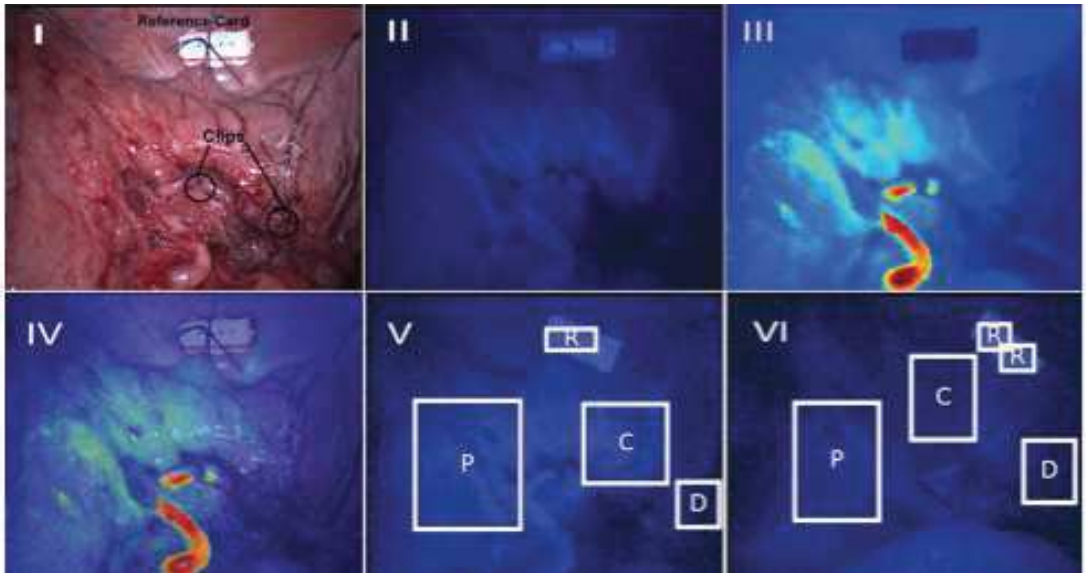


**Fig.22.** Example of FLER analysis in an arterial ischemia model. **I** White light image of the minimally invasive setting of arterial ischemia creation. **II** Near-infrared image 40s after the injection of 0.2mg/kg of ICG: bright enhancement of bowel vessels. **III** Virtual perfusion cartography, generated by computing the slope of the time-to-peak, pixel-by-pixel. **IV** FLER, showing the limits between the perfused proximal area (P) and the ischemic ROI C. **V** Near-infrared image after 10 min. **VI** Near-infrared image after 50 min.

**STUDY 5: Evaluation of hyperspectral imaging (HSI) for the measurement of ischemic conditioning effects of the gastric conduit during esophagectomy**

The aim of this pilot clinical trial was to evaluate the safety and ability of HSI to quantify the perfusion of the gastric conduit intraoperatively during hybrid (abdominal part: laparoscopic; thoracic part: mini-thoracotomy) or open esophagectomy ($n$ = 1 with simultaneous liver resection).

Intraoperative hyperspectral images of the gastric tube through the mini-thoracotomy were recorded from $n$ = 22 patients. Fourteen patients underwent laparoscopic gastrolysis first. During gastrolysis part of the stomach vasculature was interrupted (left gastroepiploic artery, short gastric artery and left gastric artery) in order to stimulate an ischemic preconditioning. 3-7 later the surgical procedure was completed through gastric tubulization, esophagectomy and anastomosis. In the rest of the patients the operation was carried out conventionally in one step. The tip of the gastric tube (later esophagogastric anastomosis) was imaged with HSI. Analysis software provided an RGB image and 3 false color images representing physiologic parameters of the recorded tissue area intraoperatively. These parameters included tissue oxygenation ($StO_2$), near-infrared perfusion index (NIR), and tissue water index (TWI) **(Figure 23)**.

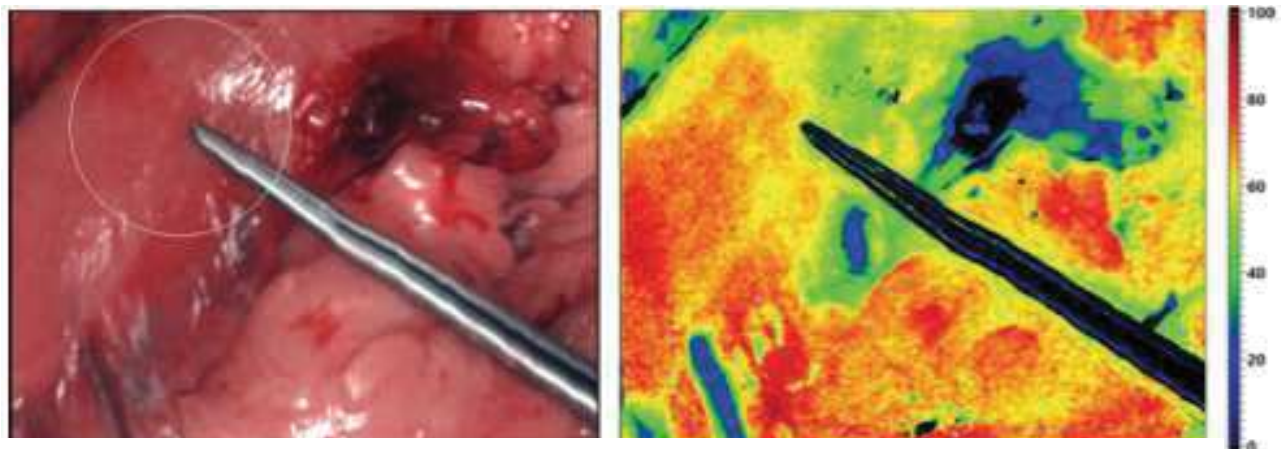


**Fig. 23.** The RGB picture is shown on the left and the $StO_2$ pseudo-color image on the right.

# RESULTS

**STUDY 1: Hyperspectral imaging quantification of mouse limb microcirculation in ischemia-reperfusion model with phosphodiesterase 5 inhibitor preconditioning**

The ischemia, not visible in the RGB pictures, could be easily visualized using the HSI in both the control and sildenafil groups (**Figure 24)**.

The control group showed a significantly lower $StO_2$ (T120, 24.8±17%, p=0.0113) during ischemia and significantly higher during reperfusion (T150, 76.8±3.77, p=0.0008) as compared with the internal control at T0 (53.3±7.04%) **(Figure 25)**. Similarly, the sildenafil group was significantly lower $StO_2$ during ischemia (T120, 28.6±20%, p=0.0312) but not significantly higher during reperfusion (T150, 73.3±19.1%, p=0.0075) as compared with the T0 value (63.3±8.46%) **(Figure 26)**.

The comparison of the $StO_2$ values at T0, T120, and T150 between the sildenafil and the control groups, did not show any statistical difference **(Figure 27)**.

During the overall ischemic phase, the $StO_2$ mean value of the ischemic limb in the control and sildenafil groups was measured at 30.2±13.4% and 30.5±18.9%, respectively. Both had significantly lower values than the mean of the non-ischemic limb in both groups (control 64.0±8.34%; sildenafil: 66.2±5.08%; p<0.0001). During the whole reperfusion phase, the $StO_2$ values of the ischemic limb were 73.8±0.477% in the sildenafil group and 77.1±1.04% in the control group, whereas values in the non-ischemic limb were 74.8±2.59% for the sildenafil and 75.6±3.45% for the control group **(Figure 28)**.

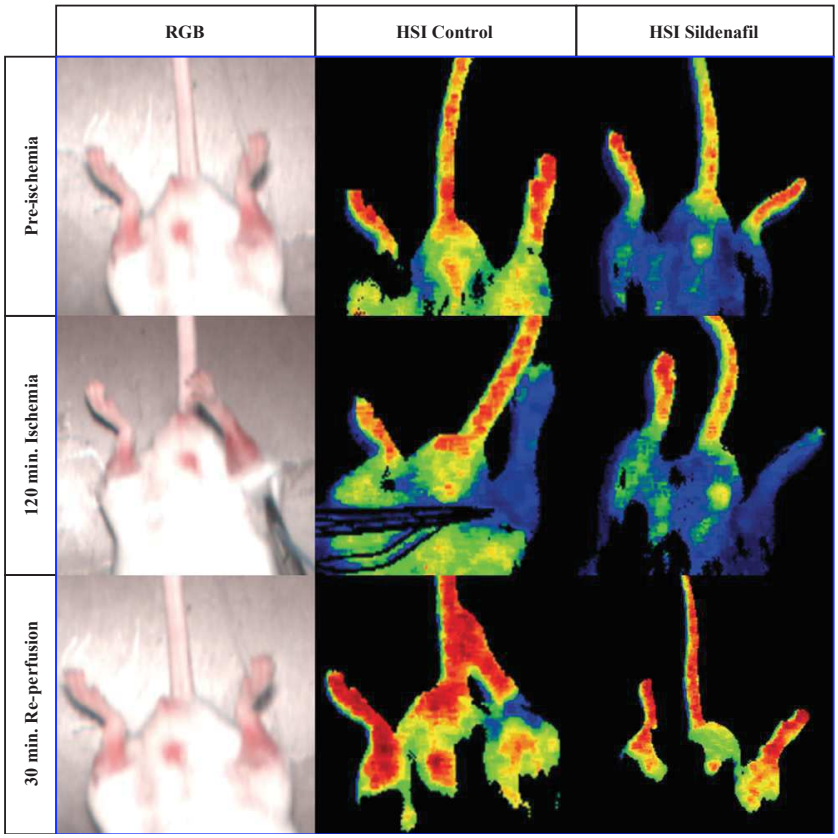


**Fig. 24.** The RGB pictures captured with the HSI camera before ischemia, after 120 minutes ischemia and after 30 minutes reperfusion are shown in the RGB column. The pseudo-color images generated by the HSI system quantify the $StO_2$ content at the different timepoints, in the control (central column) and sildenafil (right column) groups respectively. Red areas display the highest $StO_2$ values, whereas green, yellow, and blue incrementally lower perfused areas.

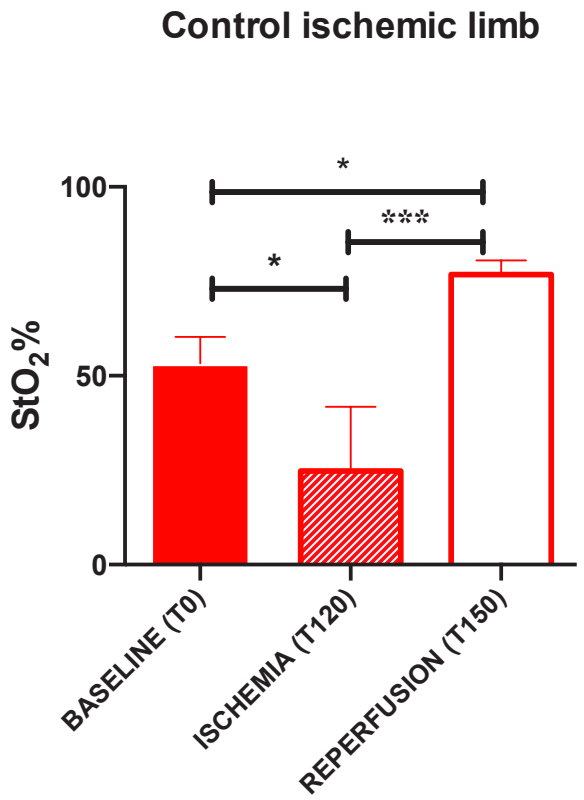


**Fig. 25.** StO2% in the control group at different timepoints, before ischemia (T0), during ischemia (T120) and during reperfusion (T150).(One-Way ANOVA p≥0.05 = ns, p<0.05 = *, p<0.01 = **, p<0.0001 = ***, p<0.00001 = ****)Fig. 25. StO2% in the control group at different timepoints, before ischemia (T0), during ischemia (T120) and during reperfusion

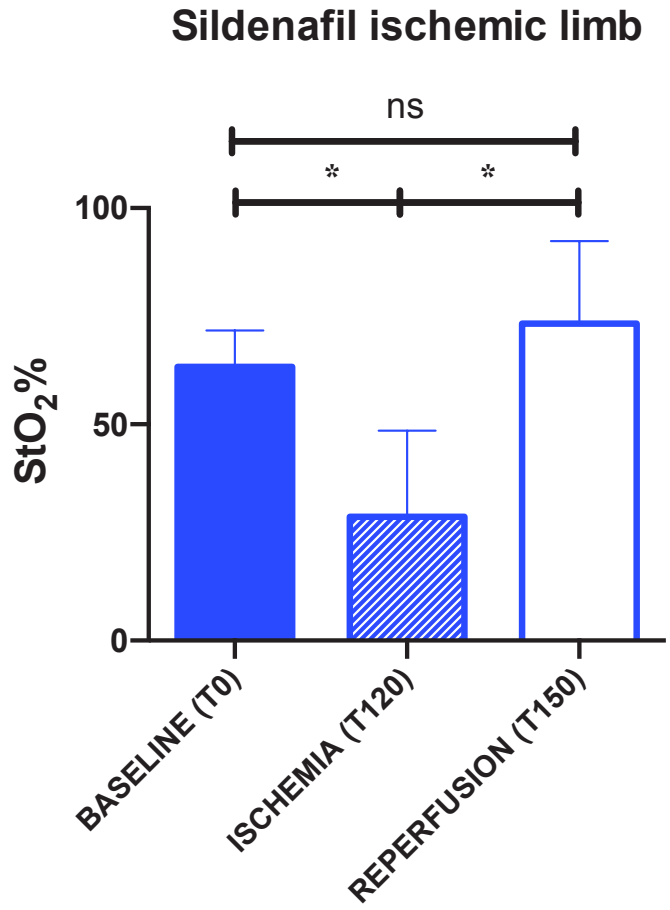


**Fig. 26.** $StO_2$% in the sildenafil group at different timepoints, before ischemia (T0), during ischemia (T120), and during reperfusion (T150). (One-Way ANOVA p≥0.05 = ns, p<0.05 = *, p<0.01 = **, p<0.0001 = ***, p<0.00001 = ****)

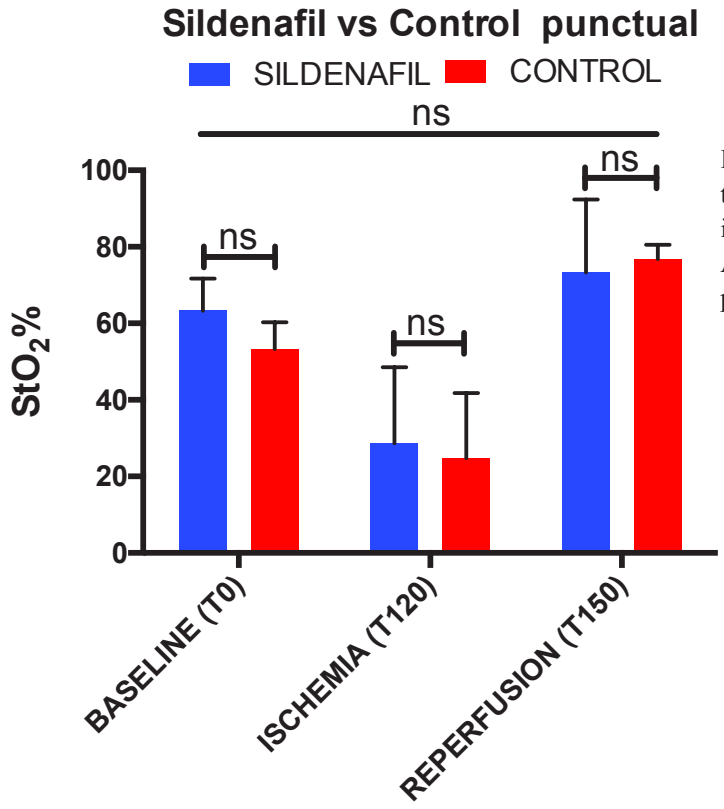


**Fig. 27**. Comparison of the StO2% control and the sildenafil group before ischemia, during ischemia, and during perfusion (Two-way ANOVA, $p \geq 0.05$ = ns, $p < 0.05$ = *, $p < 0.01$ = **, $p < 0.0001$ = ***, $p < 0.00001$ = ****)

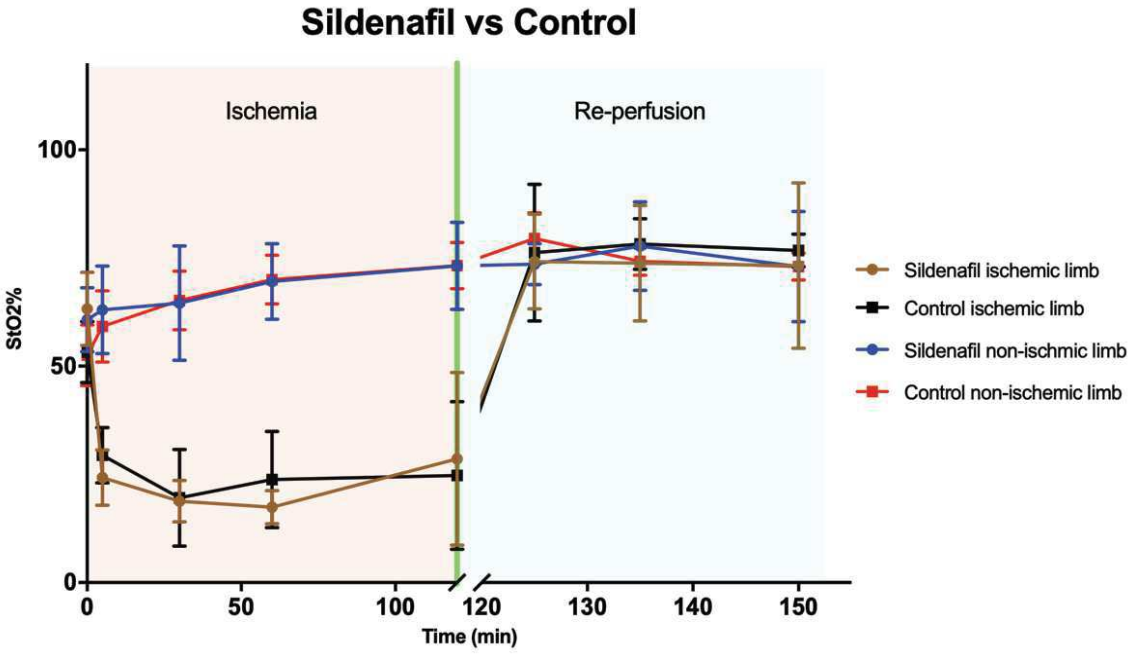


**Fig. 28.** StO2% in both groups: control and sildenafil. The graph shows all values recorded during ischemia and reperfusion. Each point is the mean of the 5 samples with SD.

**STUDY 2: HYPerspectral Enhanced Reality (HYPER): a physiology-based surgical guidance tool**

HYPER imaging could consistently and precisely identify the bowel perfusion at the various ROIs over time.

The main results were as follows:

- *Local capillary lactates (mmol/L)*

Mean cumulative (all-time points) local capillary lactate values were significantly different between the different ROIs. Mean lactate levels at the ROI ISCH (8.5±4) were significantly higher than those sampled at MI (4.12±2.16, $p<0.0001$), MV (2.33±1, $p<0.0001$), and VASC (1.78±0.79, $p<0.0001$) zones. Similarly, lactate levels were significantly different between MI vs. both MV and V ($p<0.0001$ in both cases). MV and V had similar lactate levels, throughout the entire experiment.

- *StO2%*

The mean cumulative (all timepoints) StO2% values showed statistically significant differences between all ROIs ($p <0.0001$).

- *NIR perfusion index*

Cumulative (all timepoints) NIR was significantly different at the various ROIs ($p<0.0001$), except between V and MV.

- *Tissue water index (TWI)*

ROI ISCH showed a significantly lower cumulative mean value (40.96±10.59) as compared to ROIs V (53.29±10.59, $p<0.0001$), MV (54.81±8.36, $p<0.0001$), and MI (49.49±9.65, $p<0.0001$). Statistically significant differences between ROIs occurred starting at 45' of ischemia.

- *Histopathology*

The mean Chiu's score at ROI ISCH was 2.730±1.87 and was significantly higher than ROI V (0±0; $p<0.0001$), ROI MV (0.7600±0.94; $p<0.0001$) and MI (1.37±1.43; $p=0.0021$). In addition, the MI had a significantly higher score than MV ($p=0.0002$).

- *Reactive oxygen species (µM/min/mg dry weight) generation after 2h ischemia*

The mean value of ROS at the ROI ISCH was 0.23±0.17 and was significantly higher when compared to ROI VASC (0.07±0.02; $p=0.0017$), to ROI MV (0.08±0.03; $p=0.0018$), and to ROI MI (0.093±0.04; $p=0.0053$).

The evolution and the intra-ROI differences over time are reported in **Figure 29 and Table 3**.

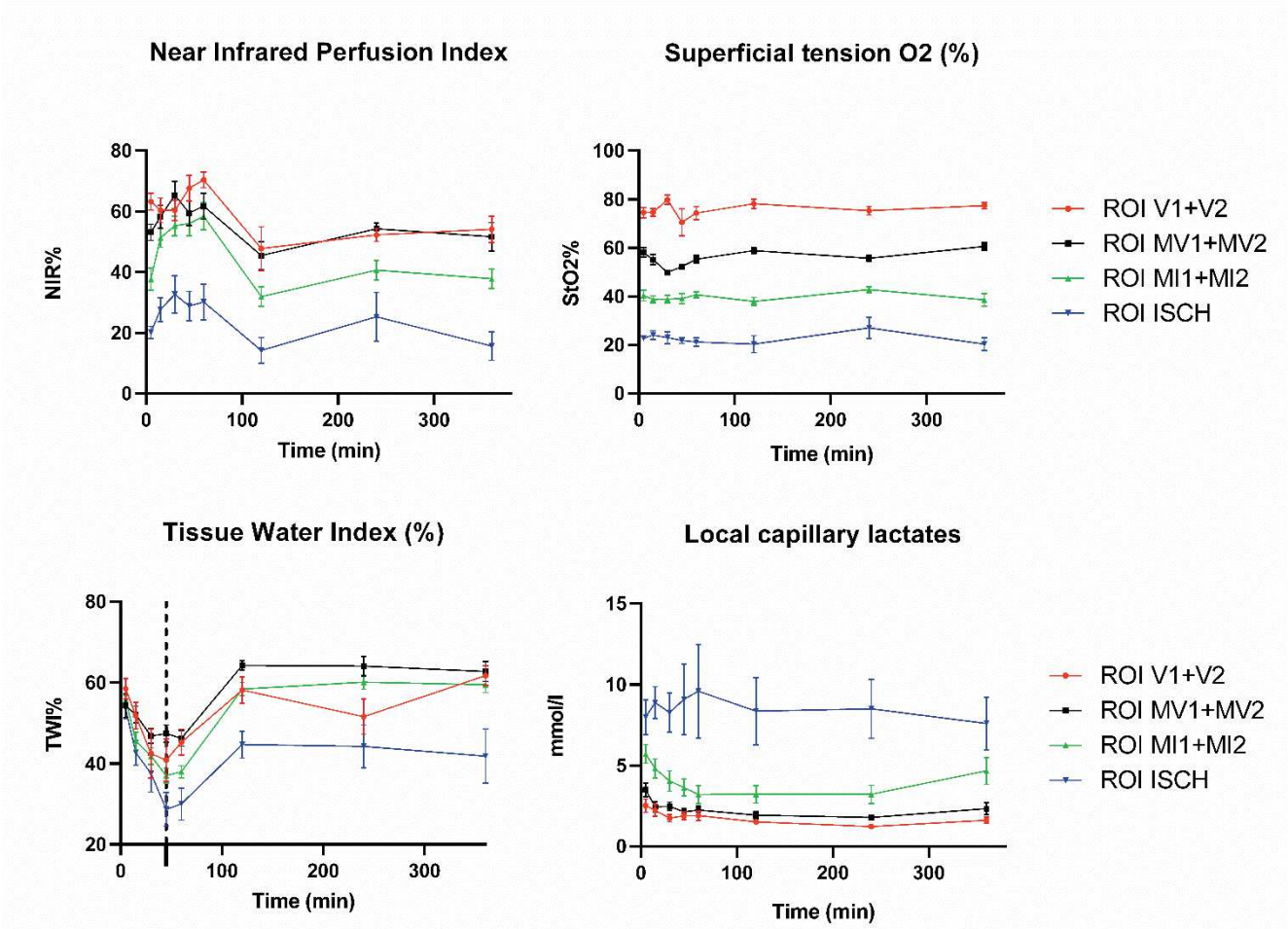


**Fig. 29.** The graph shows the evolution of HSI parameters and of capillary lactates over time at the various ROIs. For an improved graphic, the ROIs which were symmetrically proximal and distal to the ischemic area were pooled on the basis of the same StO2 levels.
The near-infrared perfusion index quantifies perfusion within the NIR wavelength, and consequently from deeper tissue layers. NIR could precisely discriminate the ischemic as well as marginal and vascularized areas throughout the entire 6h ischemia. Similarly, the StO2 imaging provided distinct curves and an accurate quantification of the oxygenated hemoglobin within the visible light wavelength at the different ROIs. The tissue water index computes the tissue water content. Upon ischemia, TWI was similarly decreased in all ROIs. From minute 45' (dotted line), TWI started to rise again, but significantly more in the perfused than in the ischemic areas. Over time, local capillary lactate curves confirmed the accuracy of the HSI images to discriminate between the ROIs based on the StO2 cartography, at any timepoint.

## Table 3. Over-time multiple comparisons between ROIs

| ROIs comparison | 5’ | 15’ | 30’ | 45’ | 60’ | 120’ | 240’ | 360’ |
|---|---|---|---|---|---|---|---|---|
| | **Local capillary lactates** | | | | | | | |
| **V vs MV** | ns | ns | ns | ns | ns | ns | ns | ns |
| **V vs MI** | 0,0128 | 0,0386 | ns | ns | ns | ns | ns | 0,0027 |
| **V vs I** | <0,0001 | <0,0001 | <0,0001 | <0,0001 | <0,0001 | <0,0001 | <0,0001 | <0,0001 |
| **MV vs MI** | ns | 0,0323 | ns | ns | ns | ns | ns | 0,0368 |
| **MV vs I** | 0,0008 | <0,0001 | <0,0001 | <0,0001 | <0,0001 | <0,0001 | <0,0001 | <0,0001 |
| **MI vs I** | ns | 0,0009 | 0,0005 | <0,0001 | <0,0001 | <0,0001 | <0,0001 | 0,0302 |
| | **StO2%** | | | | | | | |
| **V vs MV** | <0,0001 | <0,0001 | <0,0001 | <0,0001 | <0,0001 | <0,0001 | <0,0001 | <0,0001 |
| **V vs MI** | <0,0001 | <0,0001 | <0,0001 | <0,0001 | <0,0001 | <0,0001 | <0,0001 | <0,0001 |
| **V vs I** | <0,0001 | <0,0001 | <0,0001 | <0,0001 | <0,0001 | <0,0001 | <0,0001 | <0,0001 |
| **MV vs MI** | <0,0001 | <0,0001 | <0,0001 | <0,0001 | <0,0001 | <0,0001 | <0,0001 | <0,0001 |
| **MV vs I** | <0,0001 | <0,0001 | <0,0001 | <0,0001 | <0,0001 | <0,0001 | <0,0001 | <0,0001 |
| **MI vs I** | <0,0001 | <0,0001 | <0,0001 | <0,0001 | <0,0001 | <0,0001 | <0,0001 | <0,0001 |
| | **NIR** | | | | | | | |
| **V vs MV** | ns | ns | ns | ns | ns | ns | ns | ns |
| **V vs MI** | 0,0001 | ns | ns | ns | ns | 0,0236 | ns | 0,0127 |
| **V vs I** | <0,0001 | <0,0001 | 0,0009 | <0,0001 | <0,0001 | <0,0001 | 0,0002 | <0,0001 |
| **MV vs MI** | 0,0203 | ns | ns | ns | ns | ns | ns | 0,0467 |
| **MV vs I** | <0,0001 | <0,0001 | <0,0001 | <0,0001 | <0,0001 | <0,0001 | <0,0001 | <0,0001 |
| **MI vs I** | 0,0371 | 0,0019 | 0,0033 | 0,0002 | 0,0001 | 0,0334 | ns | 0,0041 |
| | **TWI** | | | | | | | |
| **V vs MV** | ns | ns | ns | ns | ns | ns | 0,0028 | ns |
| **V vs MI** | ns | ns | ns | ns | ns | ns | ns | ns |
| **V vs I** | ns | ns | ns | ns | 0,0095 | 0,0149 | ns | <0,0001 |
| **MV vs MI** | ns | ns | ns | 0,0189 | ns | ns | ns | ns |
| **MV vs I** | ns | ns | ns | 0,0001 | 0,0013 | <0,0001 | <0,0001 | <0,0001 |
| **MI vs I** | ns | ns | ns | ns | ns | 0,0094 | 0,0027 | 0,0004 |

**Table 3.** ANOVA with Tukey’s multiple comparison test. ROIs: regions of interest; V: vascularized (70-100% StO2); MV: marginal vascularized (50-70% StO2); MI: marginal ischemic (30-50% StO2); I: ischemic (0-30% StO2). NIR: near-infrared; TWI: tissue water index. A *p*- value <0.05 was considered statistically significant.

**Figure 30** displays the results of histopathology and the quantification of the radical of oxygen species at the ROIs.

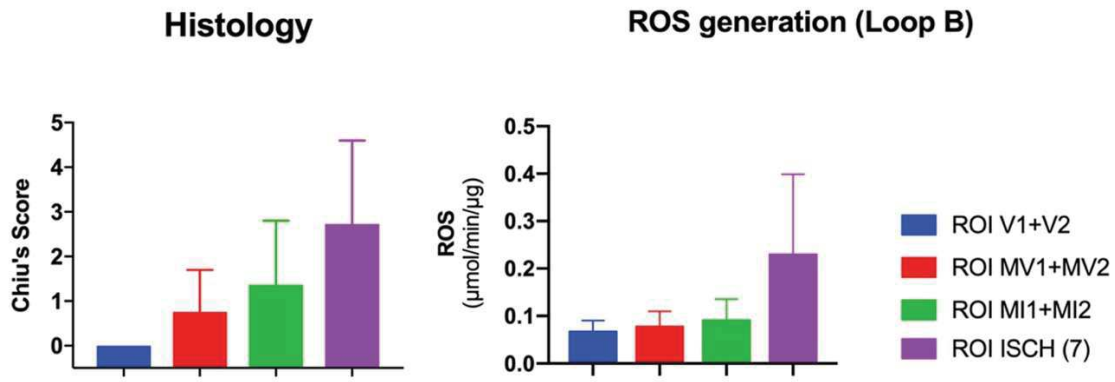


**Fig. 30.** Main differences in terms of histology at the different ROIs and ROS generation for loop B (2 hours ischemia)

- *LCL prediction from HSI StO2*

The model could predict capillary lactate values with a mean error of 1.18±1.35mmol/L. The median error was 0.7mmol/L. 95% of the errors occur for lactate values <3.44mmol/L **(Figure 31)**. The inaccuracies in predicting lactate levels occurred predominantly at levels of StO2 ranging from 0 to 30%, corresponding to the ISCH ROI. For StO2 values >30%, the mean error was 0.3±0.33 mmol/L (median error 0.164, 95th percentile 0.87).

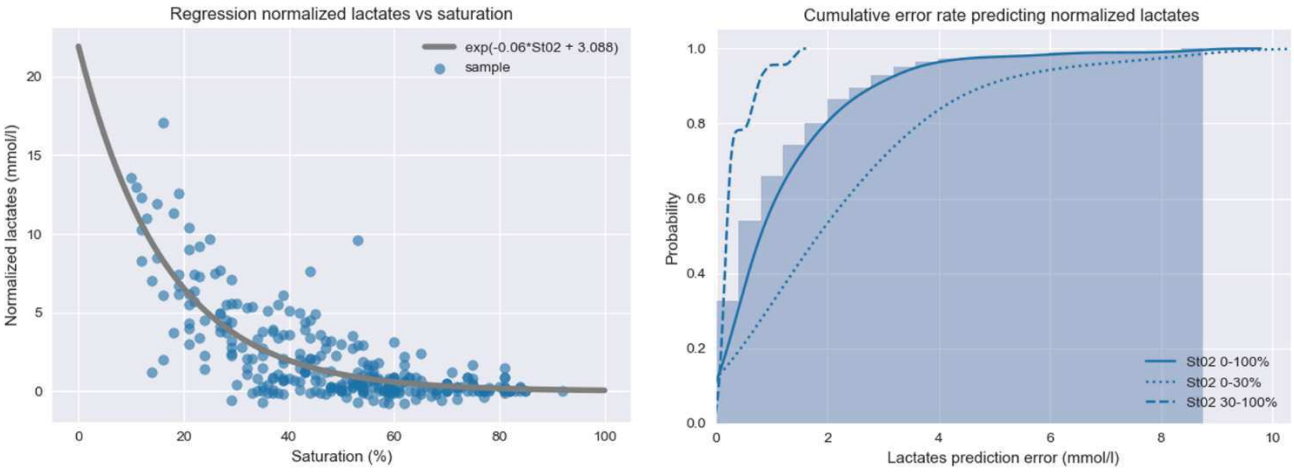


**Fig. 31.** On the left, graphical representation of the curve fitting algorithm for the relationship between StO2 and the local capillary lactate, normalized via the systemic lactate value. The graph displays the learning datasets of the 6 initial pigs and the 5 prediction animals. The graph on the right displays the error rate; the majority of the errors are found when the StO2 is lower than 30%. In the value range above 30%, the error is very low, potentially making HSI a reliable intraoperative tool to assess the perfusion of borderline perfused bowel segments, which are the most relevant ones clinically.

**STUDY 3: Quantitative fluorescence angiography vs. hyperspectral imaging to assess bowel ischemia: a comparative study in enhanced reality**

The enhanced reality environment allowed to precisely identify the ROIs on the bowel loops (n=72) and to sample serosal capillary blood to measure LCL. FLER TTP and HSI-StO2 were calculated in correspondence with the ROIs. Mean systemic lactate concentration was 2.63±2.85mmol/L. Mean LCL concentration was 4.67±4.34mmol/L, mean normalized LCL value was 2.034±2.44mmol/L, mean $StO_2$ value was 45.92±18.59% and mean TTP 10.33±9.36 sec.

- *Comparison between FLER TTP and HSI-StO2*

The Pearson analysis between FLER TTP and HSI-StO2 in correspondence with the same ROIs gave a result of R=-0.66 ($p<0.0001$) **(Figure 32)**.

- *Comparison between LCL and TTP / LCL and StO2*

The Spearman correlation between LCL values and FLER TTP gave an R=0.40 (p=0.001), and an R=-0.62 ($p<0.0001$) between LCL values and HSI-StO2.

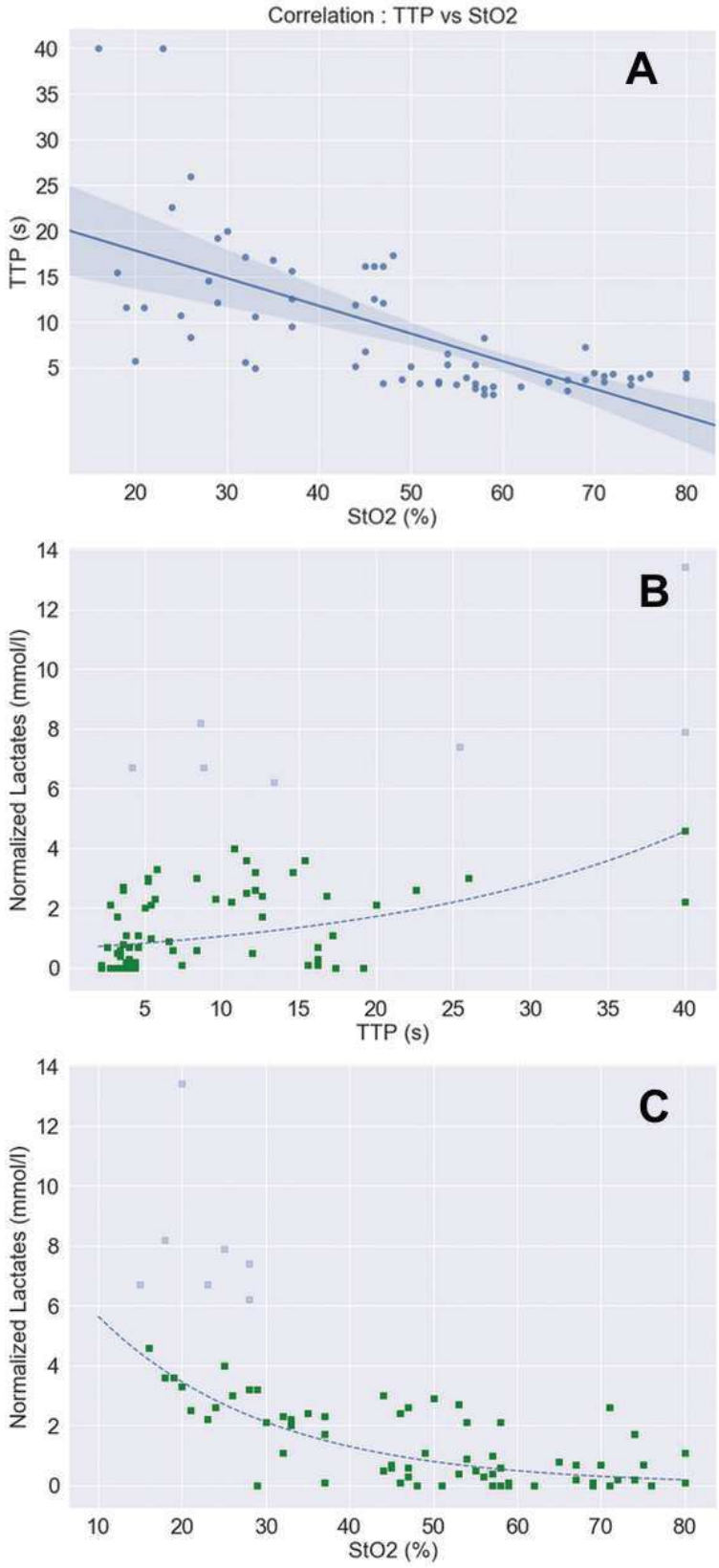


**Fig. 32.** (A) Visual representation of Pearson's correlation between HSI-StO2 and FLER TTP (R=-0.66; p<0.001). The exponential regression correlation between lactates and both FLER TTP (B) and HSI-StO2 (C) is shown. Seven datasets of highly ischemic regions (shadowed points) were excluded from the regression analysis, since we observed that, using both imaging modalities, the LCL prediction models are highly inaccurate when LCL>6mmol/L, as highlighted in the graph.

- *LCL prediction based on FLER TTP*

The mean error of the lactate prediction model was 0.95±0.74mmol/L. The median error was 0.68mmol/L. 95% of the errors occur for lactate values <2.33mmol/L.

- *LCL prediction based on HSI-StO2*

The lactate prediction model showed a mean error of 0.65±0.59mmol/L, with a median error of 0.43mmol/L. 95% of the errors occur for lactate values <2mmol/L.

- *Comparison between FLER-based and HSI-based lactate prediction models*

  The Wilcoxon test showed a significant difference between the two prediction models ($p<0.0001$), with HSI yielding a better lactate prediction performance **(Figure 33)**.

  It was observed that both prediction models were less accurate for LCL values >6mmol/L. As a result, a threshold was set at an inferior value, and led to excluding a total of 7 ROIs which were definitely outliers **(Figure 32 B-C)**.

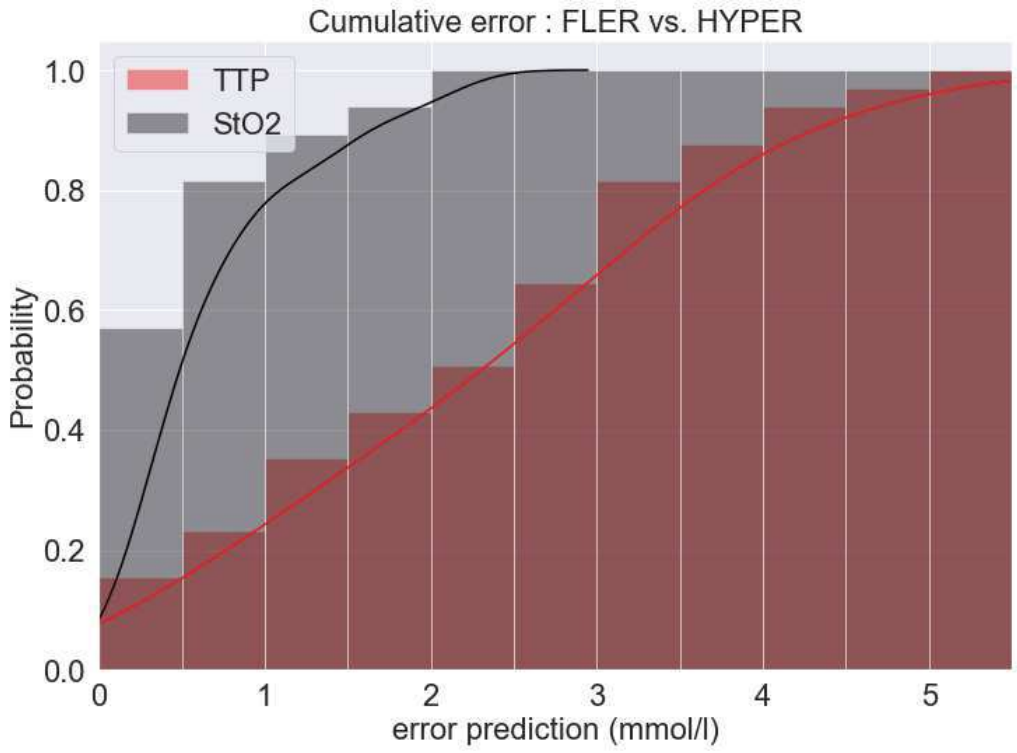


**Fig. 33.** Overall precision in predicting lactates is significantly higher when using the HSI-$StO_2$ (black line) when compared to FLER TTP (red line).

**STUDY 4: Discrimination between arterial and venous bowel ischemia by computer-assisted analysis of the fluorescent signal**

- *Slope of time-to-peak*

In group A, time-to-peak recorded at the ROI P (8.32 ± 4.16) was significantly shorter when compared to C (20.1±13; *p*=0.04). Similarly, in group A-V, time-to-peak was shorter at the ROI P (6.03±2.17) when compared to C (20.71±11.6; *p*=0.01) and when compared to D (18.56±10.75; *p*=0.01). In group V, time-to-peak was similar in the three ROIs (*p*=7.35±2.43; C=8.43±3.7 and D=8.6±2.9). Among the three groups, time-to-peak was similar at both ROIs P and D. Conversely, time-to-peak at C areas was significantly longer in group A versus V (20.1±13 vs. 8.43±3.7; *p*=0.04) and in group A-V versus V (20.71±11.6 vs. 8.43±3.7; *p*=0.03) **(Figure 34)**.

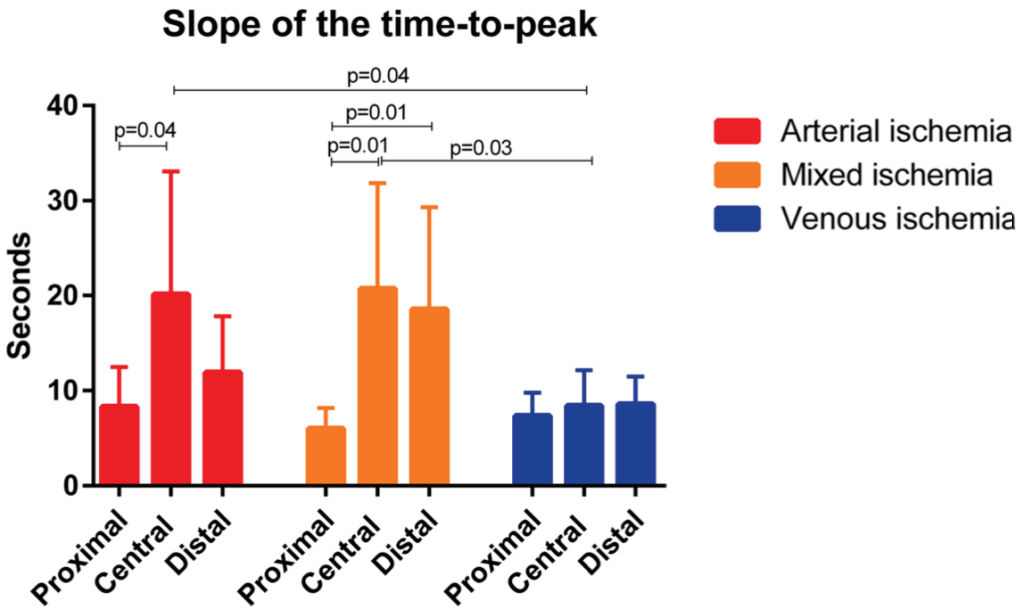


**Fig. 34.** Slope of time-to-peak (seconds) of the 3 different ischemia models at the 3 different ROIs.

- *Normalized intensity fluorescence unit (ratio between the reference card intensity and the fluorescence signal on the bowel wall; 0–1)*

At the central ischemic ROI, the maximal NIFU during the first minute after the injection of ICG, was statistically significantly higher in the V group (1.01±0.21) when compared to both the A (0.61±0.11; $p$=0.002) and to the A-V group (0.41 ± 0.2; $p$=0.0005). Similar results in terms of maximal NIFU were observed at the proximal ROI (V=0.82±0.07 vs. A=0.6±0.2; $p$=0.029; vs. A-V = 0.48±0.09; $p < 0.0001$). At the distal ROI, maximal NIFU was also higher in the V group (0.74±0.2) when compared to A (0.52±0.14; $p$=0.03) and to A-V (0.32±0.11; $p$=0.0015). The results of the over-time evolution of the signal due to the washing out of the fluorophore are reported in **Figure 35**.

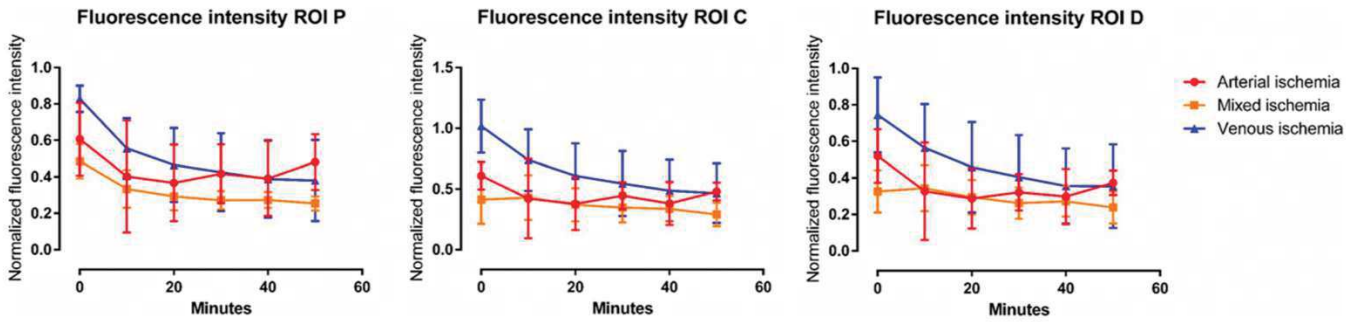


**Fig. 35.** Over-time evolution of fluorescence intensity (NIFU). In ROI C, after 10 min, in the A-V group the NIFU remained stable (0.43±0.18), while it decreased in both the A (0.42±0.32) and V (0.74±0.25) groups, with a significant difference between V and AV ($p$=0.03). Interestingly, in the A group, the signal started rising after the first 20 min of ischemia, and, after 50 min it was significantly higher than the signal observed at the same timepoint in the A-V group (0.48±0.07 vs. 0.29±0.09; $p$=0.003). The evolution of the signal was also different at the proximal and distal ROIs. After 10 min, in the P area, the signal was significantly higher in the V (0.55±0.16) when compared to the A-V group (0.33±0.1; $p$=0.02). The intensity of the signal rose proximally in the A group (0.48±0.15) and the difference was statistically significant when compared to the A-V group (0.25±0.04; $p$=0.005), after 50 min. The same thing occurred distally, after 50 min (A=0.37±0.06 vs. A–V=0.23±0.08; $p$=0.01).

- *Local bowel capillary lactates (mmol/L)*

The results of the local bowel capillary lactates are reported in **Figure 36**. There was a positive correlation between lactate levels collected at 50′ after the ischemia and the slope of time-to-peak in case of both arterial ischemia (Pearson $\rho$ 0.78), and venous ischemia (Pearson $\rho$ 0.88), while no correlation was found in case of mixed ischemia (Pearson $\rho$ 0.54).

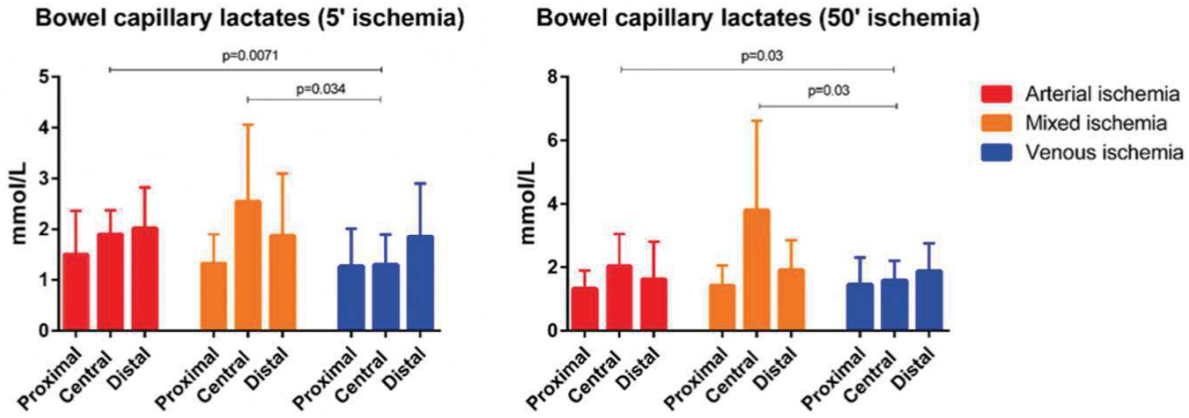


**Fig. 36.** Bowel local capillary lactates. After 5 min of ischemia, mean capillary lactates at the central area in the arterial and mixed ischemia group were statistically significantly higher when compared to those of the venous ischemia group, (A; 1.9±0.5 and A-V; 2.6±1.5 vs. V; 1.3±0.6: $p$=0.0071 and $p$=0.034 respectively). Similarly, after 50 min of ischemia, the values remained significantly higher in the ROI C in both the arterial (2±1) and mixed (3.8±2.8) ischemia when compared to the venous ischemia (1.58±0.6); $p$=0.03 for both. The over-time increase of lactates was not significant, except for ROI C in the venous ischemia (1.3±0.6 vs. 1.58±0.6; $p$=0.049)

- *Machine learning (ML) analysis*

The most accurate algorithms to discriminate the type of ischemia, taking into account the slope of time-to-peak, the maximum fluorescence signal at 1 min and the over-time evolution at 10-50 min, were the *K* Neighbor and the Linear SVM. When the ML was asked to recognize only the type of ischemia, independently of the ROI, the K nearest neighbor and the Linear SVM algorithms both provided an accuracy of 75% in discriminating between A versus V and 85% in discriminating A versus A-V. The accuracy dropped to 70% when the ML had to simultaneously identify the ROI and the type of ischemia.

**STUDY 5: Evaluation of hyperspectral imaging (HSI) for the measurement of ischemic conditioning effects of the gastric conduit during esophagectomy**

The use of HSI imaging intraoperatively proved safe and did not affect the surgical workflow. The regular operative procedure was not prolonged substantially, since the time required to obtain the pseudo-color images was approximately 10 sec. A statistically significant lower mean oxygenation was seen in the gastric conduit at the ROI representing the future anastomotic site in patients without preconditioning (one-step esophagectomy) ($StO_2$= 66%) compared to patients with ischemic preconditioning ($StO_2$=78%; *p*=0.03). Tissue water index (control TWI=59; preconditioning TWI=63) and NIR (control NIR=0.62; preconditioning NIR=0.68) did not show any statistically significant difference **(Figure 37)**. The postoperative course was uneventful in all patients, except for one non-preconditioned patient. This patient developed an anastomotic leak of the intrathoracic area without mediastinitis or sepsis on postoperative day 7, which could be successfully treated conservatively using endoscopic vacuum therapy (Endo-SPONGE®, B Braun, Melsungen, Germany).

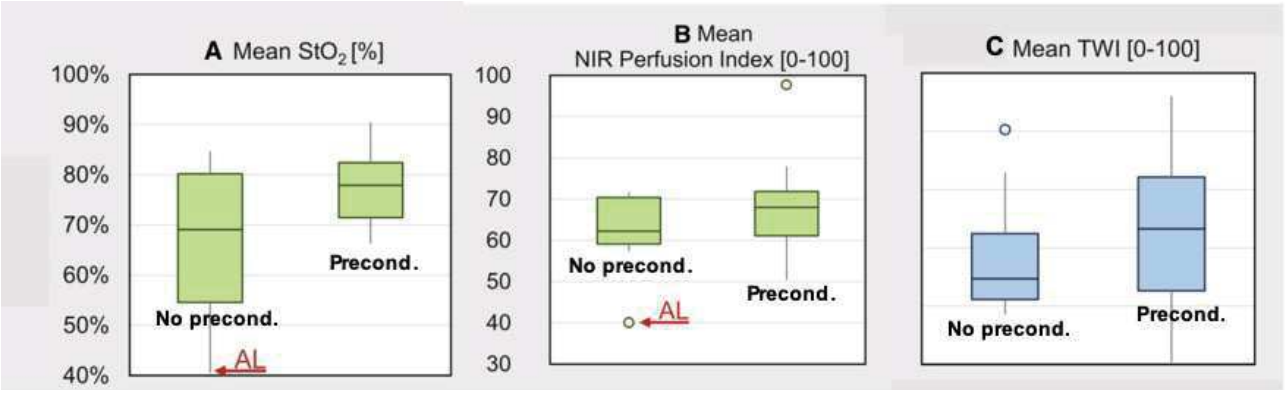


**Fig. 37.** Physiological parameters obtained with the HSI at the future anastomotic site. A) Mean $StO_2$; B) Mean NIR perfusion index; C) Mean TWI. With AL in A and B, perfusion values for the only case of anastomotic leak are graphically shown.
The $StO_2$ in the preconditioning group was higher than in the control group (p= 0.03); for the rest of the parameters, there were no significant differences.

# DISCUSSION

Despite the number of technical improvements in surgery and the increasing use of technology as part of surgical science, the AL rate is still high during gastrointestinal procedures [1, 3, 138] and intraoperative perfusion remains the main factor to be controlled in order to prevent AL [124]. Over the last few years, FA has been increasingly used to assess blood flow intraoperatively and despite its wide acceptance among the surgical community, mainly granted by the low costs, the light procedural workflow and the favorable initial results [7], it has not proven to positively influence the AL rate [11, 13]. The main reason is given by the lack of high-quality studies (heterogeneous protocols in terms of contrast dosage, NIR system used, FA timepoint, lack of published RCT), and above all by the lack of a uniformly accepted FA quantitative assessment. Although quantitative FA has been introduced and validated experimentally using the FLER tool [15, 119, 120], a few other authors have recently used quantitative FA during clinical procedures [130, 131]. The protocols used were based on similar algorithms to FLER, but did not translate the computation of time-to-peak into an enhanced reality perfusion cartography, consequently limiting the intraoperative usability. Additionally, those protocols have not undergone a validation process with controlled animal studies aiming to assess their relationship with biological parameters. A clinical protocol using FLER to assess the perfusion during laparoscopic colectomies has been recently completed, showing interesting results that will soon be available for publication. Nevertheless, the intravenous injection of a contrast agent (ICG) remains a burden from the regulatory point of view and *de facto* limits the distribution of FA solely to surgical research. Hyperspectral imaging, as described in the previous sections, does not use any contrast agent, providing a virtual real-time snapshot of the tissue's physiological state as a result of the tissue-light interaction. Akbari et al. [19] pioneered HSI to detect ischemia on the porcine bowel within a single pig proof-of-the-concept. Indeed, they could successfully identify the ischemic region wavelength (765-830nm). However, they used a rather bulky system made up of two HSI cameras, with a low spectral and spatial resolution, which operated within a large spectral range (400 to 1700nm).

Additionally, with their system a perfusion quantification was not possible. Their remarkable effort remains the first published proof-of-the-concept, with obvious limits in terms of reproducibility, sample size, and lack of biological markers to reinforce the optical imaging observation.
Successively, thanks to the technological improvements, a compact push-broom HSI system (described in the Methods section of this thesis) with a high spectral and spatial resolution, initially designed as a bed-side tool for patients suffering from chronic wounds [139, 140] has been introduced. The system was useful in the follow-up of patients with chronic wounds as it allows to assess and quantify the micro-circulation in real-time. The applicability of this camera to surgical procedures within the operating room has been tested in 2 clinical protocols not included in this thesis. In one study [41], the spectral features of the parathyroid glands from data collected *in vivo* during 9 endocrine neck procedures were successfully determined. This protocol was performed within the framework of a comprehensive HSI-based intraoperative tissue recognition project, coordinated by the writer, which goes beyond the subject of this thesis. This protocol is a joint effort between the University of Leipzig (Innovation Center of Computer-Assisted Surgery (ICCAS) and the Digestive Surgery Department and the IHU of Strasbourg. Thanks to the implementation of advanced machine learning techniques and HSI technology, the aim is an automated intraoperative recognition of target structures. In the second study [42], the system was used during various gastrointestinal procedures to observe the perfusion of gastrointestinal anastomoses *in vivo*.
With the work included in this thesis, our group started by exploring further and then validated hyperspectral imaging as a useful contrast-free tool to quantify perfusion within living animal models in real time. Additionally, in order to overcome the downside of this imaging modality, mainly due to the lack of a video rate, an innovative intraoperative navigation tool known as HYPER has been developed. HYPER was able to virtually detect real-time fine perfusion changes of the porcine gastrointestinal tract with a high degree of accuracy.

Additionally, the implementation of machine learning algorithms in the previously validated FLER concept allowed us to distinguish different ischemia patterns (arterial, venous, and mixed) with a good degree of precision.

Likewise, machine learning techniques enabled us to find the relationship between the reliable bowel ischemia biological parameter LCL and both FLER and HYPER. According to our experience, circumscribed to animal studies with a limited sample size, HYPER showed a significantly higher overall accuracy when compared to FLER.

This was taken a step further. The usability of HSI without the HYPER tool, has been tested to a further extent intraoperatively in a small patients' series, and could provide useful information about gastric conduits that underwent ischemic preconditioning prior to esophageal resection.

**STEP 1: EXPLORING THE CAPABILITY OF HYPERSPECTRAL IMAGING TO QUANTIFY TISSUE PERFUSION IN A LIVING MODEL OF ISCHEMIA (study currently submitted)**

STUDY 1 was performed using the hindlimb ischemia (HLI) murine model. This model is currently widely used in preclinical studies on peripheral arterial disease (PAD). The efficacy of the tested experimental therapies is usually assessed combining intravital (laser Doppler perfusion imaging (LDPI) or MRI angiography) and post-mortem techniques (histology, microcomputed tomography (micro-CT)) [141]. These methods are expensive, time-consuming, and provide meaningful information only if used in combination, since none of them alone are capable of providing non-invasiveness, quantification and good spatial resolution simultaneously. Considering this, as HSI is non-invasive and delivers a real-time precise quantitative perfusion analysis, it could be useful. The HLI murine model used in STUDY 1 was an ischemia/reperfusion model: 2 hours of ischemia were followed by 30 minutes of reperfusion. During reperfusion, the vessel recanalization triggers a

massive reactive oxygen species (ROS) production, causing the ischemia reperfusion injury (IRI). Several strategies have been investigated in order to limit IRI damage, one of them is the pharmacological preconditioning using a phosphodiesterase (PDE) inhibitor. The PDE5-inibitor sildenafil, has shown particularly promising protective effects against IRI on several organs [142-144], although it has recently failed to show improvement in terms of mitochondrial respiration of the skeletal muscle [145]. However, it tended to reduce ROS production, which might be linked to a change in the degree of reperfusion. Accordingly, despite recent advances in the knowledge of PAD pathophysiology [146, 147], the development of more effective therapeutic approaches still represents a strategic target of basic and clinical research.

The results of STUDY 1 demonstrated that HSI was effective in discriminating the non-ischemic and the ischemic limbs. In addition, pharmacological preconditioning using the PDE-5-inhibitor sildenafil did not increment the $StO_2$ levels over the control group and did not show a significant StO2 increase in the reperfusion when compared to the baseline level.

Several authors have previously reported the use of HSI to evaluate the outcomes of hindlimb ischemia models. Poole et al. [141] used a combination of HSI and optical coherence tomography (OCT) to assess disease severity and quantify collateral microcirculation formation in a chronical PAD model, obtained through the ligation and transection of the hindlimb femoral artery in mice. They found that HSI correlated significantly to well-established imaging modalities, such as LDPI and pulse oximetry. Additionally, Grambow et al. used HSI to successfully monitor the outcome of microsurgical anastomoses performed on the rat hind limb. They utilized the same system we used for our study and were able to successfully quantify hind limb ischemia after clamping the femoral artery [148].

Our results show a significant $StO_2$ drop after 2 hours of ischemia in comparison to the pre-ischemia baseline and reperfusion phase. Interestingly, in the control group, the $StO_2$ reperfusion was significantly higher than the baseline levels after 30 minutes. This result is in line with previous

studies on healthy human subjects, in which the $StO_2$ was measured using near-infrared spectroscopy (NIRS) [149]. NIRS clearly differentiated the ischemic phases from the non-ischemic ones, and $StO_2$ increases above the baseline during the reperfusion phase were reported. The downside of NIRS is linked to the necessity to attach several sensors to the skin's surface and to the lack of spatial coordinates. Considering this, HSI offers clear advantages over NIRS, being contactless and providing a good spatial resolution. This is especially convenient in the experimental setting, since $StO_2$ can be exactly quantified repeatedly during the procedure, providing a dynamic information. In addition, the measurement can be performed exactly at the chosen site of the future biopsy.

$StO_2$ values did not show any significant difference in the sildenafil group in comparison with the control at the baseline, after 120 min of ischemia and 30 min of reperfusion. Accordingly, in a previous study performed using only one injection of sildenafil, the protective effect of sildenafil preconditioning against IRI was explored and we could not find any improvement in mitochondrial oxidative and calcium retention capacities within the skeletal muscle [145]. However, a tendency towards ROS reduction was observed. In STUDY 1, we found no $StO_2$ difference with the baseline after 30 minutes of reperfusion in the preconditioning group, whereas a $StO_2$ statistically significantly higher than the baseline was found in the control group. As a result, one might postulate that the sildenafil-related reduced hyperemic impulse observed after ending ischemia might lead to a minor ROS production and/or a better handling of ROS by the cells during the early reperfusion phase. Besides, the beneficial effect of sildenafil on tissue perfusion might need a more chronic administration [145].

Although preconditioning with sildenafil did not improve $StO_2$, it reduced the hyperemic impulse, potentially leading to a minor ROS production during the reperfusion phase. With the completion of STEP 1, we could conclude that hyperspectral imaging is a promising technology to evaluate the

treatment efficacy in murine PAD models, since it is fast, contactless, non-destructive, and provides an objective and spatially resolved $StO_2$ quantification.

Based on the result of this preliminary study, we felt confident to proceed to the next step: the evaluation of HSI to accurately measure bowel perfusion changes in a complex bowel ischemia setup, in the large animal model.

## STEP 2: DEVELOPMENT AND VALIDATION OF HYPER IN THE PORCINE SMALL BOWEL ISCHEMIA MODEL [24]

In STUDY 2, a commercially available HSI system proved to be accurate to quantify bowel perfusion, and proved to be consistent with robust and validated biological markers, such as capillary lactates, ROS, and histopathological evaluation [15, 16, 150-152].
Additionally, with the previous customization of the HSI camera and the implementation of a Python-based software, it was possible to directly overlay the HSI augmented information on the real-time surgical images, obtaining the HYPerspectral-based Enhanced Reality effect (HYPER). The reason for developing HYPER was to overcome the limitation of current HSI systems, which provide spectral information without the corresponding real-time spatial data on the target tissue. In other words, the HSI system currently delivers the spatial information as a static-side-by-side image, which impairs the intraoperative co-localization of the spectral data on the corresponding area of the surgical field. This concept was developed in continuity and by sharing similar setting and validation markers with previous works, aiming to quantify bowel perfusion via FLER [119, 120].
The advantages of HYPER over FLER lie in the fact that HSI provides actual quantitative measures of tissue perfusion parameters and does not require an exogenous contrast agent. Additionally, HSI

can simultaneously analyze perfusion in superficial and deep layers: superficially by quantifying the oxyhemoglobin peak in the visible light and deeply in the NIR spectrum, as explained in detail in the Methods section of this thesis. HSI parameters ($StO_2$ and NIR perfusion index) were congruent with capillary lactate levels at the ROIs discriminated by HYPER. The use of local bowel capillary lactates as a robust marker of vascular supply, provided valuable insights. A high number of paired capillary lactates and StO2 datasets (291) at different timepoints were collected, and it allowed to compute a strong relationship between those two parameters, as shown in **Figure 31**. The local bowel capillary lactates were normalized via systemic lactates to reduce the variability between animals. The training dataset (6 pigs) served to build a predictive model with a machine learning approach and was tested in 5 additional animals, in the same experimental conditions. Interestingly, the prediction algorithm is highly accurate for $StO_2$ values >30%, which are the most difficult to recognize with clinical appreciation only. This has potential clinical relevance, since HSI can precisely identify marginally perfused areas, thereby cross-validating the protocol.

HYPER could also precisely discriminate differently perfused bowel segments and found boundaries with significantly different rates of ROS production and distinct histopathology damage scores **(Figure 30)**, further confirming the accuracy of this technology.

An additional parameter collected with HSI was the tissue water index (TWI). Interestingly, TWI was lower at ROI ISCH when compared to vascular areas, starting at 45' ischemia, but also when compared to the marginal ischemic (MI) segment, starting at 120'. A possible explanation could be the capillary leak induced by the pro-inflammatory cascade, triggering an accentuated edema formation at the ROIs, adjacent to the ischemic segment.

As a matter of fact, HYPER is not currently adapted to minimally invasive surgery, since the current HSI systems are too bulky. Coordinating a consortium resulting from a joint effort of the Research and Development teams of both Diaspective Vision GmbH and Karl Storz GmbH, our research team could develop a miniaturized HSI camera prototype, enabling video rate, and real-time superimposing of the hyperspectral information directly on white light images **(Figure 38)**.

Unfortunately, due to unfavorable timing, the currently undergoing preclinical validation studies of the laparoscopic HSI prototype could not be included in this thesis.

Following the introduction and validation of HYPER the next sensible step was the comparison with FLER.

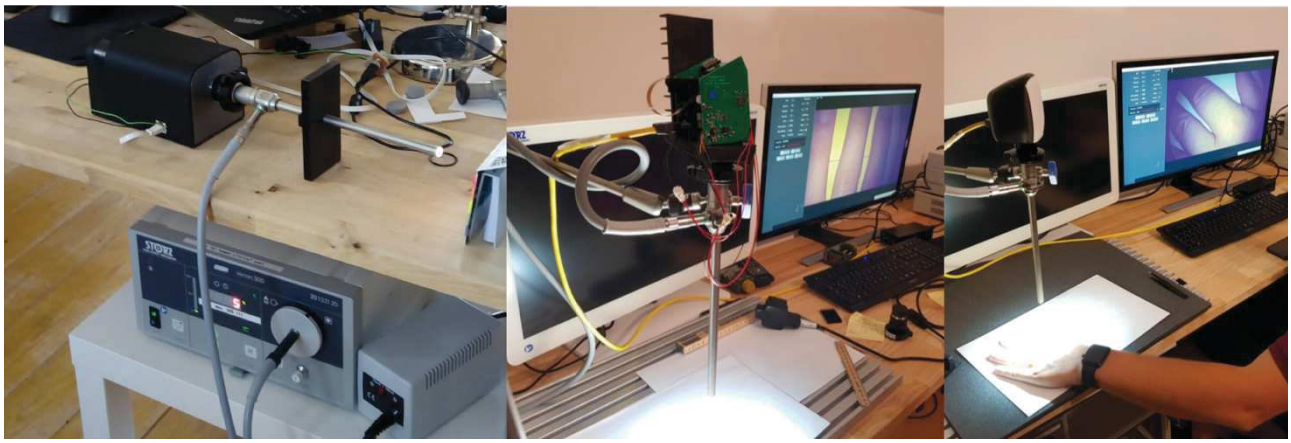

**Fig. 38.** From left to right, the evolution of the miniaturized HSI prototype is shown. The final device (right) is capable of recording with a video rate and it can directly perform HSI analysis during the video. We remain optimistic for a prompt clinical translation, after completion of the preclinical validation.

## STEP 3: COMPARISON OF FLER AND HYPER IN THE PORCINE SMALL BOWEL ISCHEMIA MODEL (study currently submitted)

In the acute experimental setting of a 30-minute porcine small bowel ischemia, described in STUDY 3, the quantitative evaluation of perfusion using hyperspectral imaging was more accurate when compared to quantitative fluorescence-based evaluation. However, the study draws a comparison between a laparoscopic camera and an open HSI camera. Additionally, the results show that both FLER and HYPER provide virtually real-time information, and TTP and $StO_2$ are significantly correlated. Besides, both parameters have a significant relationship with the local capillary lactates sampled at the ROIs [15, 16, 24, 25].

A fitting function between LCL and both FLER TTP and HSI-$StO_2$ was found and yielded two LCL prediction models based on each one of the two optical imaging parameters. It was observed that

both prediction models were less accurate for LCL values >6mmol/L. As a result, a threshold below this value was set, and led to excluding a total of 7 ROIs, which were definitely outliers **(Figure 32)**. In this manner, the precision of prediction algorithms was substantially improved. This finding is in line with the results of STUDY 2, in which we validated HYPER and observed a significantly better accuracy of the LCL prediction model for $StO_2$ values >30% [24]. In the present study, all outlying ROIs (LCL>6mmol/L) showed that $StO_2$ was <30%. Likewise, it is clinically irrelevant to precisely predict the LCL in ROIs which are frankly ischemic based on a quantitative optical imaging analysis and which are often identifiable as non-perfused to the naked eye. The regions for which it is relevant to be accurate are the marginally perfused areas, which are generally difficult to define by the sole exploration under white light and for those very areas where both prediction models showed an acceptable accuracy. The prediction model based on FLER-TTP was significantly less accurate when compared to the HYPER-$StO_2$ based model. An explanation might be given by the fact that small bowel loops underwent a short ischemia period (30 min) in our set-up. During this time, macroscopic signs of tissue suffering are rarely found. However, there are intracellular changes which provoke a reduced mitochondrial activity. As a result, reduced $O_2$ production and increased LCL already take place [16]. The HSI-detected $StO_2$ seems to better mirror those intracellular metabolic changes as compared to FLER, which finally measures a macroscopic phenomenon such as the serosal surface blood flow.

As compared to fluorescence imaging, HSI provides a larger amount of information and quantifies several tissue components, including water, oxygen, and overall hemoglobin content. Additionally, a remarkable advantage when compared to FA is that HSI does not require the use of any contrast agents. In other words, HSI enables an optical, contrast-free, and non-destructive *in vivo* "biopsy" of the surgical field, allowing one to virtually discriminate anatomical structures and characterize tissue physiology.

To the best of our knowledge, STUDY 2 is the first comparison between HSI and quantitative FA to assess bowel perfusion. The strong point of our study lies in its robust design and methodology.

Limitations lie in the fact that the results are obtained in controlled experimental conditions and the clinical application of HYPER has not been demonstrated yet.

In order to explore the influence of ICG on the spectral signal, during the execution of this protocol, we also performed HSI images after intravenous ICG administration, which was required for FLER. We noticed that ICG influences $StO_2$ quantification provided by the HSI system, leading to an $StO_2$ overestimation. The reason is given by the fact that ICG has its maximum emission spectrum at 820nm and the HSI system quantifies $StO_2$ using an algorithm based on the second derivate of the 2 main oxygenated hemoglobin peaks in the electromagnetic spectrum (500-650nm and 700-815nm). As a result, ICG generates an interference on a part of the electromagnetic spectrum corresponding to the oxygenated hemoglobin. Using a machine learning powered prediction model, trained on a large number of datasets obtained from this protocol and other similar protocols that we conducted on different organs, we could generate a prediction algorithm capable of correcting the ICG interference on $StO_2$ quantification **(Figure 39)**. This algorithm is currently undergoing a patenting process.

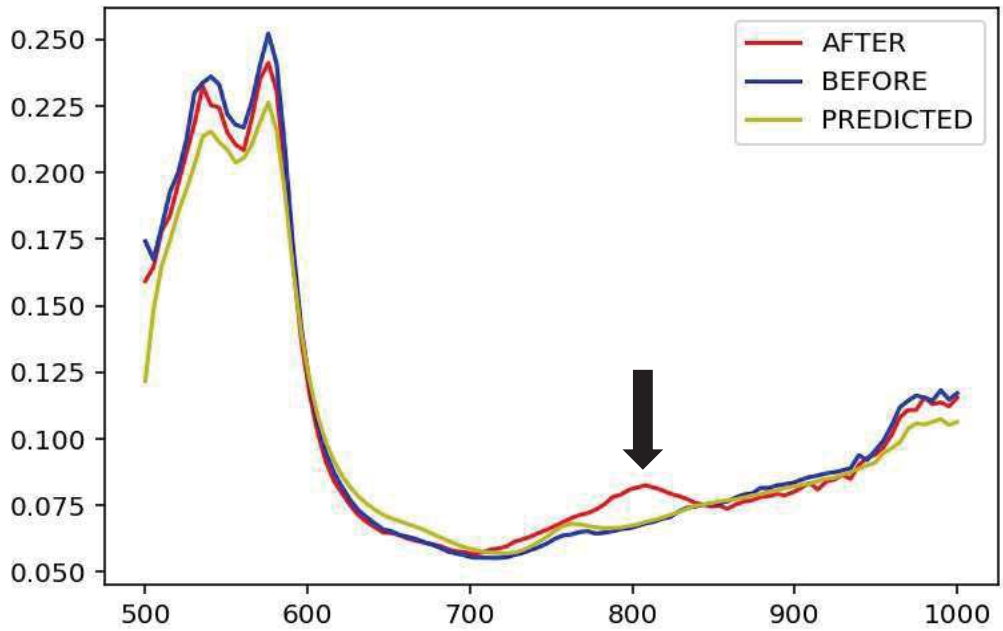


**Fig. 39.** Performance of the ICG correction algorithm. In blue, spectral curve of a bowel loop before ICG injection. In red, spectral curve after ICG injection; around 800nm, the ICG peak is visible (arrow). This peak will lead to overestimation of $StO_2$ quantification. In yellow, the curve predicted using the ML algorithm in order to "correct" the ICG influence and calculate the real $StO_2$ content.

## STEP 4: PLUGS-IN FOR FLER: IMPLEMENTING MACHINE LEARNING TO DISCRIMINATE DIFFERENT PATTERNS OF BOWEL PERFUSION [137]

As already explained in the Methods section of this thesis, during the FLER description, the main principle of quantitative FA is given by the observation that ICG rapidly highlights the vessels upon systemic injection and diffuses quickly not only to the vascularized areas of the tissues but also to the ischemic zones more slowly.

FLER has been largely validated within controlled animal experiments using robust surrogates for bowel ischemia [15, 119, 120]. As a result, several authors progressively began to use similar quantitative FA solutions based on the ICG diffusion velocity in the differently perfused areas in clinical trials [130, 131, 153]. The main difference with FLER is that none of the solution proposed allowed for a real-time enhanced reality environment. Currently, the FLER software is undergoing implementation of new features, including motion tracking and different machine learning algorithms, in order to interpret the data more accurately. In this context, in STUDY 4, we created 3 different ischemia groups (arterial, venous, and mixed) by clamping the inferior mesenteric vessels differently and by analyzing the fluorescent signal on the sigmoid colon using FLER. We hypothesized that the 3 different ischemic models would present different patterns in terms of signal increase and washout, when analyzed with the FLER software. In a nutshell, in case of venous-only ischemia, the fluorescent signal is initially brighter with a significantly shorter TTP when compared to arterial and mixed ischemia. In case of arterial ischemia, after the initial drop during the first 20 min of ischemia, the signal starts to rise again, alimented by a backflow refill of ICG not occurring with the other ischemia types, and that was significantly higher than the signal observed at the same time point in the A-V group.

Despite the low sample size, differences in the patterns allowed for a successful application of an ML approach. The most accurate algorithms, selected with the "leave-one-out cross-validation" method, could discriminate between arterial and venous ischemia with a 75% accuracy and up to an 85% accuracy to discriminate between arterial versus mixed ischemia. To validate the results and correlate with imaging, the level of capillary lactates (largely validated [118-120, 151]) on the bowel were measured with the strip-based lactate analyzer.

The capacity to accurately distinguish different types of ischemia might be useful during esophageal resection, since it was observed that poor arterial blood supply and venous congestion of the gastric conduit might lead to complications, in particular to AL [154, 155]. The ability to intraoperatively detect a vascular compromise of the gastric conduit and to discriminate between an arterial insufficiency and a venous congestion might lead to perform salvage procedures to improve blood flow and venous drainage. These include the technique of supercharged micro-vascular anastomosis, between short gastric vessels with cervical transverse artery and external jugular vein [156] and transient bloodletting to improve gastric microcirculation [157].

## STEP 5: APPLICATION OF HSI IN THE CLINICAL CONTEXT: REAL-TIME PERFUSION ASSESSMENT AT THE FUTURE ANASTOMOTIC SITE ON THE GASTRIC CONDUIT [23]

The primary aim of STUDY 5 was to assess the feasibility and reliability of HSI to intraoperatively quantify perfusion at the future anastomotic site, during a major surgical procedure such as an Ivor-Lewis esophagectomy. Secondarily, a subset of our patients' series (14 out of 22) underwent an ischemic precondition through a laparoscopic gastrolysis a few days prior to esophagectomy. Although the sample size was clearly underpowered and the time delay between ischemic

preconditioning and the main operation was variable and rather short (3-7 days), HSI could find an increase in $StO_2$ at the future anastomotic site of the preconditioning group, when compared to the control group.

To the best of our knowledge, this is the first clinical study in which HSI is used to intraoperatively assess perfusion during esophagectomy. In the past, other authors used different methods to measure the gastric tube blood flow intraoperatively, those include optical fiber spectroscopy (OFS) [158, 159] or laser Doppler flowmetry (LDF) [160, 161]. Although OFS can measure tissue oxygenation, similarly to HSI, it has a very low spatial resolution, since it is based on point measurement obtained with the optical fiber probe. Differently from HIS, LDF assesses blood flow intraoperatively, yet still with a low spatial resolution and often with a cumbersome workflow. Consequently, both OFS and LDF failed to become routine tools to assess anastomotic viability intraoperatively.

Recently, a few authors [162, 163] started to use FA to assess gastric conduit perfusion during esophagectomy. In both studies, the sample size was small, and the assessment was subjective, without quantitative analysis, and therefore larger studies with quantitative evaluation are required to understand the role of FA during esophageal surgery.

With regards to ischemic preconditioning, in the past several authors explored this technique with the aim to improve the rates of AL, which remain high during esophagectomy, ranging from 20 to 35% [33]. The previous studies supporting the concept of ischemic conditioning [164-166] were of a non-randomized character. However, the LOGIC trial [160], namely the only prospective randomized controlled trial did not show any increase in the anastomotic perfusion measured via LDF. The reason might be given by the fact that the study was underpowered and probably, since LDF exclusively measures perfusion and since ischemic preconditioning triggers neoangiogenesis at the level of the capillary network [167], this was not the appropriate tool to detect those fine microcirculatory changes. HSI has already proven to be rather effective in assessing microperfusion in the field of wound diagnosis [20, 140]. As a result, it might be a more appropriate tool to detect the viability improvement ensured by ischemic preconditioning. This is in line with the result of our small study.

Additionally, we completed another experimental study (not included in this thesis), in which a percutaneous embolic ischemic preconditioning was performed in the porcine model 3 weeks prior to surgery. After a three-week survival, a gastric tubulization was performed and perfusion was assessed at the serosal side using both FLER and HYPER and on the mucosal side using confocal microscopy. As biological parameters, we chose local capillary lactate and neoangiogenesis markers. In the preliminary results, we noticed a significant perfusion increase in the preconditioning group over the control group. This was also confirmed by biological data. The completion of data analysis and manuscript preparation is currently underway.

# CONCLUSIONS

HSI provides an accurate evaluation of bowel perfusion, which is congruent with biological markers, including capillary lactates, radicals of oxygen production, and histopathology. The HYPER tool improves the usability of HSI technology in the operating room as a bridge before the development of a fast hyperspectral video rate imaging.

In the acute experimental setting, the quantitative evaluation of perfusion using hyperspectral imaging was more accurate when compared to a quantitative fluorescence-based evaluation.

Clinical translation of HSI was successful and provided good results within major surgical procedures.

The next step is clinical translation and the evaluation of the impact of HYPER on the incidence of anastomotic leakage.

A prospective controlled clinical trial has been planned and will begin in 2020.

# References:


1. Urbanavicius L, Pattyn P, de Putte DV, Venskutonis D (2011) How to assess intestinal viability during surgery: A review of techniques. World J Gastrointest Surg 3:59-69

2. Karliczek A, Benaron DA, Baas PC, Zeebregts CJ, Wiggers T, van Dam GM Intraoperative assessment of microperfusion with visible light spectroscopy for prediction of anastomotic leakage in colorectal anastomoses. Colorectal Dis 12:1018-1025

3. Karliczek A, Harlaar NJ, Zeebregts CJ, Wiggers T, Baas PC, van Dam GM (2009) Surgeons lack predictive accuracy for anastomotic leakage in gastrointestinal surgery. Int J Colorectal Dis 24:569-576

4. Baiocchi GL, Diana M, Boni L (2018) Indocyanine green-based fluorescence imaging in visceral and hepatobiliary and pancreatic surgery: State of the art and future directions. World J Gastroenterol 24:2921-2930

5. Diana M (2017) Enabling precision digestive surgery with fluorescence imaging. Transl Gastroenterol Hepatol 2:97

6. Diana M (2017) Fluorescence-guided surgery applied to the digestive system: the cybernetic eye to see the invisible. Cir Esp

7. Kudszus S, Roesel C, Schachtrupp A, Hoer JJ (2010) Intraoperative laser fluorescence angiography in colorectal surgery: a noninvasive analysis to reduce the rate of anastomotic leakage. Langenbecks Arch Surg 395:1025-1030

8. Matsui A, Winer JH, Laurence RG, Frangioni JV (2011) Predicting the survival of experimental ischaemic small bowel using intraoperative near-infrared fluorescence angiography. Br J Surg 98:1725-1734

9. Jafari MD, Wexner SD, Martz JE, McLemore EC, Margolin DA, Sherwinter DA, Lee SW, Senagore AJ, Phelan MJ, Stamos MJ (2015) Perfusion assessment in laparoscopic left-sided/anterior resection (PILLAR II): a multi-institutional study. J Am Coll Surg 220:82-92 e81

10. Ris F, Liot E, Buchs NC, Kraus R, Ismael G, Belfontali V, Douissard J, Cunningham C, Lindsey I, Guy R, Jones O, George B, Morel P, Mortensen NJ, Hompes R, Cahill RA, Near-Infrared Anastomotic Perfusion Assessment Network V (2018) Multicentre phase II trial of near-infrared imaging in elective colorectal surgery. Br J Surg 105:1359-1367

11. Blanco-Colino R, Espin-Basany E (2018) Intraoperative use of ICG fluorescence imaging to reduce the risk of anastomotic leakage in colorectal surgery: a systematic review and meta-analysis. Tech Coloproctol 22:15-23

12. Karampinis I, Keese M, Jakob J, Stasiunaitis V, Gerken A, Attenberger U, Post S, Kienle P, Nowak K (2018) Indocyanine Green Tissue Angiography Can Reduce Extended Bowel Resections in Acute Mesenteric Ischemia. J Gastrointest Surg

13. van den Bos J, Al-Taher M, Schols RM, van Kuijk S, Bouvy ND, Stassen LPS (2018) Near-Infrared Fluorescence Imaging for Real-Time Intraoperative Guidance in Anastomotic Colorectal Surgery: A Systematic Review of Literature. J Laparoendosc Adv Surg Tech A 28:157-167

14. Vallance A, Wexner S, Berho M, Cahill R, Coleman M, Haboubi N, Heald RJ, Kennedy RH, Moran B, Mortensen N, Motson RW, Novell R, O'Connell PR, Ris F, Rockall T, Senapati A, Windsor A, Jayne DG (2017) A collaborative review of the current concepts and challenges of anastomotic leaks in colorectal surgery. Colorectal Dis 19:O1-O12

15. Diana M, Agnus V, Halvax P, Liu YY, Dallemagne B, Schlagowski AI, Geny B, Diemunsch P, Lindner V, Marescaux J (2015) Intraoperative fluorescence-based enhanced reality laparoscopic real-time imaging to assess bowel perfusion at the anastomotic site in an experimental model. Br J Surg 102:e169-176

16. Diana M, Noll E, Diemunsch P, Dallemagne B, Benahmed MA, Agnus V, Soler L, Barry B, Namer IJ, Demartines N, Charles AL, Geny B, Marescaux J (2014) Enhanced-reality video fluorescence: a real-time assessment of intestinal viability. Ann Surg 259:700-707

17. Wada T, Kawada K, Takahashi R, Yoshitomi M, Hida K, Hasegawa S, Sakai Y (2017) ICG fluorescence imaging for quantitative evaluation of colonic perfusion in laparoscopic colorectal surgery. Surg Endosc 31:4184-4193

18. Lu G, Fei B (2014) Medical hyperspectral imaging: a review. J Biomed Opt 19:10901

19. Akbari H, Kosugi Y, Kojima K, Tanaka N (2010) Detection and analysis of the intestinal ischemia using visible and invisible hyperspectral imaging. IEEE Trans Biomed Eng 57:2011-2017

20. Holmer A, Marotz J, Wahl P, Dau M, Kammerer PW (2018) Hyperspectral imaging in perfusion and wound diagnostics - methods and algorithms for the determination of tissue parameters. Biomed Tech (Berl) 63:547-556

21. Diana M, Halvax P, Dallemagne B, Nagao Y, Diemunsch P, Charles AL, Agnus V, Soler L, Demartines N, Lindner V, Geny B, Marescaux J (2014) Real-time navigation by fluorescence-based enhanced reality for precise estimation of future anastomotic site in digestive surgery. Surg Endosc 28:3108-3118

22. Jansen-Winkeln B, Holfert N, Köhler H, Moulla Y, Takoh JP, Rabe SM, Mehdorn M, Barberio M, Chalopin C, Neumuth T, Gockel IJIJoCD (2019) Determination of the transection margin during colorectal resection with hyperspectral imaging (HSI).

23. Kohler H, Jansen-Winkeln B, Maktabi M, Barberio M, Takoh J, Holfert N, Moulla Y, Niebisch S, Diana M, Neumuth T, Rabe SM, Chalopin C, Melzer A, Gockel I (2019) Evaluation of hyperspectral imaging (HSI) for the measurement of ischemic conditioning effects of the gastric conduit during esophagectomy. Surg Endosc

24. Barberio M, Longo F, Fiorillo C, Seeliger B, Mascagni P, Agnus V, Lindner V, Geny B, Charles AL, Gockel I, Worreth M, Saadi A, Marescaux J, Diana M (2019) HYPerspectral Enhanced Reality (HYPER): a physiology-based surgical guidance tool. Surg Endosc

25. Quero G, Lapergola A, Barberio M, Seeliger B, Gockel I, Saccomandi P, Guerriero L, Mutter D, Saadi A, Worreth M, Marescaux J, Agnus V, Diana M (2019) Correction to: Discrimination between arterial and venous bowel ischemia by computer-assisted analysis of the fluorescent signal. Surg Endosc

26. Mascagni P, Longo F, Barberio M, Seeliger B, Agnus V, Saccomandi P, Hostettler A, Marescaux J, Diana M (2018) New intraoperative imaging technologies: Innovating the surgeon's eye toward surgical precision. J Surg Oncol 118:265-282

27. Collins FS, Varmus H (2015) A new initiative on precision medicine. N Engl J Med 372:793-795

28. Marescaux J, Diana M (2015) Next step in minimally invasive surgery: hybrid image-guided surgery. J Pediatr Surg 50:30-36

29. Weissleder R, Pittet MJ (2008) Imaging in the era of molecular oncology. Nature 452:580-589

30. Watanabe R, Barberio M, Kanaji S, Lapergola A, Ashoka AH, Andreiuk B, Guerriero L, Pizzicannella M, Seeliger B, Saida Y, Kaneko H, Worreth M, Saadi A, Marescaux J, Klymchenko AS, Diana M (2019) Hybrid fluorescent magnetic gastrojejunostomy: an experimental feasibility study in the porcine model and human cadaver. Surg Endosc

31. Ho YH, Ashour MA (2010) Techniques for colorectal anastomosis. World J Gastroenterol 16:1610-1621

32. Oines MN, Krarup PM, Jorgensen LN, Agren MS (2014) Pharmacological interventions for improved colonic anastomotic healing: a meta-analysis. World J Gastroenterol 20:12637-12648

33. Campbell C, Reames MK, Robinson M, Symanowski J, Salo JC (2015) Conduit Vascular Evaluation is Associated with Reduction in Anastomotic Leak After Esophagectomy. J Gastrointest Surg 19:806-812

34. Frasson M, Flor-Lorente B, Rodriguez JL, Granero-Castro P, Hervas D, Alvarez Rico MA, Brao MJ, Sanchez Gonzalez JM, Garcia-Granero E, Group AS (2015) Risk Factors for Anastomotic Leak After Colon Resection for Cancer: Multivariate Analysis and Nomogram From a Multicentric, Prospective, National Study With 3193 Patients. Ann Surg 262:321-330

35. Hayden DM, Mora Pinzon MC, Francescatti AB, Saclarides TJ (2015) Patient factors may predict anastomotic complications after rectal cancer surgery: Anastomotic complications in rectal cancer. Ann Med Surg (Lond) 4:11-16

36. Ballantyne GH, Burke JB, Rogers G, Lampert EG, Boccia J (1985) Accelerated wound healing with stapled enteric suture lines. An experimental study comparing traditional sewing techniques and a stapling device. Ann Surg 201:360-364

37. Lustosa SA, Matos D, Atallah AN, Castro AA (2001) Stapled versus handsewn methods for colorectal anastomosis surgery. Cochrane Database Syst Rev:CD003144

38. Rutegard M, Rutegard J (2015) Anastomotic leakage in rectal cancer surgery: The role of blood perfusion. World J Gastrointest Surg 7:289-292

39. Bjerregaard J, Pandia MP, Jaffe RA (2013) Occurrence of severe hypotension after indocyanine green injection during the intraoperative period. A A Case Rep 1:26-30

40. Chu W, Chennamsetty A, Toroussian R, Lau C (2017) Anaphylactic Shock After Intravenous Administration of Indocyanine Green During Robotic Partial Nephrectomy. Urol Case Rep 12:37-38

41. Barberio M, Maktabi M, Gockel I, Rayes N, Jansen-Winkeln B, Köhler H, Rabe Sebastian M, Seidemann L, Takoh Jonathan P, Diana M, Neumuth T, Chalopin C (2018) Hyperspectral based discrimination of thyroid and parathyroid during surgery. Current Directions in Biomedical Engineering, pp 399

42. Jansen-Winkeln B, Maktabi M, Takoh JP, Rabe SM, Barberio M, Kohler H, Neumuth T, Melzer A, Chalopin C, Gockel I (2018) [Hyperspectral imaging of gastrointestinal anastomoses]. Chirurg 89:717-725

43. Goetz AF (2009) Three decades of hyperspectral remote sensing of the Earth: A personal view. Remote Sensing of Environment 113:S5-S16

44. Govender M, Chetty K, Bulcock H (2007) A review of hyperspectral remote sensing and its application in vegetation and water resource studies. Water Sa 33

45. Adam E, Mutanga O, Rugege D (2010) Multispectral and hyperspectral remote sensing for identification and mapping of wetland vegetation: a review. Wetlands Ecology and Management 18:281-296

46. Fischer C, Kakoulli I (2006) Multispectral and hyperspectral imaging technologies in conservation: current research and potential applications. Studies in Conservation 51:3-16

47. Liang H (2012) Advances in multispectral and hyperspectral imaging for archaeology and art conservation. Applied Physics A 106:309-323

48. Gowen A, O'Donnell C, Cullen P, Downey G, Frias J (2007) Hyperspectral imaging–an emerging process analytical tool for food quality and safety control. Trends in food science & technology 18:590-598

49. Feng Y-Z, Sun D-W (2012) Application of hyperspectral imaging in food safety inspection and control: a review. Critical reviews in food science and nutrition 52:1039-1058

50. Edelman G, Gaston E, Van Leeuwen T, Cullen P, Aalders M (2012) Hyperspectral imaging for non-contact analysis of forensic traces. Forensic science international 223:28-39

51. Malkoff DB, Oliver WR (2000) Hyperspectral imaging applied to forensic medicine. Spectral Imaging: Instrumentation, Applications, and Analysis, International Society for Optics and Photonics, pp 108-116

52. Kuula J, Pölönen I, Puupponen H-H, Selander T, Reinikainen T, Kalenius T, Saari H (2012) Using VIS/NIR and IR spectral cameras for detecting and separating crime scene details. Sensors, and Command, Control, Communications, and Intelligence (C3I) Technologies for Homeland Security and Homeland Defense XI, International Society for Optics and Photonics, pp 83590P

53. Schuler RL, Kish PE, Plese CA (2012) Preliminary observations on the ability of hyperspectral imaging to provide detection and visualization of bloodstain patterns on black fabrics. Journal of forensic sciences 57:1562-1569

54. Carrasco O, Gomez RB, Chainani A, Roper WE (2003) Hyperspectral imaging applied to medical diagnoses and food safety. Geo-Spatial and Temporal Image and Data Exploitation III, International Society for Optics and Photonics, pp 215-221

55. Li Q (2012) Hyperspectral imaging technology used in tongue diagnosis. Recent advances in theories and practice of Chinese Medicine, IntechOpen

56. Li Q, He X, Wang Y, Liu H, Xu D, Guo F (2013) Review of spectral imaging technology in biomedical engineering: achievements and challenges. J Biomed Opt 18:100901

57. Mazzer PYCN, Barbieri CH, Mazzer N, Fazan VPS (2008) Morphologic and morphometric evaluation of experimental acute crush injuries of the sciatic nerve of rats. Journal of neuroscience methods 173:249-258

58. Aikio M (2001) Hyperspectral prism-grating-prism imaging spectrograph.

59. Sun D-W (2010) Hyperspectral imaging for food quality analysis and control, Elsevier

60. Ferris DG, Lawhead RA, Dickman ED, Holtzapple N, Miller JA, Grogan S, Bambot S, Agrawal A, Faupel ML (2001) Multimodal hyperspectral imaging for the noninvasive diagnosis of cervical neoplasia. J Low Genit Tract Dis 5:65-72

61. Benavides J, Chang S, Park S, Richards-Kortum R, Mackinnon N, Macaulay C, Milbourne A, Malpica A, Follen M (2003) Multispectral digital colposcopy for in vivo detection of cervical cancer. Opt Express 11:1223-1236

62. Hattery D, Hassan M, Demos S, Gandjbakhche A (2002) Hyperspectral imaging of Kaposi's Sarcoma for disease assessment and treatment monitoring. Applied Imagery Pattern Recognition Workshop, 2002. Proceedings., IEEE, pp 124-130

63. Roblyer D, Kurachi C, Gillenwater AM, Richards-Kortum R (2009) In vivo fluorescence hyperspectral imaging of oral neoplasia. Advanced Biomedical and Clinical Diagnostic Systems VII, International Society for Optics and Photonics, pp 71690J

64. Panasyuk SV, Yang S, Faller DV, Ngo D, Lew RA, Freeman JE, Rogers AE (2007) Medical hyperspectral imaging to facilitate residual tumor identification during surgery. Cancer biology & therapy 6:439-446

65. Ogihara H, Hamamoto Y, Fujita Y, Goto A, Nishikawa J, Sakaida I (2016) Development of a gastric cancer diagnostic support system with a pattern recognition method using a hyperspectral camera. Journal of Sensors 2016

66. Zuzak K, Schaeberle M, Levin I, Lewis N, Freeman J, McNeil J, Cancio L (1999) Visible and infrared hyperspectral visualization of normal and ischemic tissue. Proceedings of the First Joint BMES/EMBS Conference. 1999 IEEE Engineering in Medicine and Biology 21st Annual Conference and the 1999 Annual Fall Meeting of the Biomedical Engineering Society (Cat. N, IEEE, pp 1118 vol. 1112

67. Zuzak KJ, Schaeberle MD, Lewis EN, Levin IW (2000) Visible spectroscopic imaging studies of normal and ischemic dermal tissue. Biomedical Spectroscopy: Vibrational Spectroscopy and Other Novel Techniques, International Society for Optics and Photonics, pp 17-26

68. Zuzak KJ, Schaeberle MD, Lewis EN, Levin IW (2002) Visible reflectance hyperspectral imaging: characterization of a noninvasive, in vivo system for determining tissue perfusion. Analytical chemistry 74:2021-2028

69. Chin JA, Wang EC, Kibbe MR (2011) Evaluation of hyperspectral technology for assessing the presence and severity of peripheral artery disease. Journal of vascular surgery 54:1679-1688

70. Zuzak KJ, Naik SC, Alexandrakis G, Hawkins D, Behbehani K, Livingston EH (2007) Characterization of a near-infrared laparoscopic hyperspectral imaging system for minimally invasive surgery. Analytical chemistry 79:4709-4715

71. Zuzak KJ, Naik SC, Alexandrakis G, Hawkins D, Behbehani K, Livingston E (2008) Intraoperative bile duct visualization using near-infrared hyperspectral video imaging. The American Journal of Surgery 195:491-497

72. Akbari H, Kosugi Y, Kojima K, Tanaka N (2010) Detection and analysis of the intestinal ischemia using visible and invisible hyperspectral imaging. IEEE Transactions on Biomedical Engineering 57:2011-2017

73. Gioux S, Choi HS, Frangioni JV (2010) Image-guided surgery using invisible near-infrared light: fundamentals of clinical translation. Molecular imaging 9:7290.2010. 00034

74. Nguyen QT, Tsien RY (2013) Fluorescence-guided surgery with live molecular navigation—a new cutting edge. Nature reviews cancer 13:653

75. Alander JT, Kaartinen I, Laakso A, Pätilä T, Spillmann T, Tuchin VV, Venermo M, Välisuo P (2012) A review of indocyanine green fluorescent imaging in surgery. Journal of Biomedical Imaging 2012:7

76. Marshall MV, Rasmussen JC, Tan I-C, Aldrich MB, Adams KE, Wang X, Fife CE, Maus EA, Smith LA, Sevick-Muraca EM (2010) Near-infrared fluorescence imaging in humans with indocyanine green: a review and update. Open surgical oncology journal (Online) 2:12

77. Matsui A, Tanaka E, Choi HS, Kianzad V, Gioux S, Lomnes SJ, Frangioni JV (2010) Real-time, near-infrared, fluorescence-guided identification of the ureters using methylene blue. Surgery 148:78-86

78. Shin D, Vigneswaran N, Gillenwater A, Richards-Kortum R (2010) Advances in fluorescence imaging techniques to detect oral cancer and its precursors. Future oncology 6:1143-1154

79. D'Hallewin M-A, Bezdetnaya L, Guillemin F (2002) Fluorescence detection of bladder cancer: a review. European urology 42:417-425

80. Tsuruki ES, Saito Y, Abe S, Takamaru H, Yamada M, Sakamoto T, Nakajima T, Matsuda T, Sekine S, Taniguchi H (2016) Evaluating the efficacy and safety of a novel endoscopic fluorescence imaging modality using oral 5-aminolevulinic acid for colorectal tumors. Endoscopy international open 4:E30-E35

81. Hellebust A, Richards-Kortum R (2012) Advances in molecular imaging: targeted optical contrast agents for cancer diagnostics. Nanomedicine 7:429-445

82. Sevick-Muraca EM, Houston JP, Gurfinkel M (2002) Fluorescence-enhanced, near infrared diagnostic imaging with contrast agents. Current opinion in chemical biology 6:642-650

83. Ntziachristos V, Bremer C, Weissleder R (2003) Fluorescence imaging with near-infrared light: new technological advances that enable in vivo molecular imaging. European radiology 13:195-208

84. Themelis G, Yoo JS, Soh K, Schulz RB, Ntziachristos V (2009) Real-time intraoperative fluorescence imaging system using light-absorption correction. Journal of biomedical optics 14:064012

85. Flum DR, Cheadle A, Prela C, Dellinger EP, Chan L (2003) Bile duct injury during cholecystectomy and survival in medicare beneficiaries. Jama 290:2168-2173

86. Navez B, Ungureanu F, Michiels M, Claeys D, Muysoms F, Hubert C, Vanderveken M, Detry O, Detroz B, Closset J (2012) Surgical management of acute cholecystitis: results of a 2-year prospective multicenter survey in Belgium. Surgical endoscopy 26:2436-2445

87. Mir IS, Mohsin M, Kirmani O, Majid T, Wani K, Hassan M-u, Naqshbandi J, Maqbool M (2007) Is intra-operative cholangiography necessary during laparoscopic cholecystectomy? A multicentre rural experience from a developing world country. World journal of gastroenterology: WJG 13:4493

88. Kaczynski J, Hilton J (2015) A gallbladder with the “hidden cystic duct”: a brief overview of various surgical techniques of the Calot’s triangle dissection. Interventional Medicine and Applied Science 7:42-45

89. Boni L, David G, Mangano A, Dionigi G, Rausei S, Spampatti S, Cassinotti E, Fingerhut A (2015) Clinical applications of indocyanine green (ICG) enhanced fluorescence in laparoscopic surgery. Surgical endoscopy 29:2046-2055

90. Ishizawa T, Bandai Y, Ijichi M, Kaneko J, Hasegawa K, Kokudo N (2010) Fluorescent cholangiography illuminating the biliary tree during laparoscopic cholecystectomy. British Journal of Surgery 97:1369-1377

91. Schols RM, Bouvy ND, van Dam RM, Masclee AA, Dejong CH, Stassen LP (2013) Combined vascular and biliary fluorescence imaging in laparoscopic cholecystectomy. Surgical endoscopy 27:4511-4517

92. Pesce A, Piccolo G, La Greca G, Puleo S (2015) Utility of fluorescent cholangiography during laparoscopic cholecystectomy: a systematic review. World journal of gastroenterology: WJG 21:7877

93. Verbeek FP, Schaafsma BE, Tummers QR, van der Vorst JR, van der Made WJ, Baeten CI, Bonsing BA, Frangioni JV, van de Velde CJ, Vahrmeijer AL (2014) Optimization of near-infrared fluorescence cholangiography for open and laparoscopic surgery. Surgical endoscopy 28:1076-1082

94. Liu Y-Y, Kong S-H, Diana M, Lègner A, Wu C-C, Kameyama N, Dallemagne B, Marescaux J (2016) Near-infrared cholecysto-cholangiography with indocyanine green may secure cholecystectomy in difficult clinical situations: proof of the concept in a porcine model. Surgical endoscopy 30:4115-4123

95. Lee J-H, Lee MS, Kim H-H, Park DJ, Lee KH, Hwang J-Y, Lee H-J, Yang H-K, Lee KU (2011) Feasibility of laparoscopic partial gastrectomy with sentinel node basin dissection in a porcine model. Surgical endoscopy 25:1070-1075

96. Mitsumori N, Nimura H, Takahashi N, Kawamura M, Aoki H, Shida A, Omura N, Yanaga K (2014) Sentinel lymph node navigation surgery for early stage gastric cancer. World journal of gastroenterology: WJG 20:5685

97. Miwa K, Kinami S, Taniguchi K, Fushida S, Fujimura T, Nonomura A (2003) Mapping sentinel nodes in patients with early-stage gastric carcinoma. British journal of surgery 90:178-182

98. Miyashiro I, Hiratsuka M, Sasako M, Sano T, Mizusawa J, Nakamura K, Nashimoto A, Tsuburaya A, Fukushima N, Group GCSS (2014) High false-negative proportion of intraoperative histological examination as a serious problem for clinical application of sentinel node biopsy for early gastric cancer: final results of the Japan Clinical Oncology Group multicenter trial JCOG0302. Gastric Cancer 17:316-323

99. Lohman RF, Ozturk CN, Ozturk C, Jayaprakash V, Djohan R (2015) An analysis of current techniques used for intraoperative flap evaluation. Annals of plastic surgery 75:679-685

100. Sekijima M, Tojimbara T, Sato S, Nakamura M, Kawase T, Kai K, Urashima Y, Nakajima I, Fuchinoue S, Teraoka S (2004) An intraoperative fluorescent imaging system in organ transplantation. Transplantation proceedings, Elsevier, pp 2188-2190

101. Arichi N, Mitsui Y, Ogawa K, Nagami T, Nakamura S, Hiraoka T, Yasumoto H, Shiina H (2014) Intraoperative fluorescence vascular imaging using indocyanine green for assessment of transplanted kidney perfusion. Transplantation proceedings, Elsevier, pp 342-345

102. Griendling KK, Touyz RM, Zweier JL, Dikalov S, Chilian W, Chen Y-R, Harrison DG, Bhatnagar A (2016) Measurement of reactive oxygen species, reactive nitrogen species, and redox-dependent signaling in the cardiovascular system: a scientific statement from the American Heart Association. Circulation research 119:e39-e75

103. Süzen S (2007) Antioxidant activities of synthetic indole derivatives and possible activity mechanisms. Bioactive Heterocycles V, Springer, pp 145-178

104. Hybertson BM, Gao B, Bose SK, McCord JM (2011) Oxidative stress in health and disease: the therapeutic potential of Nrf2 activation. Molecular aspects of medicine 32:234-246

105. Suzen S, Gurer-Orhan H, Saso L (2017) Detection of reactive oxygen and nitrogen species by electron paramagnetic resonance (EPR) technique. Molecules 22:181

106. Kohno M (2010) Applications of electron spin resonance spectrometry for reactive oxygen species and reactive nitrogen species research. Journal of clinical biochemistry and nutrition:1006170036-1006170036

107. Glinghammar B, Rafter I, Lindström A-K, Hedberg JJ, Andersson HB, Lindblom P, Berg A-L, Cotgreave I (2009) Detection of the mitochondrial and catalytically active alanine aminotransferase in human tissues and plasma. International journal of molecular medicine 23:621-631

108. Perriello G, Jorde R, Nurjhan N, Stumvoll M, Dailey G, Jenssen T, Bier D, Gerich J (1995) Estimation of glucose-alanine-lactate-glutamine cycles in postabsorptive humans: role of skeletal muscle. American Journal of Physiology-Endocrinology And Metabolism 269:E443-E450

109. De Backer D (2003) Lactic acidosis. Intensive care medicine 29:699-702

110. Adeva-Andany M, López-Ojén M, Funcasta-Calderón R, Ameneiros-Rodríguez E, Donapetry-García C, Vila-Altesor M, Rodríguez-Seijas J (2014) Comprehensive review on lactate metabolism in human health. Mitochondrion 17:76-100

111. Boekstegers P, Weidenhöfer S, Kapsner T, Werdan K (1994) Skeletal muscle partial pressure of oxygen in patients with sepsis. Critical care medicine 22:640-650

112. Shapiro NI, Howell MD, Talmor D, Nathanson LA, Lisbon A, Wolfe RE, Weiss JW (2005) Serum lactate as a predictor of mortality in emergency department patients with infection. Annals of emergency medicine 45:524-528

113. Nguyen HB, Rivers EP, Knoblich BP, Jacobsen G, Muzzin A, Ressler JA, Tomlanovich MC (2004) Early lactate clearance is associated with improved outcome in severe sepsis and septic shock. Critical care medicine 32:1637-1642

114. Demir IE, Ceyhan GO, Friess H (2012) Beyond lactate: is there a role for serum lactate measurement in diagnosing acute mesenteric ischemia? Digestive surgery 29:226-235

115. Studer P, Vaucher A, Candinas D, Schnüriger B (2015) The value of serial serum lactate measurements in predicting the extent of ischemic bowel and outcome of patients suffering acute mesenteric ischemia. Journal of gastrointestinal surgery 19:751-755

116. Noll E, Bouitbir J, Collange O, Zoll J, Charles A, Thaveau F, Diemunsch P, Geny B (2012) Local but not systemic capillary lactate is a reperfusion biomarker in experimental acute limb ischaemia. European Journal of Vascular and Endovascular Surgery 43:339-340

117. Diana M, Noll E, Diemunsch P, Moussallieh F-M, Namer I-J, Charles A-L, Lindner V, Agnus V, Geny B, Marescaux J (2015) Metabolism-guided bowel resection: potential role and accuracy of instant capillary lactates to identify the optimal resection site. Surgical innovation 22:453-461

118. Diana M, Agnus V, Halvax P, Liu YY, Dallemagne B, Schlagowski AI, Geny B, Diemunsch P, Lindner V, Marescaux J (2015) Intraoperative fluorescence-based enhanced reality laparoscopic real-time imaging to assess bowel perfusion at the anastomotic site in an experimental model. British Journal of Surgery 102:e169-e176

119. Diana M, Halvax P, Dallemagne B, Nagao Y, Diemunsch P, Charles A-L, Agnus V, Soler L, Demartines N, Lindner V (2014) Real-time navigation by fluorescence-based enhanced reality for precise estimation of future anastomotic site in digestive surgery. Surgical endoscopy 28:3108-3118

120. Diana M, Noll E, Diemunsch P, Dallemagne B, Benahmed MA, Agnus V, Soler L, Barry B, Namer IJ, Demartines N (2014) Enhanced-reality video fluorescence: a real-time assessment of intestinal viability. Annals of surgery 259:700-707

121. Tanner RK, Fuller KL, Ross ML (2010) Evaluation of three portable blood lactate analysers: Lactate Pro, Lactate Scout and Lactate Plus. European journal of applied physiology 109:551-559

122. Fujita F, Torashima Y, Kuroki T, Eguchi S (2014) Risk factors and predictive factors for anastomotic leakage after resection for colorectal cancer: reappraisal of the literature. Surg Today 44:1595-1602

123. Nachiappan S, Askari A, Currie A, Kennedy RH, Faiz O (2014) Intraoperative assessment of colorectal anastomotic integrity: a systematic review. Surgical endoscopy 28:2513-2530

124. Seike K, Koda K, Saito N, Oda K, Kosugi C, Shimizu K, Miyazaki M (2007) Laser Doppler assessment of the influence of division at the root of the inferior mesenteric artery on anastomotic blood flow in rectosigmoid cancer surgery. International journal of colorectal disease 22:689-697

125. Lee KT, Mun GH (2017) Benefits of superdrainage using SIEV in DIEP flap breast reconstruction: A systematic review and meta-analysis. Microsurgery 37:75-83

126. Fujioka M, Hayashida K, Fukui K, Ishiyama S, Saijo H, Taniguchi K (2017) Venous superdrained gastric tube pull-up procedure for hypopharyngeal and cervical esophageal reconstruction reduces postoperative anastomotic leakage and stricture. Diseases of the esophagus: official journal of the International Society for Diseases of the Esophagus 30:1-6

127. Wang W-L (2017) Venous congestion in ischemic bowel. New England Journal of Medicine 377:e10

128. Karampinis I, Keese M, Jakob J, Stasiunaitis V, Gerken A, Attenberger U, Post S, Kienle P, Nowak K (2018) Indocyanine green tissue angiography can reduce extended bowel resections in acute mesenteric ischemia. Journal of Gastrointestinal Surgery 22:2117-2124

129. Liot E, Assalino M, Buchs NC, Schiltz B, Douissard J, Morel P, Ris F (2018) Does near-infrared (NIR) fluorescence angiography modify operative strategy during emergency procedures? Surgical endoscopy 32:4351-4356

130. Son GM, Kwon MS, Kim Y, Kim J, Kim SH, Lee JW (2019) Quantitative analysis of colon perfusion pattern using indocyanine green (ICG) angiography in laparoscopic colorectal surgery. Surgical endoscopy 33:1640-1649

131. Wada T, Kawada K, Takahashi R, Yoshitomi M, Hida K, Hasegawa S, Sakai Y (2017) ICG fluorescence imaging for quantitative evaluation of colonic perfusion in laparoscopic colorectal surgery. Surgical endoscopy 31:4184-4193

132. Kulcke A, Holmer A, Wahl P, Siemers F, Wild T, Daeschlein G (2018) A compact hyperspectral camera for measurement of perfusion parameters in medicine. Biomedical Engineering/Biomedizinische Technik 63:519-527

133. Holmer A, Marotz J, Wahl P, Dau M, Kämmerer PW (2018) Hyperspectral imaging in perfusion and wound diagnostics–methods and algorithms for the determination of tissue parameters. Biomedical Engineering/Biomedizinische Technik 63:547-556

134. Noll E, Diana M, Charles AL, Singh F, Gan TJ, Pottecher J, Moussallieh FM, Namer IJ, Geny B, Diemunsch P (2017) Comparative analysis of resuscitation using human serum albumin and crystalloids or 130/0.4 hydroxyethyl starch and crystalloids on skeletal muscle metabolic profile during experimental haemorrhagic shock in swine: A randomised experimental study. Eur J Anaesthesiol 34:89-97

135. Chiu CJ, McArdle AH, Brown R, Scott HJ, Gurd FN (1970) Intestinal mucosal lesion in low-flow states. I. A morphological, hemodynamic, and metabolic reappraisal. Arch Surg 101:478-483

136. Kilkenny C, Browne W, Cuthill IC, Emerson M, Altman DG, Group NCRRGW (2010) Animal research: reporting in vivo experiments: the ARRIVE guidelines. J Gene Med 12:561-563

137. Quero G, Lapergola A, Barberio M, Seeliger B, Gockel I, Saccomandi P, Guerriero L, Mutter D, Saadi A, Worreth M, Marescaux J, Agnus V, Diana M (2019) Correction to: Discrimination between arterial and venous bowel ischemia by computer-assisted analysis of the fluorescent signal. Surg Endosc 33:2720

138. Campbell C, Reames MK, Robinson M, Symanowski J, Salo JC (2015) Conduit vascular evaluation is associated with reduction in anastomotic leak after esophagectomy. Journal of Gastrointestinal Surgery 19:806-812

139. Sicher C, Rutkowski R, Lutze S, von Podewils S, Wild T, Kretching M, Daeschlein G (2018) Hyperspectral imaging as a possible tool for visualization of changes in hemoglobin oxygenation in patients with deficient hemodynamics–proof of concept. Biomedical Engineering/Biomedizinische Technik 63:609-616

140. Daeschlein G, Langner I, Wild T, von Podewils S, Sicher C, Kiefer T, Juenger M (2017) Hyperspectral imaging as a novel diagnostic tool in microcirculation of wounds. Clinical hemorheology and microcirculation 67:467-474

141. Poole KM, Tucker-Schwartz JM, Sit WW, Walsh AJ, Duvall CL, Skala MC (2013) Quantitative optical imaging of vascular response in vivo in a model of peripheral arterial disease. Am J Physiol Heart Circ Physiol 305:H1168-1180

142. Korkmaz-Icoz S, Radovits T, Szabo G (2018) Targeting phosphodiesterase 5 as a therapeutic option against myocardial ischaemia/reperfusion injury and for treating heart failure. Br J Pharmacol 175:223-231

143. Mohey V, Singh M, Puri N, Kaur T, Pathak D, Singh AP (2016) Sildenafil obviates ischemia-reperfusion injury-induced acute kidney injury through peroxisome proliferator-activated receptor gamma agonism in rats. J Surg Res 201:69-75

144. Wang G, Zhang Q, Yuan W, Wu J, Li C (2015) Sildenafil Protects against Myocardial Ischemia-Reperfusion Injury Following Cardiac Arrest in a Porcine Model: Possible Role of the Renin-Angiotensin System. Int J Mol Sci 16:27015-27031

145. Tetsi L, Charles AL, Georg I, Goupilleau F, Lejay A, Talha S, Maumy-Bertrand M, Lugnier C, Geny B (2019) Effect of the Phosphodiesterase 5 Inhibitor Sildenafil on Ischemia-Reperfusion-Induced Muscle Mitochondrial Dysfunction and Oxidative Stress. Antioxidants (Basel) 8

146. McDermott MM (2015) Lower extremity manifestations of peripheral artery disease: the pathophysiologic and functional implications of leg ischemia. Circ Res 116:1540-1550

147. Paradis S, Charles AL, Meyer A, Lejay A, Scholey JW, Chakfe N, Zoll J, Geny B (2016) Chronology of mitochondrial and cellular events during skeletal muscle ischemia-reperfusion. Am J Physiol Cell Physiol 310:C968-982

148. Grambow E, Dau M, Holmer A, Lipp V, Frerich B, Klar E, Vollmar B, Kammerer PW (2018) Hyperspectral imaging for monitoring of perfusion failure upon microvascular anastomosis in the rat hind limb. Microvasc Res 116:64-70

149. Bezemer R, Lima A, Myers D, Klijn E, Heger M, Goedhart PT, Bakker J, Ince C (2009) Assessment of tissue oxygen saturation during a vascular occlusion test using near-infrared spectroscopy: the role of probe spacing and measurement site studied in healthy volunteers. Crit Care 13 Suppl 5:S4

150. Diana M, Noll E, Charles AL, Diemunsch P, Geny B, Liu YY, Marchegiani F, Schiraldi L, Agnus V, Lindner V, Swanstrom L, Dallemagne B, Marescaux J (2017) Precision real-time evaluation of bowel perfusion: accuracy of confocal endomicroscopy assessment of stoma in a controlled hemorrhagic shock model. Surg Endosc 31:680-691

151. Diana M, Noll E, Diemunsch P, Moussallieh FM, Namer IJ, Charles AL, Lindner V, Agnus V, Geny B, Marescaux J (2015) Metabolism-Guided Bowel Resection: Potential Role and Accuracy of Instant Capillary Lactates to Identify the Optimal Resection Site. Surg Innov 22:453-461

152. Diana M, Noll E, Agnus V, Liu YY, Kong SH, Legner A, Diemunsch P, Marescaux J (2017) Reply to Letter: "Enhanced Reality Fluorescence Videography to Assess Bowel Perfusion: The Cybernetic Eye". Ann Surg 265:e49-e52

153. Koyanagi K, Ozawa S, Oguma J, Kazuno A, Yamazaki Y, Ninomiya Y, Ochiai H, Tachimori Y (2016) Blood flow speed of the gastric conduit assessed by indocyanine green fluorescence: New predictive evaluation of anastomotic leakage after esophagectomy. Medicine 95

154. Milstein DM, Ince C, Gisbertz SS, Boateng KB, Geerts BF, Hollmann MW, van Berge Henegouwen MI, Veelo DP (2016) Laser speckle contrast imaging identifies ischemic areas on gastric tube reconstructions following esophagectomy. Medicine 95

155. Diana M, Hübner M, Vuilleumier H, Bize P, Denys A, Demartines N, Schäfer M (2011) Redistribution of gastric blood flow by embolization of gastric arteries before esophagectomy. The Annals of thoracic surgery 91:1546-1551

156. Yoshimi F, Asato Y, Ikeda S, Okamoto K, Komuro Y, Imura J, Itabashi M (2006) Using the supercharge technique to additionally revascularize the gastric tube after a subtotal esophagectomy for esophageal cancer. The American journal of surgery 191:284-287

157. Kono K, Sugai H, Omata H, Fujii H (2007) Transient bloodletting of the short gastric vein in the reconstructed gastric tube improves gastric microcirculation during esophagectomy. World journal of surgery 31:780-784

158. Pham TH, Perry KA, Enestvedt CK, Gareau D, Dolan JP, Sheppard BC, Jacques SL, Hunter JG (2011) Decreased conduit perfusion measured by spectroscopy is associated with anastomotic complications. The Annals of thoracic surgery 91:380-385

159. Bludau M, Hölscher AH, Vallböhmer D, Gutschow C, Schröder W (2010) Ischemic conditioning of the gastric conduit prior to esophagectomy improves mucosal oxygen saturation. The Annals of thoracic surgery 90:1121-1126

160. Veeramootoo D, Shore AC, Wajed SA (2012) Randomized controlled trial of laparoscopic gastric ischemic conditioning prior to minimally invasive esophagectomy, the LOGIC trial. Surgical endoscopy 26:1822-1829

161. Urschel JD, Antkowiak JG, Delacure MD, Takita H (1997) Ischemic conditioning (delay phenomenon) improves esophagogastric anastomotic wound healing in the rat. Journal of surgical oncology 66:254-256

162. Schlottmann F, Patti MG (2017) Evaluation of gastric conduit perfusion during esophagectomy with indocyanine green fluorescence imaging. Journal of Laparoendoscopic & Advanced Surgical Techniques 27:1305-1308

163. Turner SR, Molena DR (2018) The role of intraoperative fluorescence imaging during esophagectomy. Thoracic surgery clinics 28:567-571

164. Hölscher AH, Schneider PM, Gutschow C, Schröder W (2007) Laparoscopic ischemic conditioning of the stomach for esophageal replacement. Annals of surgery 245:241

165. Schröder W, Hölscher AH, Bludau M, Vallböhmer D, Bollschweiler E, Gutschow C (2010) Ivor-Lewis esophagectomy with and without laparoscopic conditioning of the gastric conduit. World journal of surgery 34:738-743

166. Nguyen NT, Nguyen X-MT, Reavis KM, Elliott C, Masoomi H, Stamos MJ (2012) Minimally invasive esophagectomy with and without gastric ischemic conditioning. Surgical endoscopy 26:1637-1641

167. Perry KA, Banarjee A, Liu J, Shah N, Wendling MR, Melvin WS (2013) Gastric ischemic conditioning increases neovascularization and reduces inflammation and fibrosis during gastroesophageal anastomotic healing. Surgical endoscopy 27:753-760

# COMMUNICATIONS

| ANNEE | CONFERENCE/VILLE | PRESENTATION | TITRE |
|---|---|---|---|
| 2018 | SMIT 2018-IBEC 2018 Joint Conference, Seoul, Corée du sud, novembre 2018 | Oral<br><br>-*Best Oral Presentation Award*<br>-*Best Researcher Award* | HYPER: HYPerspectral based Enhanced Reality to evaluate bowel perfusion |
| 2019 | EAES annual congress, Séville, Espagne, juin 2019 | Oral | Fluorescence-based enhanced reality vs. hyperspectral imaging to assess bowel perfusion |
| 2019 | EAES annual congress, Amazing Technology Symposium, Séville, Espagne, juin 2019 | Oral | Anticipating the automated intraoperative tissue recognition: intraoperative tissue classification using hyperspectral imaging and machine learning |
| 2019 | 18th Congress of the French Society of Vascular Medicine, session Ischemia reperfusion: from fundamental to clinical, Strasbourg, septembre 2019 | Conférencier invité | Mesenteric Ischemia |

# PUBLICATIONS

**Original articles**

**(included in the thesis)**

1. **Hyperspectral imaging quantification of mouse limb microcirculation in ischemia-reperfusion model with phosphodiesterase 5 inhibitor preconditioning. M. Barberio** , E. Felli….. *Submitted to Antioxidants*
2. **HYPerspectral Enhanced Reality (HYPER): a machine-learning powered, physiology based surgical guidance tool. M Barberio,** F Longo, C Fiorillo….. Surg Endosc 2019 Jul 15
3. **Quantitative fluorescence angiography vs. hyperspectral imaging to assess bowel ischemia: a comparative study in enhanced reality. M Barberio,** E. Felli…. *Submitted to British Journal of Surgery.*
4. **Discrimination between arterial and venous bowel ischemia by computer-assisted analysis of the fluorescent signal.**
   Quero G, Lapergola A, **Barberio M,** Seeliger B….Surg Endosc. 2018 Oct 16.
5. **Evaluation of hyperspectral imaging (HSI) for the measurement of ischemic conditioning effects of the gastric conduit during esophagectomy.** Köhler H, Jansen-Winkeln B, Maktabi M, **Barberio M,** Takoh J…… Surg Endosc. 2019 Jan 23.
6. **New intraoperative imaging technologies: Innovating the surgeon's eye toward surgical precision.** Mascagni P, Longo F, **Barberio M,** Seeliger B…. J Surg Oncol. 2018 Aug;118(2):265-282. doi: 10.1002/jso.25148. Epub 2018 Aug 4. Review.

**Original articles**

**(<u>NOT</u> included in the thesis)**

1. **[Hyperspectral imaging of gastrointestinal anastomoses].** Jansen-Winkeln B, Maktabi M, Takoh JP, Rabe SM, **Barberio M**, Köhler H, Neumuth T, Melzer A, Chalopin C, Gockel I. Chirurg. 2018 Sep;89(9):717-725.
2. **Hyperspectral based discrimination of thyroid and parathyroid during surgery M Barberio,** M Maktabi, I Gockel, N Rayes, B Jansen-Winkeln, H Köhler, ... Current Directions in Biomedical Engineering 4 (1), 399-402. Sept. 2018
3. **Determination of the transection margin during colorectal resection with hyperspectral imaging (HSI).** Jansen-Winkeln B, Holfert N, Köhler H, Moulla Y, Takoh JP, Rabe SM, Mehdorn M, **Barberio M,** Chalopin C, Neumuth T, Gockel I. Int J Colorectal Dis. 2019 Feb 2.
4. **Fluorescence in rectal cancer surgery.** B Seeliger, **M Barberio**, A D'Urso, V Agnus, F Longo, P Mascagni, ... Annals of Laparoscopic and Endoscopic Surgery 3 (5). May 2018
5. **[Possibilities and perspectives of hyperspectral imaging in visceral surgery]**.Gockel I, Jansen-Winkeln B, Holfert N, Rayes N, Thieme R, Maktabi M, Sucher R, Seehofer D, **Barberio M**…..Chirurg. 2019 Aug 21
6. **Simultaneous computer-assisted assessment of mucosal and serosal perfusion in a model of segmental colonic ischemia.** Seeliger B; Agnus V; Mascagni P; **Barberio M**…..*<u>Accepted by Surgical Endoscopy</u>*

**Proceedings**

**Hyperspectral imaging for thermal effect monitoring in in vivo liver during laser ablation.** M. De Landro, P. Saccomandi, **M. Barberio;** July 2019, DOI:10.1109/EMBC.2019.8856487; Conference: 2019 41st Annual International Conference of the IEEE Engineering in Medicine & Biology Society (EMBC)

# Acknowledgments

This new adventure, starting research (almost) from scratch, would not have been possible without the huge support of my parents. They helped me at every difficult moment of my life and I am really grateful for their steady love and presence throughout this path.
I want to thank my two handsome boys: Gabrielinho and Miguelito who made me laugh and brightened up my life so far. Vi amo Sarracin grande e piccolino!

I will always be grateful to Michele Diana who gave me the opportunity to start this new chapter of my life. He believed in me and had the patience to listen to every crazy idea that I came up with, calling it innovation instead of insanity. Thank you for teaching me your methods of planning, conducting and analyzing scientific works. I am grateful for your initiating me into the art of writing manuscripts properly, although I still have ways to go. Thank you for being more than a boss, you are truly a friend.

Dear Professor Marescaux, a great many thanks for trusting Michele that --it was was worth hiring me at IRCAD/IHU as a fellow and as a PhD student. It has been an honor to work in this amazing facility that you built. IRCAD is a magnet for extraordinary people and I am sincerely grateful since I was given the chance to be part of it. It has been a real life-changing experience.

Dear Professor Geny, a big thank you for always giving me the right pieces of advice on my past and future ideas. Thank you for your calm and open-minded attitude. I loved to work with you. A huge thank you goes to your team, especially to Anne-Laure and Isabelle.

Dear people of the experimental platform, Mourad, Gael, Cindy, Emilie, Manon, Thuy Mi, Alex. Thank you for listening without complaining of the music I played during my experiments. I know it must have been hard sometimes. Thank you for the brilliant assistance during the experiments.

Dear Fanelie, Pascal, Benjamin, thanks for taking care of my animals during my survival experiments. Thank you for your flexibility and understanding in the difficult situations.

Dear fellows who helped me during my experimental works, Eric Felli, Fabio Longo, Pietro Mascagni, Claudio Fiorillo, Barbara Seeliger, Taiga Wakabayashi, Takeshi Urade, Margherita Pizzicannella, Andrea Spota, Giovanni Laracca, and Emily Seyller. To Professor Paola Saccomandi, to you a sincere and big thank you for your assistance and for your friendship.

Dear Vincent Agnus, thank you for your computer skills, data analyses, and most of all for your innovative thinking solutions.

I want also to thank Professors Swanstrom, Dallemagne, Perretta, Gimenez for their precious recommendations throughout these two years, but most of all for being such extraordinary people, everyone with hers/his amazing characteristics. You are all examples to follow.

I certainly did not mention all the special people who I met during my journey in Strasbourg, but I am really thankful for the support, the friendship, and the unique moments spent and shared together.